STUDY OF ATMOSPHERIC PLASMA INTERACTION WITH SKIN TO ENHANCE PERMEABILITY

THESIS

STUDY
OF ATMOSPHERIC PLASMA INTERACTION WITH SKIN TO ENHANCE PERMEABILITY

Kristof Jaroslav

Graduate School of Science and Technology
Educational Division

Department of Optoelectronics
and Nanostructure Science

Shizuoka University

JUNE 2018

ACKNOWLEDGEMENTS

I would like to thank to master students of our laboratory, to Kentaro Hayashida, An Nhat Tran, Tomomichi Aoshima, Hideto Miyamoto and Doctor Marius Blajan for their feedback, cooperation during my study and help in experiment. I am also grateful to Professor Kazuo Shimizu for introducing me research of transdermal drug delivery and acceptance me in his laboratory.

I also would like to thank to professors Kenji Murakami, Akihisa Ogino, Daniel Moraru, Jun Kondo, and Yoshimasa Kawata for their fruitful comments and suggestions to my thesis.

Abstract

The thesis is composed of an abstract, a list of figures, a list of tables and seven chapters. The first chapter is the "*Introduction*" which introduces plasma transdermal drug delivery and experiment which were realized in this thesis.

The second chapter is dedicated to skin structure and mainly to stratum corneum which is the main barrier for transdermal drug delivery methods. The structure of stratum corneum and also its main components such as corneocytes, ceramides, fatty acids, cholesterol, their function and structure are described in the subchapters. It is also possible to find information regarding their influence on the permeability of the skin and how it can be increased or decreased.

The third chapter describes the main methods of drug delivery such as oral drug delivery, injection drug delivery and transdermal drug delivery. Their advantages and also disadvantages are briefly mentioned. The following text characterizes the basic principle of the most well-known transdermal drug delivery methods. Drug delivery using plasma is mentioned at the end. Drugs and methods successfully used for penetration through the skin are specified.

As the plasma is medium with various active particles, ions, electrons and radiations, each aspect of the plasma and possible or observed effect on skin is characterized. Chapter four starts with a description of argon and helium ions that can cause "physical sputtering" of surfaces (skin in our case). As the skin treatment is usually realized in atmospheric air, it is necessary to consider the influence of air particles such as oxygen, nitrogen or hydrogen released from hydrocarbon skin surface. This demonstrates that chemical sputtering because of the presence of radicals created in plasma can be present during skin treatment. Three subchapters describe the influence of the mentioned gases. The following subchapters characterize primary effects of plasma such as heat, UV radiation, acidifying of the skin and damage of skin by plasma. Secondary effect of lipid peroxidation receives also some dedicated space.

Chapter five entitled "*Experimental techniques and methods*" characterizes the techniques used in this thesis. The principles of XPS, FTIR, HPLC, PCA, contact angle measurement, pharmacokinetic modeling and basic information about analysis of data are mentioned.

Chapter six is the largest chapter of the thesis and includes measurements and results. It is composed of six subchapters: Plasma discharges, Interaction of plasma and skin surface, Plasma treatment of lipids, Plasma treatment of the skin, Permeability of plasma treated skin and Pharmacokinetics.

The section "*Interaction of plasma and skin surface*" interprets skin surface activation through water angle measurement using different gasses or distances from plasma source. X-ray photoelectron spectroscopy helped to determine the concentration of surface atoms and created bonds. Histological skin sections show roughness and change of thickness of the stratum corneum.

The section "*Plasma treatment of lipids*" characterizes changes of isolated lipids after plasma treatment by Fourier transform infrared spectroscopy and X-ray photoelectron spectroscopy.

The section "*Plasma treatment of the skin*" characterizes the skin surface mostly by FTIR, change of lipid fluidity or packing density of the lipids in the lipid matrix..

The section "*Permeability of plasma-treated skin*" is dedicated to the experiments which investigate the ability of the skin to be permeable for molecules such as H_2O and Cyclosporine A.

The section "*Pharmacokinetics*" analyzes the amount of drug (Cyclosporine A) in blood after successful permeation through the skin. There is determined treatment area and concentration of drug for successful medical application.

Chapter seven entitled "*Conclusion*" summarizes the results of all experiments mentioned in the thesis.

In the last section, a list of publications is displayed.

Content

List of Figures

List of Tables

1 Introduction

According to Laroussi [1], plasma was used in biological application in 1850s when dielectric barrier discharge generated ozone to clean water from biological contaminates. However, systematic research started only in the 1990s. These days, there is a huge amount of publications in the field of the decontamination of surfaces, wound healings or treatment of cancer cells. As a result, human skin became the center of attention of plasma researchers, but only very few publications are dedicated directly to drug delivery experiments where the plasma is used as an enhancer of skin permeability. There are only a few contributions analyzing the interaction of the most upper layer of the skin – stratum corneum and plasma, and even fewer contributions which tested penetration of any molecule through the stratum corneum. Three of these contributions were published in our laboratory. However, the number of publications is slowly increasing and this year (2018) three papers from three laboratories have been published. There are several techniques to perform drug delivery. One of the most convenient techniques is oral drug delivery. However, the problems of swallowing or low bioavailability of drug, danger of under dosing or over dosing, interaction with food or drink and existence of other problems indicate that it is required new pathway for drug administration. Also application of the drug by injection is not solution because it is the reason of huge amount of infection, not only undeveloped but also in developed countries. The drawbacks of subcutaneous delivery are that it is possible to use only for certain kinds of drugs [2].

This thesis has three main aims. These are: “Successful penetration of heavy drug after plasma treatment of the skin”, “Analyzing of processes leading to improvement of skin permeability” and “Observation of skin damage by other interactions with plasma source”.

“Observation of skin damage made by plasma source” was realized by microscopic observation of the skin section which showed etching of the stratum corneum by microplasma discharge and some serious disruptions by plasma jet treatment.

Penetration of the heavy drug was tested by Cyclosporine A which has molecular weight 1203 Da. This drug penetrated through the skin only after plasma treatment. The experiment was realized by using Franz cells for a period of 24 hours. Pharmacokinetic model showed that, under some conditions, this amount could be sufficient in medical praxis, but another improvement of permeability is necessary to be able to compete with other methods.

Improvement of permeability was also confirmed by measurement of trans-epidermal water loss from the skin realized also using Franz cell.

"Analyzing of processes leading to improvement of skin permeability" was realized by two ways. At first, as the skin is the material with many molecules inside, we investigated interaction of the plasma and lipid molecules such as erucic acid, stearic acid, cholesterol or ceramide C4. Observed changes can help us to understand, how improving of permeability happens. As the second step, interaction of plasma and the stratum corneum was realized by FTIR and TEM observation of the skin sheet. And these observations were compared with changes of lipids with plasma treatment which showed similar behavior in some cases.

References

[1] M. Laroussi, IEEE TRANSACTIONS ON PLASMA SCIENCE 36(4), 1612 (2008).
[2] J. Gabriel,Br. J. Nurs. 23, S10 (2014).

2 Skin structure

Skin is composed of several layers such as the epidermal layer composed of stratum corneum (composed of dead cells) and viable epidermis. Other layers are dermis and hypodermis which connect our skin to bones and muscles. Stratum corneum is the most important part of the skin for transdermal drug delivery. In the next section, the structure and composition of the stratum corneum will be described.

2.1 Stratum corneum structure

Stratum corneum, an upper layer of the skin, is a lipid-rich matrix with embedded corneocyte cells that are dead keratinocytes. This layer is the main barrier of the skin which protects the body against loss of water and ensures that molecules from outside will not enter the body. The stratum corneum is composed of corneocyte cells placed in a lipid-rich matrix. Human stratum corneum (thickness of 10 – 20 μm) contains from 10 to 25 layers of corneocytes. Corneocytes are composed of fibrillary keratin and water, inside a cornified envelope. The cornified envelope is composed of crosslinked fillagrin, loricrin and involucrin [1]. Corneocytes are tied together by a protein called corneodesmosome (Figure 2.1.1). Lipid-rich matrix is used for transdermal drug delivery (TDD) – intercellular pathway. The lipid-rich matrix is composed of hydrophilic domain – head of ceramides and lipophilic domain – tails (Figure 2.1.1). Lipids in the lipid matrix are organized in lamellar layers following a tri-layer broad-narrow-broad arrangement [2]. The width of the tri-layer structures can be 6 or 13 nm. These lamellae can be packed in dense orthorhombic, less dense hexagonal or disordered liquid phase [1]. The lipid matrix consists of ceramides (41%), cholesterol (27%), cholesterol esters (10%), fatty acids (9%) with a small fraction of cholesterol sulphate (2%) [3] and glucosylceramides. The presence of ceramides indicates that lipids will be structured [7]. Lipid chains are usually in a solid crystalline or gel state. At higher temperatures, lipids change state to a liquid crystalline and they are more permeable (Figure 2.1.1).

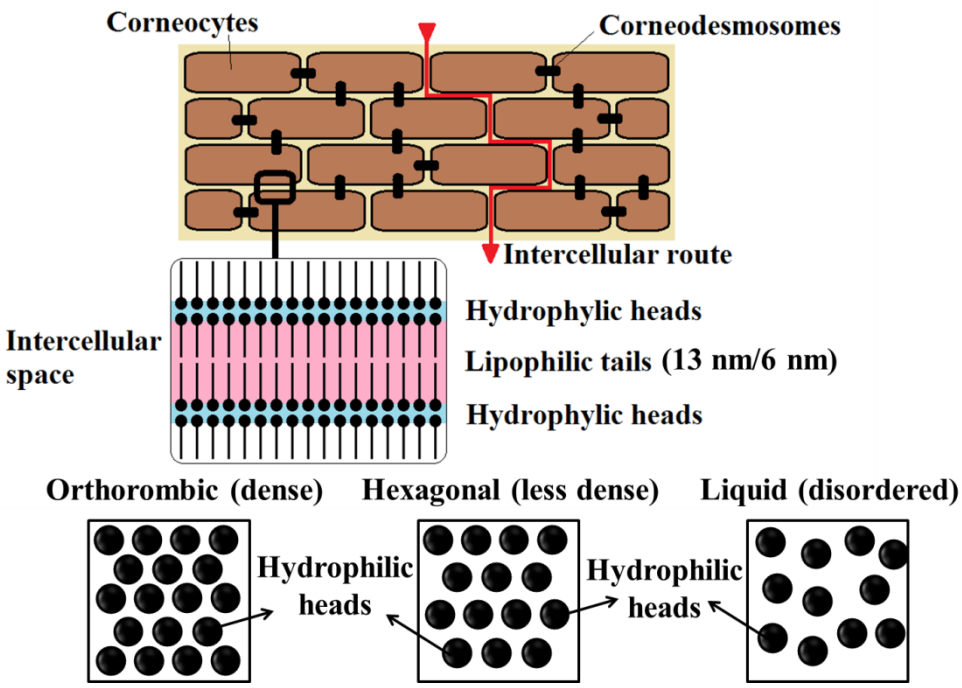

Figure 2.1.1: Model of the stratum corneum and with lateral and lamellar organization of lipids in the lipid matrix [2].

The permeability of stratum corneum lipid membranes depends strongly on the ceramide composition of these membranes. Molecular dynamics simulations show that ceramides with shorter (four- to eight-carbon acyl chains) fatty acid chains increase skin permeability, while further shortening of the chain leads to increased resistance to penetration almost as good as that of ceramides from healthy skin (24 carbons long on average) [4]. In order to enhance skin permeability, mechanisms like alternation of lipids of stratum corneum and its fluidity, or creation of the disordering effect between alkyl chains of lipids of stratum corneum have been proposed [5]. After disruption of the stratum corneum, cholesterol synthesis leads to repairing of the barrier and it starts 90 min after barrier disruption [6]. Renewal of the stratum corneum occurs every 14 days [7].The stratum corneum can be divided into three main layers with different compositions and barrier functions [8]. The layers can be characterized by the concentration of K, Na, ceramides and fillagrin (Figure 2.1.2).

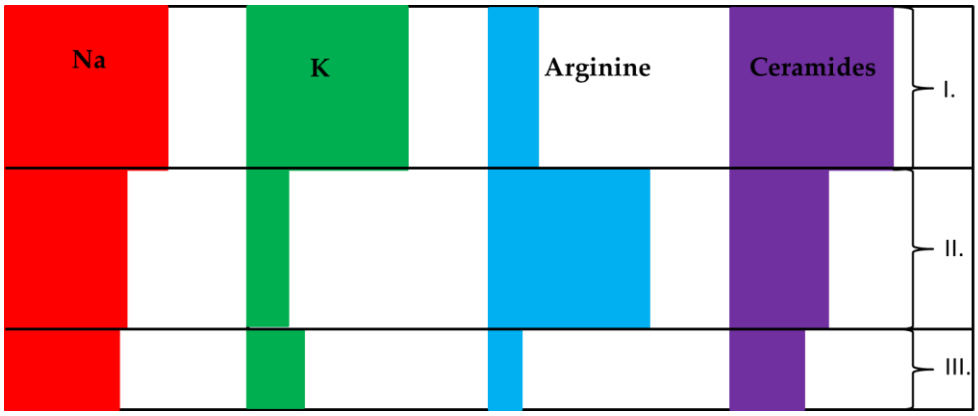

Figure 2.1.2: Three layers of the stratum corneum characterized by normalized amount of Na, K, arginine and ceramides [8]. The thickness of red, green blue and violet rectangular indicates relative concentration. I. denotes the upper layer, II. denotes the middle layer, and III. denotes the lower layer.

Concentration of Na is high in the whole stratum corneum and concentration of K is high in the upper layer but low in the rest of the stratum corneum. Concentration of ceramides decreases from the upper layer to the lower layer. Concentration of arginine, which is the product of fillagrin, is the highest in the middle layer and low in the rest of the stratum corneum. The upper layer of the stratum corneum with dimension of 2/5 of the whole thickness (~ 8 μm) appears as a layer which allows passive flow of ions inside and outside. The amount of Na and K can be changed by the influence of the outer environment. Liquid and ions can easily penetrate the corneocytes in this layer and intracellular Na can be flushed out when cornecytes absorb water or other liquids. The middle layer of the stratum corneum appears as a first real barrier. The thickness is approximately 2/5 of the whole stratum corneum as in the previous case. Ions such as K^+ or Cr^{6+} cannot penetrate this layer. Hydration of the skin is a function of the second layer because of a high concentration of arginine. It was observed that Cr^{3+} was able to penetrate the middle layer of the stratum corneum but not the third layer, which is the reason why the third layer can be called a second barrier. The third layer has a thickness of 1/5 of the stratum corneum (~ 4 μm) and the barrier function of the stratum corneum increases towards the viable epidermis. We can say that only 3/5 of whole thickness of stratum corneum is the real barrier of the skin.

2.1.1 Corneocytes

Corneocytes contain a lipid envelope bounded to the exterior by a protein envelope. Corneocytes of the lipid envelope functions as a semipermeable membrane that allows water molecules to penetrate but not larger hygroscopic molecules [9]. Intercellular lipid lamellae

and lipids of the lipid envelope of cornecytes are connected through an ester bond (R-CO-O-R1) [10].

2.1.2 Role of ceramides

The percentages of some ceramides in the lipid matrix are 29.9% of ceramide 6, 21.7% of ceramide 2, 14.8% of ceramide 4, 13.9% of ceramide 5, 11.9% of ceramide 3 and 7.8% of ceramide 1 [11] (Figure 2.1.3).

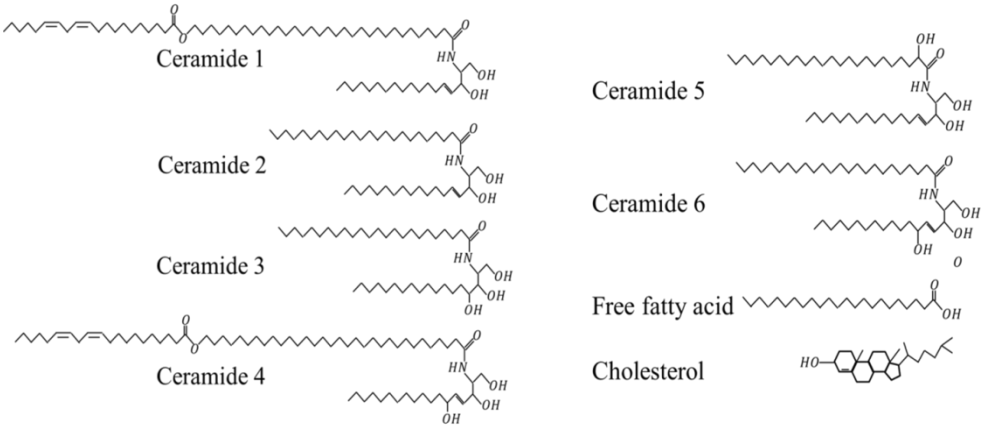

Figure 2.1.3: Structure of some ceramides fatty acid and cholesterol in the lipid matrix [11].

The permeability of this membrane can be increased by decreasing the concentration of cholesterol, increasing the amount of short tailed fatty acids and unsaturated fatty acids. A decrease of ceramides also decreases the barrier function of the skin. Ceramides form a multilayer lamellar structure with other lipids. Ceramides also act as a water modulator and their decrease also decreases the water-holding capacity [12]. The majority of ceramides of the stratum corneum has an even number of carbons and the most abundant has 44 and 46 carbons. Ceramides with numbers of carbons higher than 60 were also observed in a not negligible concentration [13]. The permeability of the synthetic lipid membrane was not changed with the length of the ceramides. Changes in head groups of ceramides also did not change the permeability [14]. Other research showed that the chain length of ceramides has a huge influence on the barrier permeability. It was also observed that a synthetic barrier composed of a limited amount of ceramides (3 in this case) has some effect on barrier properties. Comparison with ceramides from a pig which contains a wider distribution of ceramides showed higher permeability. This can be explained by mismatches between various lengths in the lipid lamellae. Wider distributions of ceramide chains affect lamellar and also lateral organization. The wider distribution leads to a hexagonal organization, and synthetic

ceramides with a low ceramide chain distribution leads to an orthorhombic organization [15]. A long periodic phase (Figure 2.1.1 13 nm long lipid tails) is formed in the presence of a certain level of unsaturated ceramides, and a long periodic phase is associated with fluid-like structure inside. Saturated Ceramide EOS-S is important for the stabilization of the orthorhombic phase [16].

2.1.3 Role of fatty acids

Reduction of free fatty acid (FFA) chains was observed in skin diseases which are known by impaired skin barrier function. Reduction of the fatty acid chain can be caused by an increase in the amount of shorter FFA chains such as with 16 or 18 carbons. A shorter chain allows an increase in vibrations followed by conformational disordering. An increase in the number of unsaturated FFA reduces the packing density of the lipid organization [13]. An analysis of the composition of free fatty acids of human stratum corneum showed a dominant presence of saturated free fatty acids with carbon chain lengths from 16 to 30. The most abundant were FFAs with 24 and 26 carbons (50% of all FFAs). The content of unsaturated FFAs appeared to be around 2% of all FFAs; mostly with 18 carbons and with traces of FFAs with 16, 17 and 20 carbons; 1% of di-unsaturated FFAs (chain length of 18 carbons) [14].

2.1.4 Role of cholesterol

Cholesterol is situated near the ester bond of ceramides and this position allows formation of a hydrogen bond between the cholesterol –OH group and the carbonyl group C=O. The presence of cholesterol has an influence on the formation of the long periodicity phase of ceramides (13 nm). There is a minimal amount of required cholesterol for the formation of the long periodicity phase of ceramides (without cholesterol, long periodicity phase is not formed). Cholesterol does not influence only the presence of long periodicity phase, but also the packing density in the long periodicity phase [17]. Cholesterol is very important for correct skin barrier function [18].

2.1.5 Sebum

Sebaceous glands are placed on the most parts of body. There are several theories about their function from antibacterial effect, antioxidant effects and transport of pheromones, but their actual function is not known. Changes in sebum are very often connected with creation of acne. Human sebum is composed of 57% of weight of triglycerides, diglycerides

and free fatty acids, 26% of weight of wax esters, 12% of weight of squalene and 2% of weight of cholesterol [19]. According to Lovászi *et al.* [20], desaturation of fatty acids and accumulation of lipid peroxides in the sebum can lead to creation of acne and hydrolysis of sebaceous lipids lead to decreasing of triglycerides. An increase of free fatty acids causes irritation, but depends on the composition of fatty acids [21, 22]. Follicular and sebaceous glands are investigated as a route for drug delivery [23, 24]. The effects of sebum on skin barrier function have not been yet investigated [25].

References

[1] Van Smeden J., Janssens M., Gooris G.S., Bouwstra J.A., Biochimica et Biophysica Acta 1841, 295 (2014).
[2] Hill J. R., Wertz P.W., Biochimica et Biophysica Acta1616, 121 (2003).
[3] Suhonen T M , Bouwstra J A , Urtti A., Journal of Controlled Release. 59, 149 (1999).
[4] Paloncyova M ,Vavrova K, Sovova Z, DeVane R, Otyepka M, Berka K., J. Phys. Chem. B. 119, 9811 (2015).
[5] Moghadam S H, Saliaj E, Wettig S D, Dong Ch, Ivanova M V, Huzil J T, and Foldvari M., Mol. Pharmaceutics 10, 2248 (2013).
[6] Dayan. N., Cosmetics & Toiletries magazine 121(1) 37 (2006).
[7] Hadgraft J and Lane M E., Phys. Chem. Chem. Phys. 13, 5215 (2011).
[8] Kubo A., Ishizaki I., Kubo A., Kawasaki H., Nagao K., Ohashi Y., Amagai M., Scientific Reports. 3, 1731 (2013).
[9] Elias P.M., Gruber R., Crumrin D., Menon G., Williams M.L., Wakefield J.S., Holleran W.M., Uchida Y., Biochimica et Biophysica Acta (BBA) - Molecular and Cell Biology of Lipids. 1841(3), 314 (2014).
[10] Downing D. T,.Journal of Lipid Research 33, 301 (1992).
[11] Wertz P.W., Adv. Drug Deliv. Rev. 18, 283 (1996).
[12] Imokawa G., Koichi I., J Clin Exp Dermatol Res. 5(1), 1000206 (2014).
[13] Van Smeden J., Boiten W. A., Hankemeier T., Rissmann R., Bouwstra J. A., Vreeken R. J., Biochimica et Biophysica Acta 1841, 70 (2014).
[14] Uchiyama M., Oguri M., Mojumdar E. H., Gooris G. S., Bouwstra J. A., Biochimica et Biophysica Acta 1858, 2050 (2016).
[15] Mojumdar E.H., Kariman Z., van Kerckhove L., Gooris G.S., Bouwstra J.A., Biochimica et Biophysica Acta 1838, 2473 (2014).
[16] De Sousa Neto D., Gooris G., Bouwstra J., Chemistry and Physics of Lipids 164, 184 (2011).
[17] Mojumdar E.H., Gooris G.S., Groen D., Barlow D.J., Lawrence M.J., Demé B., Bouwstra J.A., Biochimica et Biophysica Acta (BBA) - Biomem-branes. 1858(8), 1926 (2016).
[18] Vávrová K., Kováčik A., Opálka L., Eur. Pharm. J. 64(1), 1 (2017).
[19] K. R. Smith, D. M. Thiboutot, The Journal of Lipid Research 49, 271 (2008).
[20] M. Lovászi, A. Szegedi, Ch. C. Zouboulis, D. Törőcsik, Dermato-Endocrinology 9(1),e1375636, (2017)
[21] X. Li, C. He, Z. Chen, Ch. Zhou, Y. Gan, Y. Jia, J Cosmet Dermatol. 1, 6 (2017).
[22] N. AKAZA, H. AKAMATSU, S. NUMATA, M. MATSUSUE, Y. MASHIMA, M. MIYAWAKI, S. YAMADA, A. YAGAMI, S. NAKATA, K. MATSUNAGA, Journal of Dermatology 41, 1069, (2014).
[23] J. W.Fluhr, M. Mao-Qiang, B. E.Brown, P. W.Wertz, D. Crumrine, J. P.Sundberg, K. R.Feingold, P. M.Elias, Journal of Investigative Dermatology 120(5) 728.
[24] R. Reddy, J. H. Cary, A. Elmahdy, H. Maibach, Journal of Dermatological Treatment (2018).
[25] Tsai JC., Lan CC.E., Sheu HM. (2017) Effects of Sebum on Drug Transport Across the Human Stratum Corneum. In: Humbert P., Fanian F., Maibach H., Agache P. (eds) Agache's Measuring the Skin. Springer, Cham.

3 Drug delivery methods

There are several drug delivery methods such as oral drug delivery, injection drug delivery, nasal drug delivery, ocular drug delivery, transdermal drug delivery and some others. In this chapter, a brief description of oral drug delivery, injection drug delivery and transdermal drug delivery is introduced.

3.1 Oral drug delivery

One of the most convenient techniques of drug delivery is oral drug delivery. Drugs are easy to store, they are noninvasive, and no special instructions are needed. They exist in solid form as tablets and capsules or liquids. One of the limitations of liquid forms of drugs is the uncontrolled release of their active agent, which leads to multiple doses during the day [1]. On the other hand, solid formulations are economical, and they are well established in pharmaceutical companies, but large tablets can be a problem to swallow for children or patients with difficulty in swallowing. Tablets with very small dimensions (in the range of millimeters) [2] can be produced, but the size is limited by the required dose. First-pass metabolism causes low bioavailability [3] of orally administrated drugs, which leads to higher doses that have to be delivered, which can also be toxic for some organs.

3.2 Injection drug delivery

The first experiments with intravenous injections were carried out in 1642, but because of lethal accidents, they were not favored as a treatment therapy. Later, in 1853, injection methods that allowed an exact dosage was invented [4]. When injection is used, there is still a risk of infection. These days, the reuse of injections causes 20 million of infections with hepatitis B and 250 000 infections with HIV in the world every year [5].It means that trained people are needed for drug administration, and pain that can occur is inevitable and causes fear. The advantage apart from other techniques is that the drug is completely absorbed [6]. When the preferences of patients were investigated between intravenous and subcutaneous delivery, patients mostly chose subcutaneous delivery [7].

Hutin *et al.* [5] published the best practices to decrease infections by injection:

1. Elimination of the usage of unnecessary injections.
2. Using sterile injection equipment for each injection (ideally using new single-use syringe and needle or, if single-use syringe is not available, sterilize in equipment for steam sterilization)

3. Prevent contamination of injection equipment and medication (preparation of each injection in a clean area)
4. Prevent needle-stick injuries to the provider
5. Prevent access to used needles

Intravenous infusion or injection is used when an immediate therapeutic effect is necessary or other techniques are not suitable for drug administration. Such case is for example the administration of insulin. These days, diabetes is a very common disease and it requires multiple injections during the life of the patient. Mostly, insulin application is very often without any infections, but skin infection was detected in rare cases.

However, microneedles represent some hope for the future. If microneedles are shorter than 0.5 mm, they are not painful. But redness of the skin can cause increased sensitivity to the sun in the place of the administration [8].

3.3 Transdermal drug delivery

3.3.1 Advantages and disadvantages of TDD

As the stratum corneum provides a barrier to any chemical entering to the body, only small molecules having a molecular weight of less than 500 Da (Daltons) can passively diffuse through the skin at rates resulting in therapeutic effects. There are several methods for overcoming this barrier, such as using chemical enhancers or physical ways using electric current or plasma discharge. Transdermal drug delivery is an alternative to oral and parenteral routes of administration. It can offer some advantages over other methods of drug delivery [9, 10]:

1. Reduction of dosing frequency, due to longer duration of delivery.
2. Lower dosing of drugs
3. Circumvention of first-pass inactivation by liver that can metabolize drugs
4. Reduction of gastrointestinal irritation
5. Lower probability of over or under dosing
6. No pain
7. No risk of infection by a contaminated needle or via wounds caused by a needle
8. Suitable for patients with problems swallowing

Disadvantages of TTDS:

1. Only some drugs are permeable through the skin

2. Limited to drugs with a daily dose 10 mg and less
3. Slow drug delivery
4. Possible skin irritation

3.3.2 Chemical enhancers in transdermal drug delivery

Chemical enhancers are substances that change the properties of skin for better penetration of drugs. The most well-known chemical enhancers are alcohols, fatty acids, terpenes and azone. An increase in permeability is very often caused by fluidizing the lipids in stratum corneum. However, it is not valid for high concentration of short chain alcohols (like ethanol), where there was observed only a decrease of the absorbance of CH_2 stretching bands and no shift of their position; thus, there is only the extraction of lipids [11]. Many enhancers have long hydrocarbon chains and it was found out that for fatty acids and fatty alcohols, enhancement is related to the length of the hydrophobic group chain [12]. The enhancer can interact with the polar head or with hydrophobic tails of lipid bilayer or with proteins. Water increases fluidity of stratum corneum by insertion of water molecules between polar head groups. DMSO (dimethylsulfoxid) interacts with intercellular lipids and keratin. Azone disrupts lipid structure, and oleic acid increases fluidity of intercellular lipids. The most effective enhancers are those which interact with lipids and also with proteins of stratum corneum [13]. Combinations of chemical enhancers have been used to maximize the effect of the permeability of drugs, and chemical enhancers are also combined with physical-enhancing methods such as iontophoresis [14].

3.3.3 Iontophoresis in transdermal drug delivery

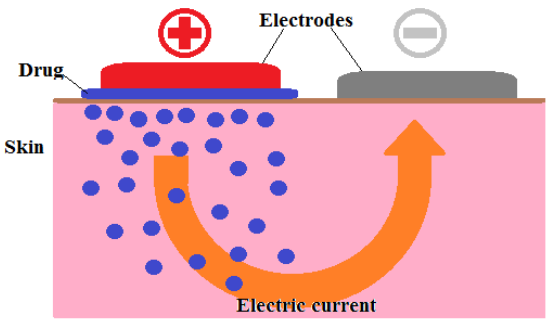

Figure 3.3.1 Application of iontophoresis to skin.

Iontophoresis (Figure 3.3.1) is a class of non-invasive methods to increase penetrations of ions through the skin by applying electric current using low voltages up to 10 V (Figure 3.3.1). Various waveforms of applied current has been investigated [15], and it has been shown that various waveforms have various effectivity for skin permeability [16]. Iontophoresis enhances transdermal drug delivery by three mechanisms:

1. Ion-electric field interaction causing moving of drug (ions) away from the electrode through the skin.
2. Flow of electric current increases skin permeability.
3. Electro-osmosis caused by solvent flow from the anode to cathode because of negatively charged skin due to amino acids in cell membranes.

Iontophoresis is used for ionisable drugs and it is most effective for molecules with weight up to 7 kDa [17] or 10-15 kDa according to Kalluri *et al.* [18]. The disadvantages of iontophoresis are: difficulties with stabilizing the therapeutic agent in the application vehicle, complexity of the drug release system, and prolonged skin exposure to an electric current [19]. The main changes on skin after iontophoresis are an increase of the hydration of stratum corneum, and a decrease of electrical resistance of the skin [20]. Analysis of asymmetric CH_2 peak, in ATR-FTIR spectra, did not show lipid alkyl chain disorders characterized by band shift or band broadening even at high current densities in some previous works [21, 22, 23, 24]. On the other hand, in the recent work of Prased *et al.* [25], they observed a shift of asymmetric CH_2 band with increasing of current density that achieved 8 cm^{-1} at 0.2 mA/cm^2. Also, decreasing of lipid and protein bands intensity indicates lipid and protein extraction. The spectra also demonstrated a split in amide II band into 1553 cm^{-1} and 1541 cm^{-1}. The split could be due to the disruption in hydrogen bonding associated with the head of ceramides, breaking interlamellar hydrogen bonding of the lipid bilayer and disrupting the barrier property of stratum corneum, resulting in loosening of lipid-protein domains, thus allowing higher flux as compared to the passive treatment [26]. Reversibility studies were conducted *in vivo* after 24 and 48 h of the application of iontophoresis. It was observed that the recovery process had started in 24 h and almost total recovery of epidermal as well as dermal changes was found in 48 h with low current density DC iontophoresis. However, with iontophoresis using 0.5 mA/cm^2 current density, edema along with focal disruption of the epidermis persisted [26].

3.3.4 Electroporation in transdermal drug delivery

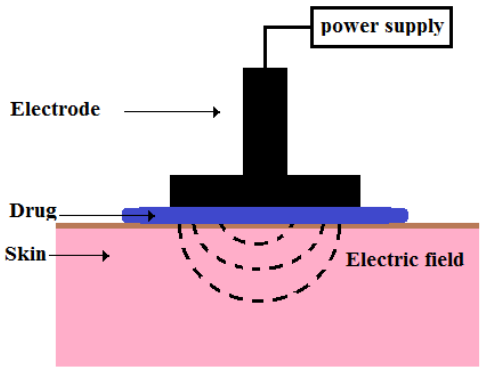

Figure 3.3.2: Application of electroporation application.

Unlike iontophoresis, electroporation (Figure 3.3.2) uses high voltage (over 100 V) pulses for short time (in range of microseconds to milliseconds). Cells exposed to an electrical pulse open pores in the cell membrane and allow macromolecules to enter. It was confirmed that delivery of drugs at least 40 kDa can be achieved [27]. The disadvantages of electroporation are:

(1) if the pulses have not adequate length and intensity, pores can be too large or cause cell damage, and a non-specific amount of material can be released to the cell [28];

(2) the created pores can persist several hours, which allows a higher amount of drug to be delivered [29].

3.3.5 Plasma transdermal drug delivery

DBD plasma discharge in direct contact with skin was used for transdermal delivery in the air [30]. The time of plasma application was set up to 2 min in pulsed mode 1-10 μs and frequency ranged from 50 Hz to 3.5 kHz. Delivery of large molecules such as dextran molecules with a molecular weight 10 kDa can penetrate to a depth of 600 μm within one hour and larger molecules such as albumin (66 kDa), IgG human immunoglobulin (115 kDa) and SiO_2 nanoparticles with a diameter of 50 nm can penetrate to a depth of 200 μm within one hour. Even liposomes with a diameter of 100 nm were delivered to a depth of 100 μm after one hour. Remote microplasma or plasma jet in argon gas was investigated for transdermal delivery of Galantamine Hydrobromide (368 Da) [31] in our laboratory.

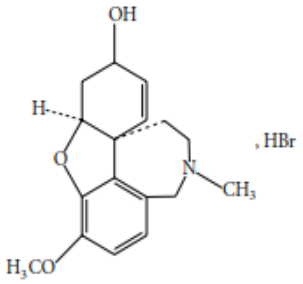

Figure 3.3.3: Chemical structure of Galantamine hydrobromide.

Galantamine hydrobromide (Figure 3.3.3) is an alkaloid, isolated from plant species such as Narcissus and Lycoris species [32]. Treatment of Alzheimer's disease occurs by inhibition of acetylcholinesterase enzyme. The chemical structure of Galantamine hydrobromide is shown in Figure 3.3.3.

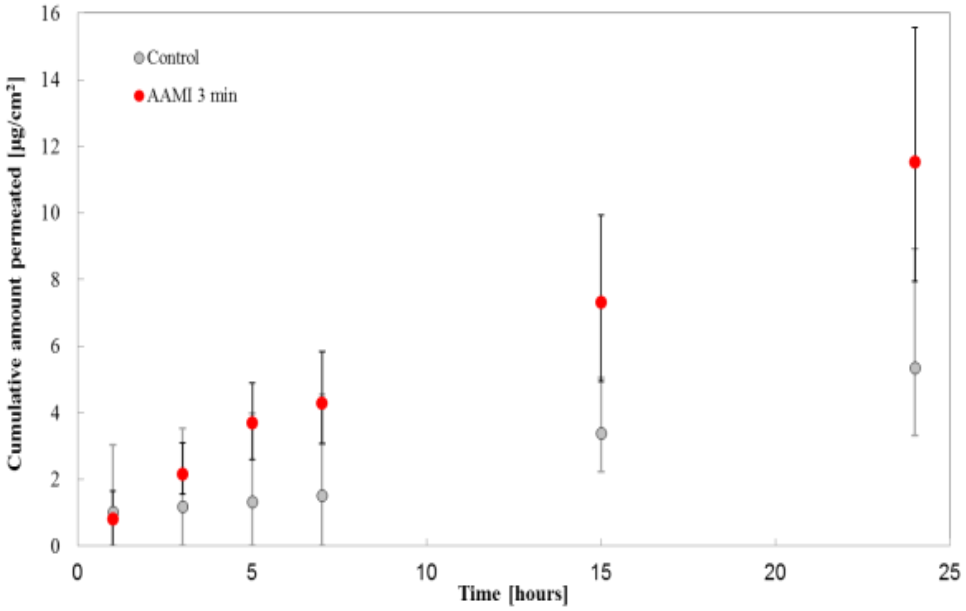

Figure 3.3.4: Amount of penetrated GaHBr – passive diffusion and after microplasma irradiation (red circles) [31].

As GaHBr is a hydrophilic molecule with a low molecular weight (368 Da), usually transdermal patches with chemical enhancers are used for transdermal delivery [33]. Using microplasma for the first time for enhancement of transdermal delivery of GaHBr, a slight improvement was observed with comparison of passive diffusion (Figure 3.3.4). Pig skin was

irradiated for 3 minutes and then a water solution with GaHBr was applied on the skin. The permeation profiles of GaHBr through the pig skin delivered 5.35 ± 2.34 μg/cm^2 and 11.53 ± 2.89 μg/cm^2 for the control and the plasma-irradiated sample after 24 h post-experiment, respectively [31]. These results lead to the expectation that microplasma discharge can be used to enhance the skin delivery of hydrophilic drugs and larger molecular drugs in the future. Choi *et al*. [34] investigated transdermal drug delivery using argon atmospheric discharge and they found out that plasma can reduce the barrier function by reducing the expression of E-cadherin and skin barrier will be recovered 3 hours after plasma treatment. E-cadherin is cell adhesion molecule important in the formation of junctions to bind cells to each other. Lee *et al.* [35] compared argon and helium discharge. Argon discharge was more effective than helium discharge. They observed that ions played a key role in enhancing of skin permeability. Gelker *et al.* [36] successfully tested the permeability of human skin after air atmospheric plasma treatment for molecules from 332 Da to 500 000 Da.

References

[1] F. L. Lopez, T. B. Ernest, C. Tuleu, and M. O. Gul,Expert Opin. DrugDelivery12, 1727 (2015).
[2] N. Spomer, V. Klingmann, I. Stoltenberg, C. Lerch, T. Meissner, and J.Breitkreutz,Arch. Dis. Child.97, 283 (2012).
[3] J. H. Lin, M. Chiba, and T. A. Baille, Pharmacolog. Rev.51, 135 (1999).
[4] H. Feldmann, Laryngo-Rhino-Otol 79(4), 239 (2000).
[5] Y. Hutin, A. Hauri, L. Chiarello, M. Catlin, B. Stilwell, T. Ghebrehiwet, J. Garner & the Members of the Injection Safety Best Practices Development Group, Bulletin of the World Health Organization 81(7), 491 (2003).
[6] D. Josephson, "Patient preparation and site selection for peripheral IVinfusion therapy," inIntravenous Infusion Therapy for Nurses: Principlesand Practice, 2nd ed. (Thomson Delmare Learning, New York, 2004).
[7] K. L. Stoner, H. Harder, L. J. Fallowfield, and V. A. Jemkins,Patient8,145 (2015).
[8] B. Koch, I. Rubino, F.-S. Quan, B. Yoo, and H.-J. Choi, Materials 9, 646 (2016).
[9] Jhawat V Ch, Saini V, Kamboj S, Maggon N., Skin. Int. J. Pharm. Sci. Rev. Res. 20(1), 47 (2013).
[10] Prausnitz M R and Langer R.. Nat Biotechnol. 26, 1261 (2008).
[11] Levang A K, Zhao K, Singh J., International Journal of Pharmaceutics 181, 255 (1999).
[12] Suhonen T M , Bouwstra J A , Urtti A., Journal of Controlled Release 59, 149 (1999).
[13] Barry B W., Journal of Controlled Release. 6, 85 (1987).
[14] Prasad R, Anand S, Khar R K, Dinda A K, Koul V., Drug Development and Industrial Pharmacy 35, 1281 (2009).
[15] Coston A F and Li J K-J., Cardiovascular Engineering: An International Journal. 1, 127 (2001).
[16] Prasad R, Koul V, Anand S, Khar R K., Int J Pharm. 333, 70 (2007).
[17] Turner N G, Ferry L, Price M, Cullander Ch, Guy R H., Pharm. Research.14, 1322 (1997).
[18] Kalluri H and Banga A K., AAPS Pharm Sci Tech.12, 431 (2011).
[19] Krueger E, Junior J L C, Scheeren E M, Neves E B, Mulinari E, Nohama P. Fisioter Mov. 27, 469 (2014).
[20] Jadoul A , Bouwstra J, Preat V., Advanced Drug Delivery Reviews. 35, 89 (1999).
[21] Pardeike J, Hommoss A, Müller R H., Int J Pharm. 366, 170 (2009).
[22] Thysman S, Van Neste D, Preat V., Skin Pharmacol.8, 229 (1995).
[23] Jadoul A, Doucet J, Durand D, Preat V., J. Control. Release. 42, 165 (1996).
[24] Van der Geest R, Elshove D A R, Danhof M, Lavrijsen A P M, Bodde H E., J. Control. Release 41, 205 (1996).
[25] Prasad R, Anand S, Koul V., Int J Pharm Investig 1, 234 (2011).
[26] Kazarian S G and Chan K., BBA-Biomembranes 1758, 858 (2006).
[27] Lombry C, Dujardin N, Preat V., Pharmaceutical Research 7, 32 (2000).
[28] Weaver J C and Chizmadzhev Y A., Biochemistry and Bioenergetics. 41, 135 (1996).
[29] Prausnitz M R and Langer R., Nat Biotechnol.. 26, 1261 (2008).
[30] Kalghatgi S., Tsai C., Gray R., Pappas D.. Transdermal drug delivery using cold plas-mas. In: 22nd Int'l Symposium on Plasma Chemistry; 5-10 July; Antwerp, Belgium. 2015. p. O-22-6.
[31] Shimizu K., Tran A. N., Kristof J., Blajan M.. Investigation of atmospheric microplasma for improving skin permeability. In: Proceedings of the 2016 Electrostatics Joint Conference; 13-18 June; Lafayette, USA. 2016. p. I4.
[32] Martin G T, Pliquett U F, Weaver J C., Bioelectrochemistry. 57, 55 (2002).
[33] Yen W F, Basri M, Ahmad M, Ismail M. 2015, 495271 (2015).
[34] J.-H. Choi, S.-H. Nam, Y.-S. Song, H.-W. Lee, H.-J. Lee, K. Song, J.-W. Hong, G.-Ch. Kim, Arch. Dermatol. Res. 306(7), 635 (2014).
[35] H. Y. Lee, J. H. Choi, J. W. Hong, G. Ch. Kim, H. J. Lee, J. Phys. D: Appl. Phys. 51, 215401 (2018).
[36] M. Gelker, Ch. C. Müller-Goymann, W. Viöl, Clinical Plasma Medicine 9, 34 (2018).

4 Plasma effects on skin barrier and transdermal drug delivery

Plasma can interact with the skin by several ways at the same time as it produces heat, UV radiation, ions, metastable states radicals and carious long living particles. Some of the effects of plasma will be described in the next section.

4.1 Sputtering/etching

Sputtering is very often the result of an interaction of the target surface or molecule with ion fluency. When the energy of an ion exceeds a certain value during collision, an atom absorbing this energy can leave its position in the molecule and a vacancy is created vacancy (free bond). If the atom that has left still has enough energy, other atoms can be released by following collisions and other vacancies can be created. Some of the atoms can be released from the target material which leads to a process called “physical sputtering”.

4.1.1 Physical sputtering

The key parameter of physical sputtering is the binding energy in the target molecule and also the energy and mass of the impinging ion. The dependency on temperature is weak. The threshold energy is relatively high (in the range of 10 eV – 100 eV) depending on the target/impinging ion combination. The sputtered yield changes with the angle of incidence, the substrate material or the roughness of the surface. Eroded species consist of atoms or small clusters of target material. Investigation of metallic targets with impinging metallic ions showed that the mechanism of sputtering depends on the ratio of impinging ion mass (M1) and the mass of the atom in the sample (M2) [1]. In the case $M1 < M2$, the threshold energy does not depend on the mass M1 or M2. As the mass M2 increases, the probability of reflection of the ions increases. The mechanism of sputtering follows the next steps:

1. The ion penetrates through the surface layer
2. The ion is implanted in sublayer and deforms the structure of the material
3. The atom of the first layer is sputtered by the impinging ion

If $M2 \geq M1$, the threshold energy for sputtering is higher than in the first case. The threshold energy also does not depend on the mass of M1 and M2, and sputtering follows the mechanism:

1. The ion penetrates through the surface layer and create vacancy releasing atom
2. The impinging ion and also the released atom deform the structure of the material
3. The atom of the first layer is sputtered by the released atom.

The threshold is higher in the second case because atoms of the target are sputtered by secondary atoms which were released by ion bombardment. Pure physical sputtering can be achieved mostly in discharges with inert gasses. Bombardment of lipids inside the stratum corneum will follow mostly the second mechanism when argon is used and the first one in the case of helium. Physical sputtering is present also in nitrogen, oxygen or air plasma but chemical sputtering can be much more dominant.

4.1.1.1 Argon bombardment/Argon plasma

Argon is one of the simplest media for treatment of biological material. Excited states of Ar (Ar*), metastable states (Ar_m) and Ar ions (Ar^+, Ar_2^+) [2] can be produced in any electrical discharge. Ionization energy of Ar^+ and Ar_2^+ is 15.8 eV and 15.5 eV, respectively. Argon metastable states have a relatively long lifetime equal to 38 s [3] in vacuum. However, this time is reduced in atmospheric pressure. The energy difference between the ground state and the metastable state of Ar is 11.55 eV, which can be released by collision. A molecular dynamics simulation demonstrated sputtering of a lipid-like material by argon ions (Figure 4.1.1 A, B). The sputtering threshold energy was between 10 – 20 eV. The yield of sputtered particles increases to 4 Carbon atoms per ion impacting the surface at an energy of 50 eV and increases more slowly up to 10 at 100 eV [4]. If we suppose a similar behavior of lipids and polymers during bombardment, argon ion bombardment of the polymers can lead to decreasing of side chains of the polymer and lead to volatile CH_4, CO, CO_2, $HCOOCH_3$ and H_2, and target structure will disorder [5]. Sputtering of polymer surface by Ar ions leads to graphite-like structure decreasing the rate of sputtering [6]. If the surface consists of too much O and H, a thin C-rich layer is not created because released O and H atoms can cooperate in surface sputtering and react with free carbon bonds [4]. Comparison of the lipid-like surface and polymethylmethacrylate in Figure 4.1.1 A, B shows forming of carbon like surface in the case of polymer but this surface is not formed in the case of the lipid-like surface. Etching of skin surface was confirmed by measuring of the thickness of the stratum corneum in the skin cross section (Figure 4.1.2) [7]. The first layer of the stratum corneum was etched after 5 minutes of irradiation. If argon plasma treatment is realized in atmospheric air, air particles

can participate in treatment with processes other than physical sputtering. Chemical sputtering or surface functionalizing can start to be effective. In this case, plasma treatment causes wettability and hydrophilicity of surfaces by increasing the number of functional groups, such as oxygen or nitrogen. Argon plasma treatment is able to increase oxygen functional groups on polymer surface if argon plasma discharge is working in atmospheric air [8]. MD (Molecular Dynamics) simulation of bombardment of polymers showed that the main products of etching are CO or H_2, polymer units and C_xH_y fragments during transient sputtering. After formation of a damaged layer, the products of sputtering are H, H_2, CO, C_n. Oxygen leaves polymers more difficult than hydrogen because oxygen is larger and less mobile. That is the reason why oxygen is concentrated under a damaged layer with strong C-O-C bonds. In consequence, the surface of polymer is transformed into a layer of amorphous carbon. This process is not valid for all polymers. If polymers are composed of many H or O atoms, amorphous layer of carbon is not formed because the released H and O atom can etch carbon atoms [9].

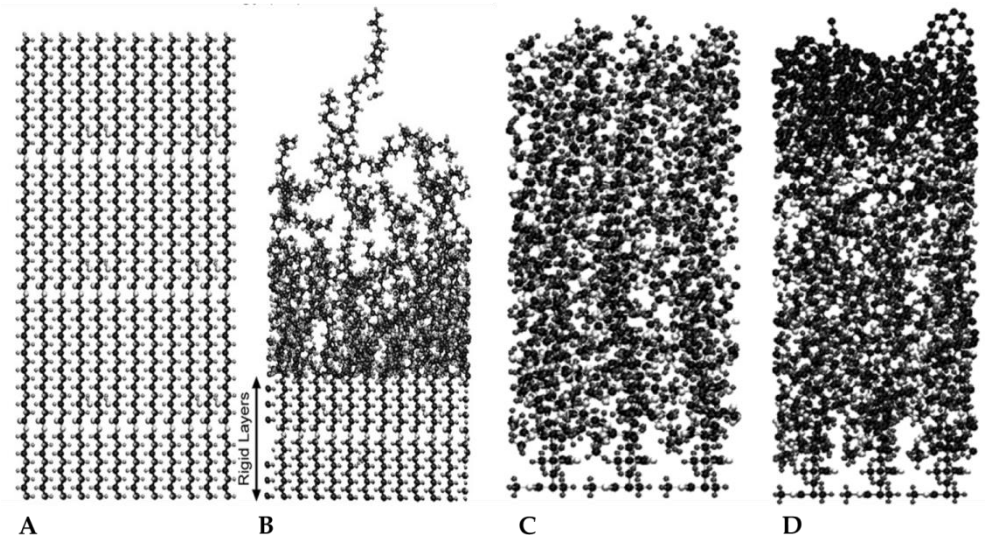

Figure 4.1.1:Molecular Dynamic simulation. A. Lipid-like surface (Black – C, Grey – H, White – O). B. Lipid-like surface after bombardment by argon ions [4]. C. Virgin polymethylmethacrylate (composed of C - Black, H - Grey and O – White) D. Polymethylmethacrylate after bombardment by argon ions (Damaged, carbon rich layer is formed on surface) [9].

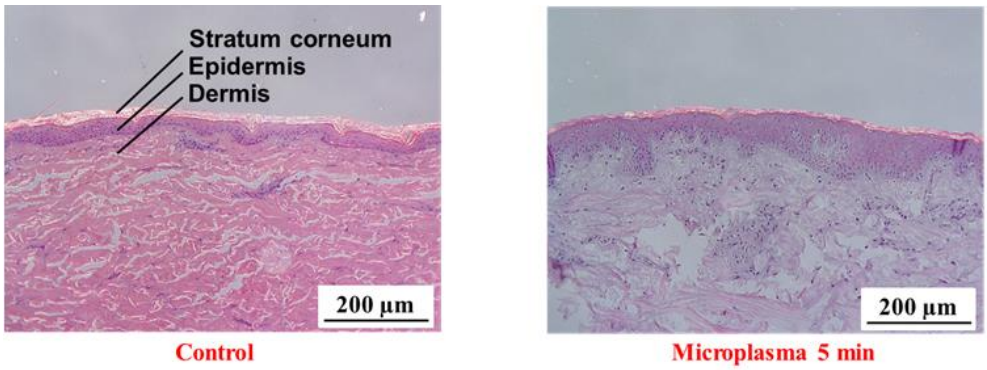

Figure 4.1.2: Cross section of pig skin before atmospheric plasma irradiation, the stratum corneum thickness: 18.09 ± 1.64 µm (left – control), and after atmospheric plasma irradiation (right), the stratum corneum thickness: 13.40 ± 1.46 [10, 7].

4.1.1.2 Helium bombardment/Helium plasma

Helium is an inert gas with light atomic mass, which means that sputtering of any surface is lower in comparison with argon. All atoms in the lipid matrix of the stratum corneum are heavier than helium, so atoms are sputtered mostly by the first mechanism described in the introduction of the section 4.1.1. Investigation of sputtering of polymers by high energy (1 keV) He and Ar ions demonstrated that light atoms such as hydrogen are sputtered at first, followed by heavier carbon and oxygen [11]. On the other hand, the penetration depth increases with decreasing atomic mass, which means that an atomic mass of helium allows penetration deeper inside the surface than argon [12]. However, helium plasma treatment of crystalline carbon with low energy ions (ion temperature ~0.1 eV) demonstrated mass loss and disorder in carbon structure [13]. Helium plasma treated polycarbonate containing C, O, H atoms did not change the number of C and O atoms, but a change of structure by breaking carbonate groups was observed [14]. Helium is effective in increasing oxygen and also nitrogen functional groups coming from the surrounding atmospheric air [8].

4.1.2 Chemical sputtering

Unlike physical sputtering, chemical sputtering (sometimes known as reactive etching) has no or a very low threshold. Chemical sputtering varies strongly with surface temperature and it is highly selective depending on the target/impinging particle combination. The impinging particle also involves neutral reactive species which help to increase the number of sputtered atoms. Eroded species consist of molecules involving impinging atoms and target. The number of sputtered atoms increases by decreasing the energy of bonds and also by decreasing the molecular weights of the atoms in the molecule. The rate of reactions on the

surface depends on its structure. If the surface is damaged by sputtering, the reaction rate can increase by orders of magnitude. Atoms react with free bonds after ion bombardment. Chemical sputtering is much more effective, sometimes even by 1 or 2 orders.

4.1.2.1 Reactive etching/plasma treatment by gases containing oxygen

The dominant mechanism of sputtering by oxygen plasma discharge is the bombardment of the sample by ions creating vacancies. Oxygen molecules, ozone or radicals react with these defects and form H_2O, CO or CO_2. When an unsaturated bond is created in argon plasma, this bond cannot react with any chemically active species to form a volatile by-product. The only way to form those carbon-carbons unsaturated bonds is to react with others carbons and form a highly cross-linked material. Physical sputtering of hydrocarbon film by argon ions can be increased by a beam of molecular oxygen which leads to chemical sputtering. Molecular oxygen alone cannot sputter the surface, but can be adsorbed. Bombardment induces reactions between adsorbed molecular oxygen and bonds created by Ar^+ bombardment on hydrocarbon film. The sputtered amount of atoms and molecules is proportional to the flux of molecular oxygen and the ratio of O_2/Ar^+. An increase of molecular flux increases the number of adsorbed molecules and the number of chemical reactions on the surface [15]. A similar effect can be achieved in Ar/O_2 plasma discharge, where except molecular oxygen, also other active species such as O_3, radicals O and metastable states $O_2(a)$ and Ar_m are present. Unsaturated bonds created by Ar/O_2 plasma treatment leads to crosslinking and oxidation [16]. Pure oxygen post-discharge treatment of hexatriacontane resulted in a mass decrease, which corresponds to etching, but no chemical modifications were observed [17]. In this case, only long-living particles can interact with hexatriacontane. Wertheimer *et al*. [18] showed that oxygen radicals $O(^3P)$ and metastable $O(^1D)$ alone are not very effective in interacting with a polymer surface with saturated aliphatic carbons. When hexatriacontane was treated in N_2-O_2 discharge, grafting with etching compete to each other. Joubert *et al.* showed that molecular oxygen does not participate in plasma surface reaction when they compared discharges of N_2O plasma and N_2-O_2 plasma with the same concentration of atomic oxygen. They concluded that O_2 only provides oxygen radicals [19].

4.1.2.2 Reactive etching/plasma treatment by gases containing nitrogen

Nitrogen is a very stable molecule and its concentration of atomic radicals is low in comparison with oxygen. On the other hand, nitrogen creates a lot of metastable states. It was

observed that even so, nitrogen states coming from nitrogen discharge can cause chemical sputtering [20]. Bombardment of carbon film by N_2^+ ions with an energy under threshold of physical sputtering demonstrated formation of CN radicals. If these radicals are formed on the surface, it creates HCN and OHCN after reaction with hydrogen and water. If the radical is formed in sublayers, C_2N_2 molecule is created [21]. In the case of nitrogen plasma of hydrocarbon film, we can also observe erosion of the surface and formation CN radicals. However, an admixture of methane can cause deposition of C_xH_y groups. Erosion will compete with deposition and CN, CNH and C_2N_2 groups can be incorporated into the film [22, 23].

4.1.2.3 Reactive etching/plasma treatment by gases containing hydrogen

Hydrogen is the lightest atom, so similar to helium, the sputtering effect of hydrogen ions H^+, H_2^+ and H_3^+ is much lower than by heavy ions. Hydrogen atomic radicals can be formed in discharge which leads to more effective reactive etching. Etching by hydrogen plasma causes incorporation of H and reduction of dangling bonds, unlike oxygen plasma which increases the number of dangling bonds [24]. It was observed that sputtering of the surface with a combination of hydrogen atoms and argon ion enhances sputtering more than their sum. A hydrogen rich surface is easier to etch than a surface with a deficiency of hydrogen or a more crosslinked carbon network, as the hydrogen atoms can react with free carbon bonds after bombardment by Ar^+ ions. The ratio of the flux of hydrogen atoms and Ar^+ ions is crucial for effective etching. It is the most effective at a ratio 400:1. It means that the atomic flux should be several times higher than the ion flux. If the flux ratio is too low most of the ion-induced defects recombine before they can be passivated by incident H [25]. Another way to increase sputtering is using an N_2-H_2 mixture. Ions N^+, NH_2^+, NH_3^+, NH_4^+, N_2H^+ and H_3^+ increase the etching rate to a higher value than N_2 or H_2 plasma alone [26].

4.2 Lipid peroxidation

Lipids in the lipid membrane of the stratum corneum do not have to be etched by ions but radicals created in plasma or secondary created in the stratum corneum can degrade lipids by process called lipid peroxidation. Lipid peroxidation is an oxidative degradation of lipids. The reaction occurs on unsaturated fatty acids. As molecular oxygen is not reactive enough to start oxidation, it must be changed to a more reactive state such as hydroxyl radical (OH), superoxide anion (O_2^-), hydrogen peroxide (H_2O_2), hydroperoxyl radical ($HO_2\cdot$), lipid

peroxyl radical (LOO·), alkoxyl radical (LO·), metastable singlet oxygen (O_2(a)), or iron-oxygen complexes (ferryl-, perferryl radical) [27]. Reactive oxygen species abstract hydrogen atoms from the methylene group and create a lipid radical. The rate of lipid peroxidation exponentially increases with the number of bis-allylic carbons because this bond is the weakest in the molecule with no relation to chain length. After abstraction of hydrogen, the lipid radical can react with molecular atmospheric oxygen and form a lipid peroxyl radical. At a low concentration of atmospheric oxygen, lipids can react with each other in the lipid membrane [27]. The lipid peroxyl radical can abstract hydrogen from another lipid to form lipid radical (L·) which can react with atmospheric oxygen and again to form lipid peroxyl radical (LOO·). Oxidized lipids form more rigid domains. LOOH is more polar than fatty acids; it can disrupt the structure of the lipid membrane.

Superoxide anion radical (O_2-·) reactivity is low in aqueous environments, but it increases in hydrophobic environment.

Hydroperoxyl radical (HO_2·) is much more reactive than superoxide anion radicals. Deprotonation can lead to formation of O_2-· at a pH of 4.8. Weak reactivity of O_2-· allows penetrating deeper in the lipid bilayer than HO_2·. The poor reactivity and relatively long half-life of O_2-· allows it to diffuse more effectively from its generation site to targets such as membrane lipid bilayers than HO_2· or other reactive species.

Hydrogen peroxide (H_2O_2) has limited reactivity, can diffuse to target longer time and has potential to create other reactive short living species near the lipid membrane. Creation of lipid radical can be realized in the presence of iron as a catalyst.

Hydroxyl radical (OH·) reactivity is very high, its lifetime is very short and it can react with any molecule in tissue. It can be created from H_2O_2 by catalysis of iron or ultrasound in water [27]:

$$\text{Fe(II)-complex} + H_2O_2 \rightarrow \text{Fe(III)-complex} + OH^- + OH \quad (1)$$

4.3 Effect of heating on skin barrier

Heating of the skin can increase permeability of stratum corneum [28]. The reasons of improving of transdermal delivery through the skin by increasing temperature are structural changes of stratum corneum lipids. Plasma can raise skin temperature from 30°C to more than

100°C which depends on the irradiated time, power of plasma source or used gas. Structural changes of stratum corneum lipids occur between (20-40)°C, from orthorhombic to hexagonal ordered lipids. These changes can be indicated by CH_2 symmetric stretching frequency with increase 0.5 cm^{-1} in ATR-FTIR spectra or it is possible to observe by CH_2 scissoring mode where transition is revealed by splitting of the scissoring modes to produce a doublet with components at 1473 cm^{-1} and 1463 cm^{-1}. Ordered lipid chains change to disordered chains at around (80-90)°C. But some scientific groups identified more transitions in lipid structure [29]. For example, four phase transitions in temperature ranges (35–42)°C, (65–75)°C, (78–86)°C and (90–115)°C, respectively. Transitions below 75°C are reversible [30]. Between 35°C and 42°C two transitions can occur belonging to solid fluid transition and disruption of lipids covalently linked to corneocites at 37°C and at 40°C to 'orthorhombic to hexagonal' change in structure. But too high a temperature can cause damage to the skin. Thermal conditions that cause burns of the skin are functions of the time and method of how the skin is exposed to the heat. Longer exposure of skin to a temperature higher than 43 °C can lead to the formation of blisters [31]. It was found out that fast heating of skin can increase skin permeability without damaging deeper tissues. Investigation of high temperatures up to 315°C applied to skin for 100 ms, 1 s and 5 s showed small variations between drug deliveries of calcein [32]. Exposure for 1 s or 5 s should be sufficient to equalize temperature in the full thickness of skin, but the 100 ms exposure should have influence only on straum corneum. Between (100-150)°C, permeability of skin was increased a few fold. This increase was attributed to lipid melting in the stratum corneum. In the range 150°C to 250°C, transdermal flux increased by two orders, attributable to disruption of stratum corneum keratin network structure. Above 300°C, transdermal flux increased three orders, attributable to decomposition and vaporization of the stratum corneum [32].

4.4 Effect of UV radiation on skin barrier

The wavelength range of 100-400 nm is called UV light, and is usually divided into three ranges; UVA (320-400nm), UVB (280-320nm) and UVC (100-280) nm. UV light can cause damage to skin. It is well-known that atmospheric plasma can generate wide range of UV light dependent on the used gas [33, 34]. UVC radiation can reach only stratum corneum and it consists of emission of excited NO molecule (200-280 nm – NO-gama system) or nitrogen molecule (120-200 nm - LBH system) in plasma discharges. The source of UVB radiation is the emission of OH and nitrogen (2^{nd} positive system of nitrogen). UVA is

composed mostly of 2nd positive system of nitrogen. UVA and UVB can reach deeper layers of skin like epidermis and UVA also dermis. UV radiation can cause formation of hydroxides and epoxides, hydrogenation of double bonds and breaking of carbon chains. The effect of UV on lipids depends on their structure, and only double bonds of fatty acids are sensitive to the formation oxygenated molecules by oxygen in the air. These changes can be amplified or weakened by surrounding atmosphere around treated skin. When lipids of stratum corneum like cholesterol, cholesterol sulphate, ceramide III, linolenic acid, and Dipalmitoylphosphatidylcholine were irradiated by UV light up to 240 min, peroxidative changes occurred only in lipids with double bonds such as cholesterol and linolenic acid [35]. However, the changes are not permanent and the order of stratum corneum lipids and water-loss protection can recover after three days and it return to its initial state thanks to repair processes in the skin [36]. Reactive oxygen species like superoxide anion radicals, singlet oxygen, hydrogen peroxide, and hydroxyl radical can be created by UV light. For example, superoxide anion radicals are precursors to other oxygen reactive species, and it was found that there exists a correlation between the superoxide anion radical's concentration and the degree of oxidation of lipids [37]. UV light is also used for treatment of some skin diseases, but delivered doses have to be controlled and maintained in safety level to not penetrate to deeper layers of skin [38].

4.5 Acidifying effect of plasma on skin

Acidifying effect was observed after applying plasma to stripped lipids from stratum corneum. A higher decrease of pH was observed in discharges, which produced a higher amount of NO_x species. The same effect was observed on human skin, but after 30 minutes after plasma treatment, the pH of skin return to initial value [39]. The decrease of pH depends on parameters of the plasma discharge and the treatment time. Nitrates formed in water droplets could form nitric acid. NOx species could adhere on lipid surface or deposited nitric acid on the film surfaces by gaseous HNO_3 [40]. The recovery of pH in the post-plasma phase was attributed to the decrease of acidifying agents on the substrate surfaces by both diffusion and desorption processes.

4.6 Skin etching and skin damage by plasma

The etching effect of plasma is demonstrated in Figure 4.6.1 by a cross section of the skin. The stratum corneum layer (the white part in (a) control sample) was removed after 20

tape stripping cycles, as shown in (b). After 30 seconds of atmospheric plasma jet irradiation, most of the stratum corneum layer was removed, as shown in (c). In the microplasma case, even after 5 min irradiation (d), the stratum corneum layer remained similar to the control sample (a) [7]. Little difference in physical appearance was observed between the control pig skin sample and after microplasma irradiation. For the tape stripping test, surface asperity was decreased and after 10 s of atmospheric plasma jet irradiation, small pores (ranging from 40 to 100 μm) were observed. Physical damages on skin could be considered to arise from the electric field or an etching effect from bombardment with charged particles [41].

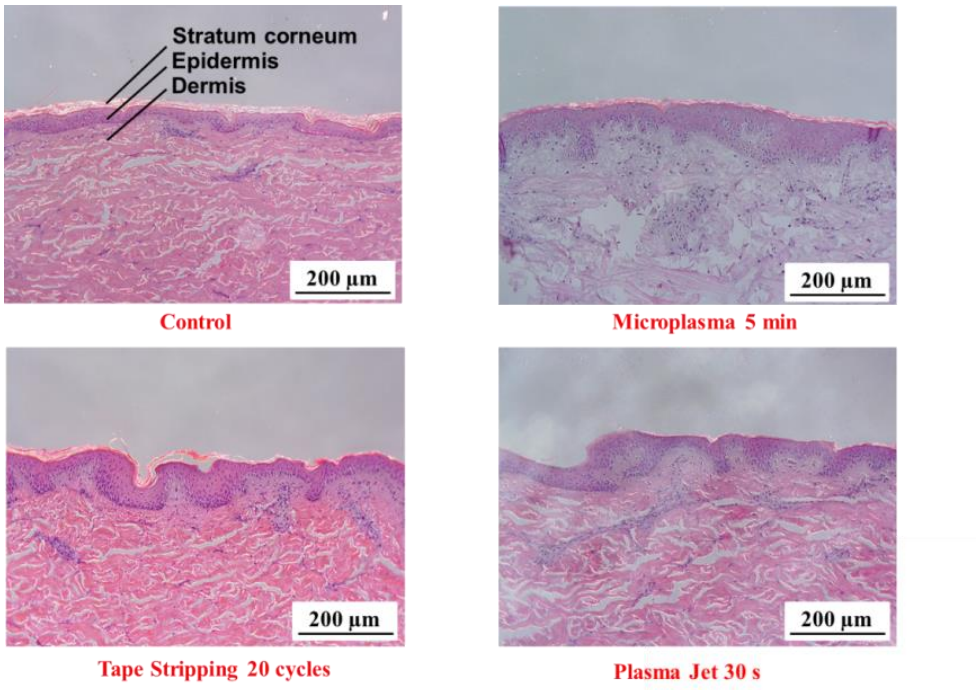

Figure 4.6.1: Cross section of pig skin after atmospheric plasma irradiation, and tape stripping test. (a) control sample, stratum corneum thickness: 18.09 ± 1.64 μm; (b) tape stripping test - 20 times, stratum corneum thickness: 5.99 ± 1.24; (c) plasma jet - 30 seconds, stratum corneum thickness: 3.49 ± 0.61; (d) microplasma - 5 min, stratum corneum thickness: 13.40 ± 1.46 [7].

Surface potential can lead to a strong electric field across the skin and finally penetrate the skin to form holes. Holes were confirmed after longer operation (3 to 5 min) of atmospheric plasma jet irradiation. Pores and holes are shown in Figure 4.6.2 after 10 s and 30 s of operation of the plasma jet.

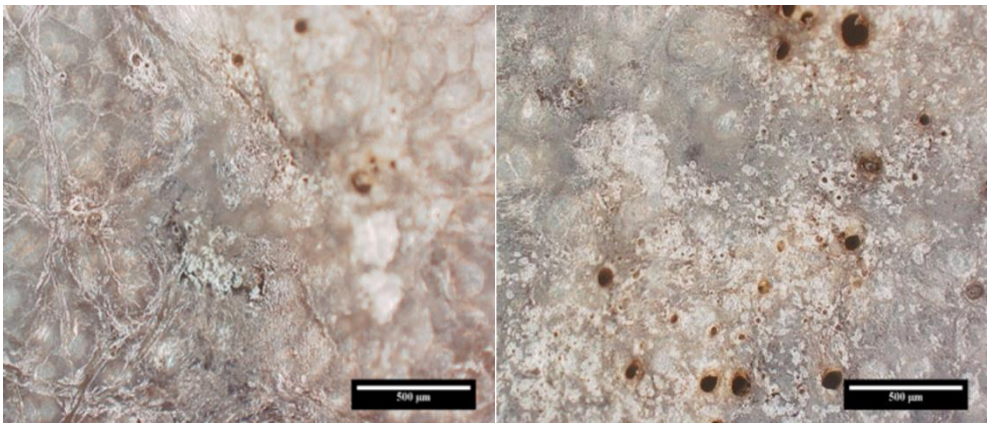

Figure 4.6.2: Left: 10 seconds of treatment by plasma jet; Right: 30 seconds of treatment by plasma jet [7].

This physical damage could affect the barrier function of skin samples. When the effect of plasma jet was tested on PEN film, after 10 s of plasma jet irradiation, the surface potential increased to about 10% of the driven voltage. After long-term operation, it reached almost the same value as the driven voltage [7]. A similar problem could happen in electroporation, but it uses very short operation times in the range of microseconds or milliseconds. High surface potential can induce current flow through the skin, it will increase the skin temperature and might affect cells of skin and cause thermal damage of skin [42]. On the contrary, the surface potential remained low in the microplasma case. The thickness of stratum corneum after 30 s of treatment of plasma jet is equivalent to 20 times of striping by tape.

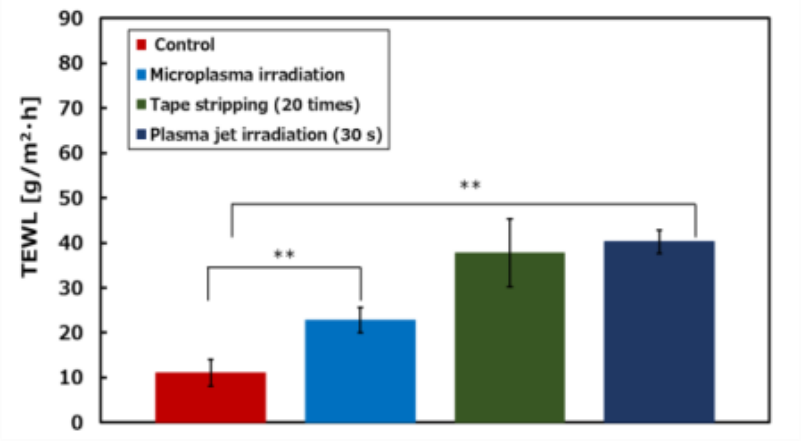

Figure 4.6.3: Variations of TEWL values before and after microplasma irradiation, tape striping test and plasma jet irradiation [7].

This is also confirmed by TEWL (TransEpidermal Water Loss) (Figure 4.6.3) which shows also the same values. On the other hand, TEWL after 5 min of microplasma irradiation of the pig skin sample, TEWL increased to almost double its original value, suggesting that the barrier properties were decreased through atmospheric microplasma irradiation, but it is less effective than plasma jet [7].

References

[1] Yan C., Zhang Q. Y., AIP Advances., 2, 032107 (2012).
[2] Bashir M., Rees J. M., Bashir S., Zimmerman W. B., Physics Letters A. 378(32–33), 2395 (2014).
[3] Zinner M., Spoden P., Kraemer T, Birkl G., Ertmer W.. Physical Review A., 67, 010501 (2003).
[4] Babaeva N. Y., Ning N., Graves D. B., Kushner M. J., J. Phys. D: Appl. Phys. 45, 115203 (2012).
[5] Pignataro B., Fragal M.E., Puglisi O., Nucl. Instr. and Meth. in Phys. Res. B. 131, 141 (1997).
[6] Bachman B. J. and Vasile M. J., J. Vac. Sci. Technol. A. 7(4), 2709 (1989).
[7] Shimizu K, Hayashida K and Blajan M. , Biointerphases 10, 029517 (2015).
[8] Van Deynse A., Morent R., De Geyter N.. Surface modification of polymers using at-mospheric pressure cold plasma technology. In: Méndez-Vilas A. and Solano A., editors. Polymer science: research advances, practical applications and educational aspects. Formatex Research Center; 2016. p. 506-516.
[9] Choudhary G. K., Vegh J. J., Graves D. B., J. Phys. D: Appl. Phys. 42, 242001 (2009).
[10] Shimizu K., Kristof J.. Enhancement of Percutaneous Absorption on Skin by Plasma Drug Delivery Method. In: Maiti S., Sen K. K., editors. Advanced technology for delivering therapeutics. InTech; 2017. p. 111.
[11] Rzeznik L., Fleming Y., Tom Wirtz T., Philipp P., Beilstein J. Nanotechnol. 7, 1113 (2016).
[12] Livengood R., Tan S., Greenzweig Y., Notte J., McVey S.. Subsurface damage from helium ions as a function of dose, beam energy, and dose. J. Vac. Sci. Technol. B. 27(6), 3244 (2009).
[13] Kim H. S., Noh S. J., Kweon J. J., Lee Ch. E. Journal of the Korean Physical Society 63(7), 1422 (2013).
[14] Bergeron A., Klemberg-Sapieha J. E., Martinu L., J. Vac. Sci. Technol. A. 16(6), 3227 (1998).
[15] Hopf C., Schluter M., Jacob W., Appl. Phys. Lett. 90, 224106 (2007).
[16] Murillo R., Poncin-Epaillard F., Segui Y., Eur. Phys. J. Appl. Phys. 37, 299 (2007).
[17] Hody V., Belmonte T., Czerwiec T., Henrion G., Thiebaut J.M., Thin Solid Films. 212, 506 (2006).
[18] Wertheimer M.R., Fozza A.C., Hollander A.. Nucl. Instrum. Methods, Phys. Res., B Beam Interact. Mater. Atoms 151 ,65 (1999).
[19] Joubert O., Pelletier J., and Arnal. Y., J. Appl. Phys. 65(12), 5096 (1989).
[20] Vázquez L., Buijnsters J. G., J. Appl. Phys. 106(3), 033504 (2009).
[21] Hammer P., Gissler W., Diamond and Related Materials. 5(10), 1152 (1996).
[22] Hong J., Granier A., Goullet A., Turban G., Diamond and Related Materials. 9(3-6), 573 (2000).
[23] Hong J., Turban G., Diamond and Related Materials 8(2-5), 572 (1999).
[24] Yun D. Y., Choi W. S., Park Y. S., Hong B.. Applied Surface Science 254, 7925 (2008).
[25] Hopf C., von Keudell A., Jacob W., Nucl. Fusion 42, L27 (2002).
[26] Voitsenya V.S., Masuzaki S., Motojima O., Sagara A., Jacob W., Problems of Atomic Science and Technology. Series: Plasma Physics 6(12), 141 (2006).
[27] Min B., Ahn D.U., Food Sci. Biotechnol. 14(1), 152 (2005).
[28] Petersen K K, Rousing M L, Jensen C, Arendt-Nielsen L, Gazerani P., Int J Physiol Pathophysiol Pharmacol. 3, 236 (2011).
[29] Mendelsohn R, Flach C R, and Moore D J., BBA-Biomembranes 1758, 923 (2006).
[30] Wood D G, Brown M B, Jones S A., European Journal of Pharmaceutics and Biopharmaceutics 81, 642 (2012).
[31] Hao J, Ghosh P, Li S K, Newman B, Kasting G B, Raney S G. Expert Opinion on Drug Delivery 13, 755 (2016).
[32] Park J-H, Lee J-W, Kim Y-Ch, Prausnitz M R., Int J Pharm. 359, 94 (2008).
[33] Yu L, Laux Ch O, Packan D M, and Kruger Ch H., J. Appl. Phys. 91, 2678 (2002).
[34] Sewraj N, Merbahi N, Gardou J P, Rodriguez Akerreta P and Marchal F., J. Phys. D: Appl. Phys. 44, 145201 (2011).
[35] Trommer, M. Plätzer, R. Wolf, R.H.H. Neubert, Skin Pharmacol Appl Skin Physiol 16, 291 (2003).
[36] Merle C, Laugel C and Baillet-Guffroy A., Photochem Photobiol 86, 553 (2010).
[37] Kaneko T, Kaise Ch, Kimoto Y, Suzuki S, Kondo T, Yuasa M., J Oleo Sci. 60, 647 (2011).
[38] Lademann J, Richter H, Alborova H, Humme D, Patzelt A, Kramer A, Weltmann K D, Hartmann B, Ottomann Ch, Fluhr J W, Hinz P, Hübner G, Lademann O., J Biomed Opt. 14, 054025 (2009).
[39] Hirschberg J, Gerhard C, Braun A, Grottker S, Krupp A, Emmert S and Viöl W. Open Journal of Applied Sciences. 5, 40 (2015).
[40] Helmke A, Hoffmeister D, Mertens N, Emmert S, Schuette J and Vioel W., New J. Phys. 11, 115025 (2009).
[41] Babaeva N Yu, Ning N, Graves D B, Kushner M J., J. Phys. D: Appl. Phys. 45, 115203 (2012).
[42] Martin G T, Pliquett U F, Weaver J C., Bioelectrochemistry 57, 55 (2002).

5 Experimental techniques and methods

There are wide varieties of methods available for analyzing skin structure and other properties including its barrier function, such as Raman spectroscopy [1], X-ray diffraction [2], electron diffraction [3] and transmission electron microscopy [4]. Barrier properties of the stratum corneum can be confirmed by the TEWL test, which indicates water evaporation from the inner body through skin [5]. ATR-FTIR spectra can give us information about hydration of skin [6], structure of proteins [7] and lipids [8] and about their changes during skin treatment by chemical or other drug enhancers [9, 10]. There are several vibrational bands associated with chemical functional groups. Vibrational bands at 2850 cm^{-1} and 2920 cm^{-1} belong to CH_2 symmetric and asymmetric stretching modes, respectively [11]. The absorbance of the spectrum decreases as the thickness of the skin decreases and the wavenumber indicates a change in chain conformation, especially a change in peak shape [8]. This chapter will describe techniques used in the thesis.

5.1 Optical emission spectroscopy

When we want to observe emission spectra of molecules or atoms, we have to get these particles to the excited states. We can observe this phenomenon in the plasma, where the particles are excited by electron collisions. Particles returning to the lower state emit light which can be recorded by an emission spectrometer. The spectrum of the plasma of two-atomic molecules is much richer than spectrum of atomic gases. Two-atomic molecule stores energy except in electronic states in translational movement and also in rotational and vibrational movements. Values of these energies can be ordered as:

$$E_e >> E_v >> E_r \tag{2}$$

where E_e is the electronic energy, E_v is the vibrational energy and E_r is the rotational energy.

Rotational spectrum

If we imagine a molecule as a rotor with constant distance between atoms, we can write for rotational energy:

$$E_r = \frac{h^2 J(J+1)}{8\pi^2 I} = BJ(J+1), \tag{3}$$

where J is the rotational quantum number with values 0, 1, 2 ... and I is the moment of inertia of the molecule.

Vibrational spectrum

Two atoms of a molecule can also vibrate. The vibrational movement can be described by equation:

$$E_v = h\nu_{osc}(v + \frac{1}{2}) = hc\omega(v + \frac{1}{2}), \quad (4)$$

where v_{osc} is the frequency of vibration and v is the vibrational quantum number with values 0, 1, 2 ... . This model is very simple and can be more precise by adding other elements to the formula. If the energy of the vibration is higher than a certain energy, the molecule will dissociate.

Ro-vibrational spectra

Rotational spectrum is composed of a lot of emission lines. This is the reason why these lines are very often overlapped and they create together a vibrational band. The shape of the vibrational band depends very often on the temperature of the plasma.

Emission spectrometer

Emission spectra of discharges were measured by Echelle spectrometer. Echelle spectrometer has two dispersion elements. The principle of this spectrometer is based on Echelle grating used under high angle in such a way that diffraction occurs in higher orders which are overlapped. Separation of the diffraction orders is realized by prism which disperses light in perpendicular direction to the dispersion of grating. The principle is described by Figure 5.1.1 that allows to record the spectrum of whole range in one moment. Echelle spectrometer Mechelle 5000 has resolution $\lambda/\Delta\lambda$ = 5000, what means that at entrance slit size of 50 μm FWHM = 0.04 nm at 200 nm and FWHM = 0.1 nm at 500 nm. Wavelength range is 200 – 975 nm.

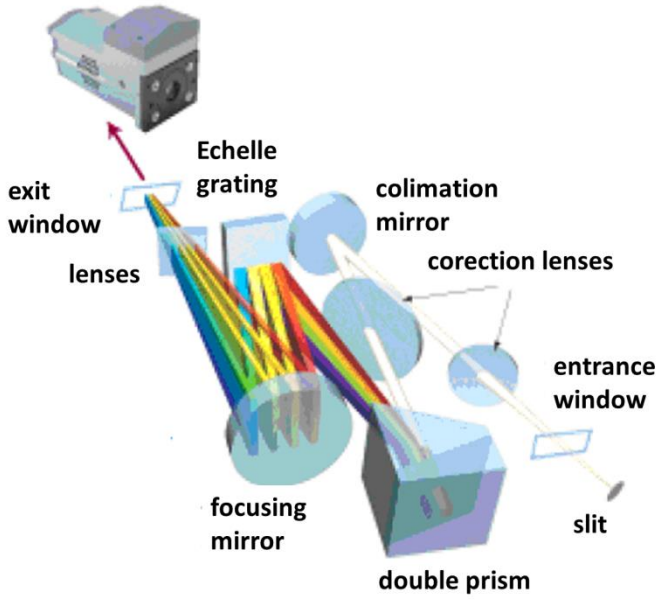

Figure 5.1.1: Spectrometer Mechelle 5000 – principle of working.

5.2 Absorption spectroscopy

In absorption spectroscopy, a photon is absorbed by an electron which is excited to the higher level according the to photon energy. As in emission spectroscopy, we can get ro-vibrational spectra also in absorption spectroscopy. Light is absorbed by a sample according Beer-Lambert law:

$$\boldsymbol{ln\frac{I_0}{I_T} = \varepsilon cl = A}, \qquad (5)$$

where c is the concentration of absorbing particles, l is the length of the absorbing medium, ε is the extinction coefficient and A is the absorbance. A simple design of the absorption spectrometer is depicted in Figure 5.2.1.

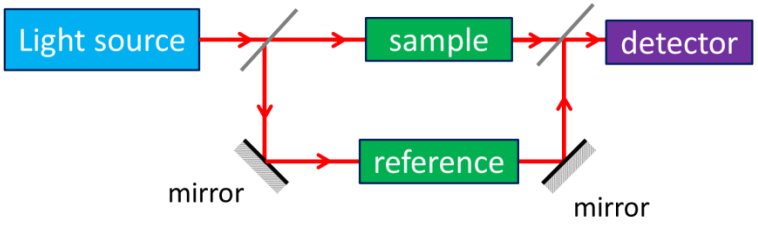

Figure 5.2.1: Principle of absorption pectrocopy.

The light source of the absorption spectrometer is usually tungsten or deuterium lamp. They have continuous emission from ca. 190 nm – 400 nm (deuterium lamp) and from 220

nm – more than 3000 nm (tungsten lamp). The absorption spectrometer compares a reference beam I_0 with the beam going through the sample (I_T). The advantage of absorbance is proportionality to concentration of elements of our interest. The disadvantage is that spectra gained by the method in Figure 5.2.1 are very broad and overlapped with various molecules in sample and it makes analysis difficult. Among more advanced absorption spectroscopies are FTIR spectroscopy, Raman spectroscopy or HPLC.

5.3 FTIR spectroscopy

Fourier-transform infrared (FTIR) spectroscopy is absorption infrared spectroscopy of liquid, solids or gases. The main part of the spectrometer is a Michelson's interferometer depicted in Figure 5.3.1. The light beam from the source is sent through the beam splitter. The first beam is reflected to the stationary mirror and reflected back through the beam splitter and sample to the detector. The second beam goes through the beam splitter to the moving mirror and beam is reflected back and after reflection on beam splitter goes through the sample to the detector. Moving mirror makes total path length variable in comparison with stationary mirror. Beams going toward sample interfere. This interferogram is recorded by the detector as energy versus time. The mathematical conversion from time spectrum to frequency spectrum is called Fourier transformation.

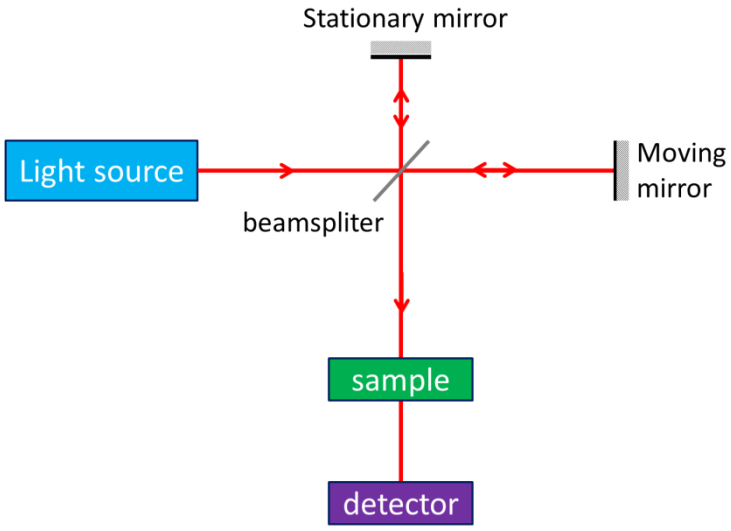

Figure 5.3.1: Principle of Fourier transform spectroscopy.

If solid or liquid samples are necessary to analyze, Fourier-Transform InfraRed-Attenuated Total Reflectance (FTIR-ATR) spectroscopy is used.

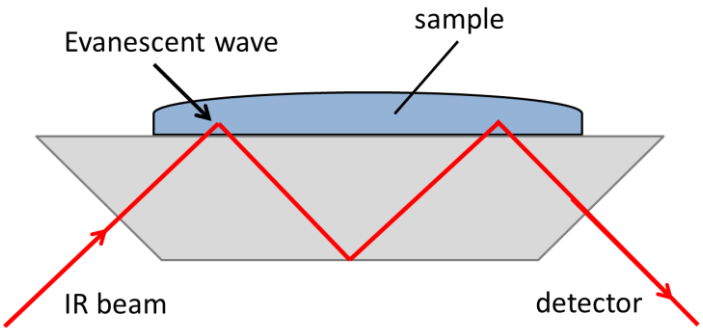

Figure 5.3.2: Principle of FTIR-ATR spectroscopy.

FTIR-ATR measures spectra after total reflection of infrared beam which came into contact with a sample (Figure 5.3.2). Reflectance of the beam on surface of crystal creates evanescent wave which is extended into the sample. The sample has to be in contact with the crystal and this wave can enter 0.5-5 μm into the sample. In regions of the infrared spectrum where the sample absorbs energy, the evanescent wave will be attenuated or altered. Refractive signal of crystal has to be significantly greater than refractive signal of the sample. Diamond crystal is very often used, with the refractive index 2.4 at 850 nm [12].

The intensity of the evanescent wave is

$$\boldsymbol{I_{ev} = I_0 exp\left(-z/d_p\right)}, \tag{6}$$

where z is the distance from the normal of optical interface of evanescent wave, d_p is the penetration depth of the wave and I_0 is the intensity at $z = 0$.

The penetration depth is given by formula:

$$\boldsymbol{d_p = \frac{\lambda}{2\pi n_c \sqrt{sin^2\theta - \left(n_s/n_c\right)^2}}}, \tag{7}$$

where λ is the wavelength if infrared beam, n_s is the refractive index of the sample, n_c is the refractive index of the crystal and θ is the angle of reflection of the evanescent wave. Two important factors for infrared absorption are the absorption wavenumber and the molecular dipole moment. Infrared absorption is active if molecular vibration change dipole moment of molecule and frequency of infrared radiation from source is equal to the frequency of molecular vibration. Dipole moments of uncharged molecules derive from partial charges on the atoms, which can be determined from molecular orbital calculations. As a simple approximation, the partial charges can be estimated by comparison of the electronegativity of the atoms.

5.4 Principal component analysis

Principal component analysis is a mathematical method that helps us to find relationships between samples and their parameters. Such methods create new variables called "principal components". They are created in directions of the highest variability of parameters of our samples. Data are put into a matrix where Y- values are parameters and X- values are different samples. PC1 – the first principal component is in direction of the highest variability data. PC2 – the second principal component is also in direction of the highest variability but perpendicular to PC1 (Figure 5.4.1). PC3 – the third principal component is in direction of the highest variability but perpendicular to PC1 and PC2, and so on. Principal component analysis helps us to describe matrix of our data by principal components and decrease the dimension of our problem. The main results are "score plot" and "loading plot" (Figure 5.4.2). The score plot is a summary of the relationship among samples. If points are close to each other, it means that they have similar behavior. The loading plot represents the parameters – interpretation of patterns seen in the score plot. If points in the loading plot are close to each other, it means that parameters have similar behavior.

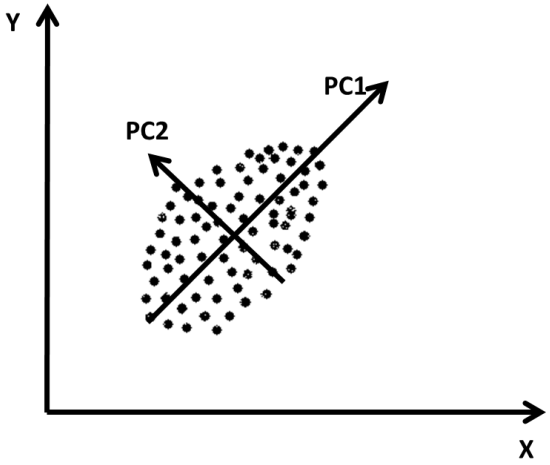

Figure 5.4.1: Principal component PC1 and PC2 show direction of the highest variability.

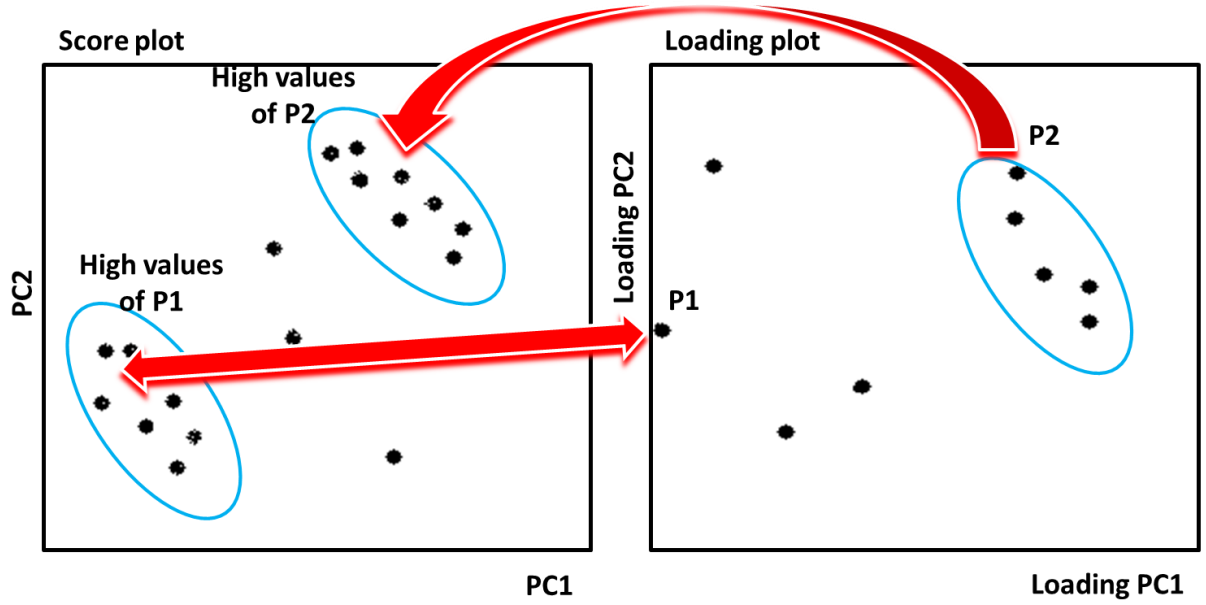

Figure 5.4.2: Example of Score plot and Loading plot.

5.5 High performance liquid chromatography

High performance liquid chromatography (HPLC) is an analytical chemical method used for separation of mixed compounds.

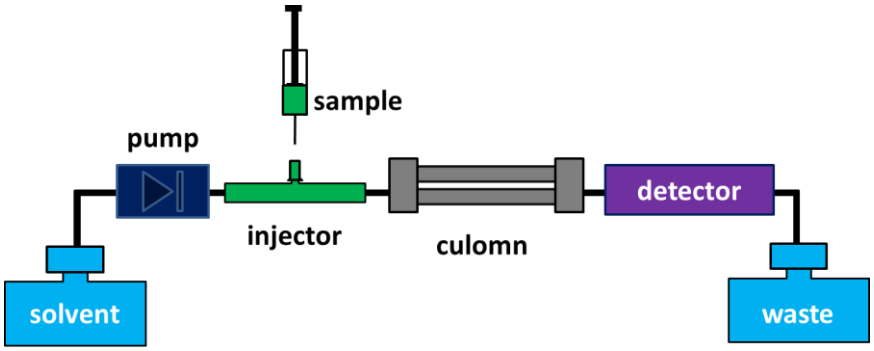

Figure 5.5.1: Set-up of HPLC.

Solvent creates mobile phase by pumping it to the system under high pressure of several atmospheres. A sample is mixed with the solvent in the injector. The column is in a stationary phase. The sample is carried by mobile phase to the column. When the column is reached, the sample leaves the mobile phase and enters to the stationary phase. Various components of mixture are separated in the column and detected by measurement of absorption of molecules and then the liquid will go to the waste (Figure 5.5.1).

The most usual HPLC is so-called “reverse phase” HPLC. In the reversed phase HPLC, the mobile phase is polar and the stationary phase is non polar (hydrophobic). The column is

composed of silica spherical particles. To make silica non polar, 8 or 18 carbon atoms are added to one spherical silica sphere. Non polar molecules adsorb on the silica surface and pass slow through the column. However, polar molecules will pass more quickly and it is also how separation occurs. Other parameters such as column temperature, concentration of chemicals in mobile phase or flow rate can increase or decrease separation. Separation is characterized by a retention time, what is the time while the sample goes from injection to the detector. The spectrum measured by detector is called chromatograph when absorbance is function of time.

At beginning of the chromatogram, we can find some peaks created by mobile phase and particles which do not interact with column. The time while these peaks appears is called "dead time" and the corresponding volume ("dead volume") is the volume of mobile phase inside of the column. Dead volume V_m can be estimated as

$$\boldsymbol{V_m \approx 0.5 L d_c^2 / 1000}, \tag{8}$$

where V_m is in mm^3, L is the length of column in mm and d_c is the diameter of the column. Dead time is

$$\boldsymbol{t_0 = V_m / F} \tag{9}$$

where F is the flowrate in mm/min [13]. The peak which we want to detect should always appear in chromatogram after dead time t_0.

5.6 X-ray photoelectron spectroscopy

X-ray photoelectron spectroscopy (XPS) is a technique for surface analysis. The investigated sample is irradiated by X-ray photons. If the photon has enough energy, a core electron is emitted (Figure 5.6.1). The energy is analyzed by the spectrometer. The kinetic energy (*EK*) of the electron depends on binding energy (*EB*) of the electron in the atom and energy of photon ($h\upsilon$) according formula:

$$\boldsymbol{EB = h\upsilon - EK - W} \tag{10}$$

where W is the spectrometer work function. If the electron is excited and can escape without energy loss, it contributes to the characteristic peak in the spectrum. Electrons which lose energy, they contribute to the background. Characteristic peaks can help to identify chemical bonds on the surface, as well as the concentration of elements.

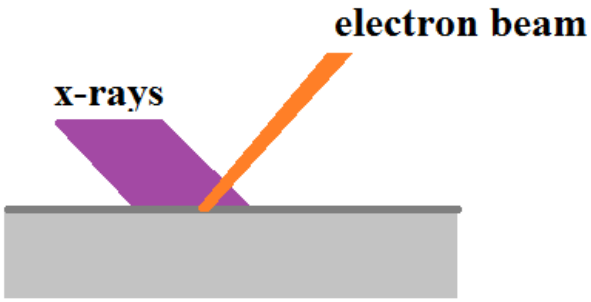

Figure 5.6.1: Principle of XPS spectroscopy.

Due to charging of samples which are insulators, XPS spectra can be shifted. Usually, position of peaks in spectrum is calibrated by carbon peak at 285 eV. During calibration, all peaks are shifted to the same direction by the same value in such a way that carbon peak will appear at 285 eV. Typical chemical characteristic peaks for organic materials are in Table 1.

Table 1: Positions of characteristic peaks of molecules in organic material.

C 1s	E_{BE} (eV)	O 1s	E_{BE} (eV)	N 1s	E_{BE} (eV)
C=C	284.8	COO-	531.1-531.6	C=N	389.5-399.7
C-C/C-H	285	O=C-OH	531.8-532.5	C-N	399.0-401.1
C-N	285.6-286.4	N-C=O	531.1-532.2	N-C=O	399.0-400.9
C-O	286.1-287.0	C-O	532.4-533.6	$C=NH^+$	401.2-401.9
C=O	287.0-287.9	NO_2	532.5	$C-NH^+$	401.4-402.1
O-C-O	287.8-288.2	O-C-O	532.9-533.6	NO_2	405.4-406
N-C=O	287.8-288.7	O=C-OH	533.0-533.9	ONO_2	408.1
O=C-OH	288.6-289.9				

5.7 Trans-epidermal water loss

Figure 5.7.1: TEWL device with probe.

Moisture inside TEWL probe (Figure 5.7.1) is measured due to evaporation from a surface. The measurement is based on the change of the evaporation rate. The skin is a mechanical barrier which prevents the loss of water. This test expresses the amount of water in grams evaporated per square meter in one hour. The better barrier functions of the skin, the higher water content inside the skin and the lower TEWL value. Measurement of the TEWL is the direct way of barrier function of the skin. Measuring the amount of water evaporating from the skin surface includes not only TEWL, but also the water delivered to the skin by other way such as sweating. This method was used for evaluation of the barrier function of the skin several times [14].

5.8 Contact angle measurement

Attachment of gaseous or liquid molecules on surface is called adsorption. Physical adsorption is the process without energetic activation and it is explained by Van der Waals's force between adsorbent and absorber. Because of Van der Waals's force, atoms or molecules are attached on the solid surface only for a short time. The adsorbed particles leave the surface when the amplitude of vibration of atoms on the surface is high enough. Physical adsorption is effective at low temperatures when the number of adsorbed particles increase.

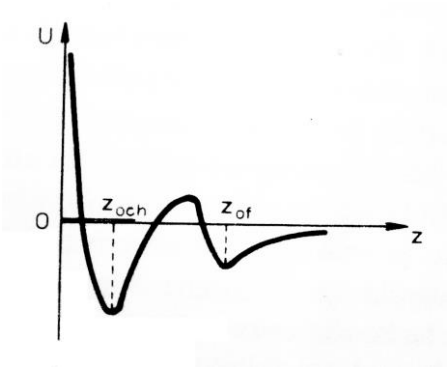

Figure 5.8.1: Potential energy depending on distance of atoms in case of physical adsorption and chemisorption (z_{och} – equilibrium position at chemisorption, z_{of} – equilibrium position at physical adsorption) [15].

Chemisorption can be characterized by stronger bonds than in the case of physical adsorption. The bond has a character of covalent bond. Chemisorbed molecules are in the distance of tens of nanometers. Chemisorption is dominant at high temperatures and very weak at low temperatures. At low temperatures, the number of adsorbed atoms is high. Increasing the temperature decreases number of the adsorbed molecules, but from a certain value of the temperature, the number of adsorbed molecules increases. The ability to adsorb molecules can be characterized by contact angle. The contact angle can be characterized by using θ/2 method using the portable contact angle meter (Kyowa Interface Science Co., Ltd, PCA-1). A droplet of water is put on investigated surface. The contact angle is determined as

$$\boldsymbol{\theta = 2\arctan(h/r)} \qquad (11)$$

where θ, r, and h represent the contact angle, the radius of droplet and the height of the droplet, respectively.

5.9 Skin section and microscopy

A small piece (approximately 15 × 15 mm^2) of the treated skin was cut and fixed in 10% neutral buffered formalin for four days. The formalin solution contains stock of formaldehyde solution (35% CH_2O, 1 L), sodium phosphate monobasic ($NaH_2PO_4 \cdot H_2O$: 44 g), sodium phosphate dibasic anhydrous (Na_2HPO_4, 65 g) and distilled water (9 L). After four days, the skin was dehydrated and embedded into paraffin mold. The paraffin-embedded skin sample was sectioned at a thickness of several micrometers using a microtome and placed on a glass side. In order to visualize the micro-scale change in the stratum corneum, hematoxylin-eosin staining was then performed. The process of preparation samples is described in more details in Table 2.

Table 2: preparation of skin section samples

Process	Realization
Deparaffinization	Clear Plus, 5 min Clear Plus, 5 min Clear Plus, 5 min 99.5% ethanol, 5 min 95% ethanol, 5 min 90% ethanol, 5 min 80% ethanol, 5 min 70% ethanol, 5 min
Dyeing	Water washing, 10 min Hematoxylin, 4 min Water washing, 10 min Eosin, 4 min
Dehydration	90% ethanol, washing few times 95% ethanol, washing few times 99.5% ethanol, washing few times 100% ethanol, washing few times 100% ethanol, washing few times 100% ethanol, 4 min 100% ethanol, 4 min
Penetration	Xylene, 4 min Xylene, 4 min Xylene, 4 min

5.10 Transmission electron microscopy

Optical microscope is not able to resolve very small objects because of the limitation given by the wavelength of the light. Transmission Electron Microscopy (TEM) can resolve smaller details. Electron beam passes through the very thin sample. As the beam interacts with sample, image is created by transmitted electrons. A simplified model of the transmission electron microscope is in Figure 5.10.1.

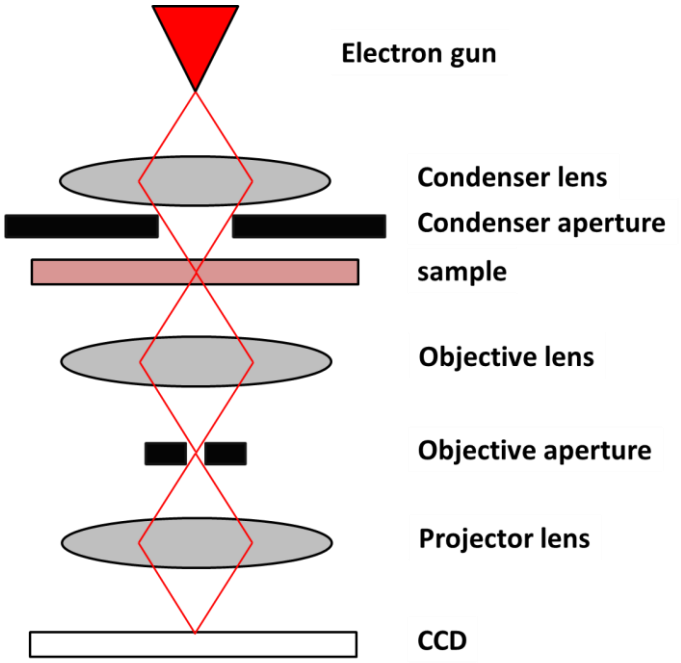

Figure 5.10.1: Model of the Transmission electron microscope.

Electrons are produced by an electron gun and focused to the thin beam by the condenser lens to the sample. The condenser aperture filters the unwanted scattered electrons. The electrons interact with the sample by several ways: elastically scattered electrons, inelastically scattered electrons and unscattered electrons (transmitted). The objective lens focuses transmitted electrons into an image and objective aperture increases the contrast by blocking scattered electrons. The projector length expands the beam on the surface of a phosphor screen which is generating light detected by CCD camera. TEM samples have to be very thin because of the absorption of electrons. In the case of the skin, thickness of several nanometers is realized by ultramicrotome. However, the preparation of the sample is complicated process, as it is seen in Table 3.

Table 3: Process of preparation of the skin sample for TEM.

Process	Realization
Pre-fixation	2% glutaraldehyde (0.1 M phosphate buffer) 4 ° C
Washing	0.1 M phosphate buffer 4 ° C. overnight
Post-fixation	2% osmium solution at 4 ° C for 3 hours
Washing	distilled water 4 ° C. 1.5 hours
Pressing fixation	2% ruthenium tetroxide aqueous solution, 3.6 kg Pressure 4 ° C for 3 hours
Washing	distilled water 4 ° C. overnight
Dehydration	Soaking in sequential high concentration of ethanol (50, 70, 90, 100, 100, 100%) 4 ° C (50% only), rest in room temperature, 15 minutes each
Substitution	Propylene oxide, room temperature 45 min Mixture of propylene oxide + epoxy resin Room temperature 1.5 hours
Embedding	Epoxy resin (EPON 812) is placed in a capsule together with cured epoxy resin and hardened at 60 ° C for 48 hours
Curing agent	Methyl nadic anhydride (MNA)
Curing agent	Dodecenyl Succinic anhydride (DDSA)
Accelerator	Dimethylaminomethyl phenol (DMP-30)
Slicing	Slicing with ultramicrotome
Dyeing	2% uranyl acetate, stain section with lead staining solution
Reinforcement	Carbon deposition (Reinforcement of section relative to electron beam)

5.11 Pharmacokinetics - Two-compartment model

In Figure 5.11.1, the central compartment X_1 represents blood. Cyclosporine A is delivered to blood with flux k_{01} (in μg/h) and it is eliminated from the body at rate constant k_e. The second, peripheral compartment X_2 consists of tissues, bones, skin, etc. Drug exchange between the central and peripheral compartments is controlled by rate constants k_{12} and k_{21}. The process can be described by differential equations, as shown in (12) and (13), where X_1 and X_2 are the amounts of drug in μg:

$$\frac{dX_1}{dt} = k_{01} - k_e X_1 - k_{12} X_1 + k_{21} X_2 , \tag{12}$$

$$\frac{dX_2}{dt} = k_{12} X_1 - k_{21} X_2 . \tag{13}$$

The concentration of Cyclosporine A in blood can be expressed by

$$C_b = \frac{X_1}{V_1} \tag{14}$$

where V_1 is the volume of the central compartment, which usually depends on the weight of the patient. Equations (12) and (13) were calculated by the Runge-Kutta method of 4th order with initial conditions $X_1(t=0)=0$ and $X_2(t=0)=0$. We divided the drug flux into several intervals and we supposed that the flux is constant in these intervals with a value $k_{0i,}$ where i is index of the interval (infusion). At the end of the interval, the infusion was stopped. Infusion and oral drug delivery were compared with transdermal delivery. In the case of oral delivery, k_{0i} was replaced by $F \cdot Dose \cdot k_a \cdot e^{-k_a t}$, where F is the bioavailability of the drug, and k_a is the absorption constant of the gastro-intestine tract.

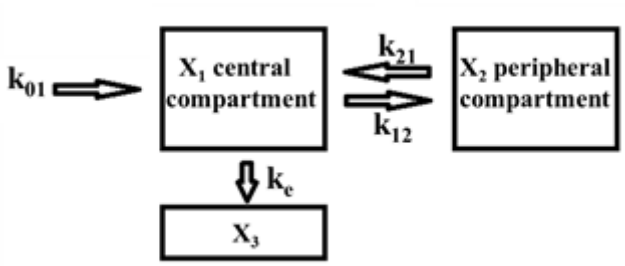

Figure 5.11.1: Two-compartment model.

References

[1] Caspers P J, Lucassen G W, Wolthuis R, Bruining H A, and Puppels G J., Biospectroscopy 4, S31 (1998).
[2] Bouwstra J A, Gooris G S, Weerheim A, Kempenaar J, and Ponec M., J. Lipid Res. 36, 496 (1995).
[3] Nakazawa H, Imai T, Hatta I, Sakai S, Inoue S, and Kato S., BBA-Biomembranes 1828, 1424 (2013).
[4] Honeywell-Nguyen P L, de Graaff A M, Groenink H W, Bouwstra J A., Biochim Biophys Acta 1573, 140 (2002).
[5] Ya-Xian Z, Suetake T and Tagami H., Arch. Dermatol. Res. 291, 555 (1999).
[6] Lucassen G W;van Veen G N A;J. Jansen A J., J. Biomed. Opt. 3, 267 (1998).
[7] Karande P, Jain A, Ergun K, Kispersky V, Mitragotri S., Proc Natl Acad Sci U S A. 102, 4688 (2005).
[8] Boncheva M, Damien F, Normand V., Biochim Biophys Acta 1778, 1344 (2008).
[9] Zhang D, Wang H-J, Cui X-M, Wang Ch-X., Evaluations of imidazolium ionic liquids as novel skin permeation enhancers for drug transdermal delivery. Pharm Dev Technol. 2016;DOI: 10.3109/10837450.2015.1131718
[10] Balázs B, Sipos P, Danciu C, Avram S, Soica C, Dehelean C, Varju G, Erős G, Budai-Szűcs M, Berkó S, Csányi E., Biomedical Optics Express 7:67 (2016).
[11] Mendelsohn R, Flach C R, and Moore D J., BBA-Biomembranes 1758, 923 (2006).
[12] H. R. Phillip and E. A. Taft. Kramers-Kronig Analysis of Reflectance Data for Diamond, Phys. Rev. 136, A1445-A1448 (1964).
[13] J. W. Dolan, LCGC North America 32(1), 24 (2014).
[14] Shimizu K., Tran A. N., Kristof J., Blajan M.. Investigation of atmospheric microplasma for improving skin permeability. In: Proceedings of the 2016 Electrostatics Joint Conference; 13-18 June; Lafayette, USA. 2016. p. I4.
[15] Lukáč P., Martišovitš V.: Netesnosti Vákuových Systémov, Alfa Bratislava (1981) 73

6 Results

6.1 Plasma discharges

6.1.1 Plasma Jet

The experimental set-up of plasma jet treatment is shown in Figure 5.11.1. The source of plasma (plasma jet) consists of a Pyrex tube (outer diameter 6 mm, length 100 mm), and a central tungsten (0.8 mm in diameter) high voltage (HV) electrode covered by a glass layer except for a 10-mm long region close to outlet of Pyrex tube. The grounded electrode is an aluminum ring (8 mm wide) located on outer surface of the Pyrex tube, 12 mm from the end of the plasma jet. The electrodes have been coupled by using a Neon transformer (ALPHA Neon M-5) with an AC frequency of 16 kHz. The voltage and current were monitored with a Tektronics P60015A high-voltage probe and a Tektronics P6021 current probe. The distance between the skin sample and the outlet of the plasma jet was usually set to 2 mm via a grounded micrometric sample holder. The sample was isolated from the holder by a 30-mm thick PVC isolator. The treatment time of the sample was set to 1 min, and the sample was in contact with plasma during this time. The gas is introduced into the plasma jet through a Yamato flow meter.

The discharge voltage and discharge current waveforms are shown in Figure 5.11.2. Gas flow of argon was set to 3 L/min by using a flow meter (Yamato). The treatment time of skin was set to 1 minute.

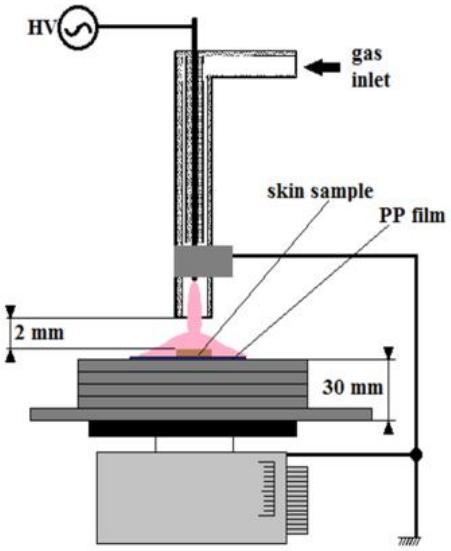

Figure 5.11.1: Experimental set-up of the skin treatment by plasma jet.

6.1.2 Microplasma dielectric barrier discharge

A dielectric barrier discharge was generated by a thin-film electrode with a thickness of 105 μm (Figure 5.11.2b). Both high-voltage and grounded electrodes were encapsulated in the dielectric. The thickness of electrodes was 18 μm separated by a 14 μm thick dielectric. The outer side of each electrode was covered by a dielectric with a thickness of 27.5 μm. Plasma was generated at the surface closer to the grounded electrode. Atmospheric argon plasma was generated at a voltage of 950 V and a frequency of 25 kHz by a Neon transformer (ALPHA Neon M-5, LECIP). The discharge voltage and discharge current waveforms are shown in Figure 5.11.2b. Gas flow of argon was set to 5 L/min by a flow meter (Yamato). The treatment time of skin was set to 5 minutes after the gas flow started. The thickness of the plasma was negligible in comparison with the distance between electrode and skin surface, which was set to 0.5 – 1 mm.

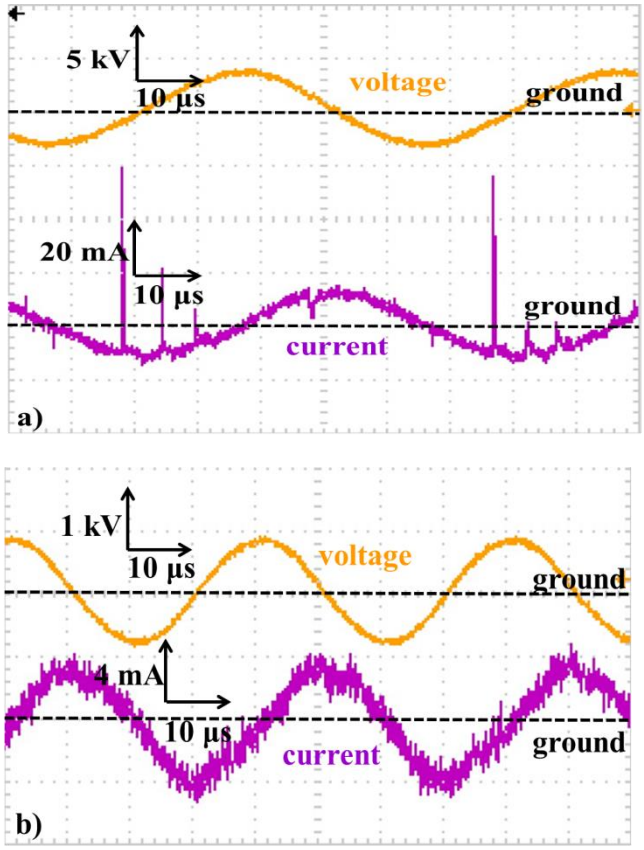

Figure 5.11.2: a) Discharge current (violet) and applied voltage (orange) on electrodes of plasma jet.
b) Discharge current (violet) and applied voltage (orange) on electrodes of microplasma dielectric barrier discharge.

6.1.2.1 Fourier transform infrared spectroscopy of microplasma

Analysis of the composition of gases which are in contact with the pig skin was implemented by the set-up in the Figure 5.11.3. The tube with a diameter of 3 cm and with a length of 10 cm was at the distance of 1 mm from the surface of the electrode. The tube was covered with a plastic shield with 9 holes to allow gas to enter. The other part of the tube was connected to the chamber with the O_2 monitor (OXY-1). At the end of the chamber was a pressure gauge followed by a 509 cm long plastic tube (diameter 0.4 cm) and another pressure gauge. The last pressure gauge was connected to an FTIR (Furrier Transform InfraRed) spectrometer pumped by the oil rotary vacuum pump. The gas flow to the FTIR spectrometer was set to a low value of F = 0.5 – 1 l/min depending on the used gas according to the following formula (15):

$$\boldsymbol{F = \frac{\pi(P1-P2)r^4}{8\eta l}} \qquad (15)$$

where F is the gas flow, $P1$ ($P1$ = atmospheric) is the pressure at the chamber with the O_2 monitor, $P2$ ($P2$ = 99-99.5 kPa) is the pressure at the side of the FTIR spectrometer, l is the length of the tube connecting 2 pressure gauges, r is the radius of the tube and η is the viscosity of the gas. The low gas flow was chosen to have minimal influence on the flow of gases between the electrode and the plastic shield mentioned above.

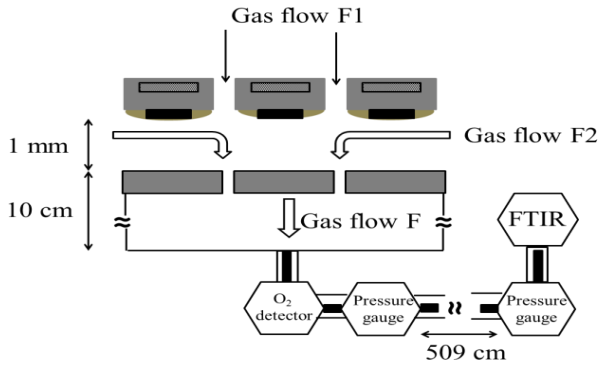

Figure 5.11.3: Experimental set-up for the measuring of the production of long living molecules in microplasma.

Plasma particles production

The O_2 monitor detected an increasing percentage of O_2 with the gas flow $F1$ through the electrode. The higher was gas flow $F1$ the lower could be flow $F2$ from air surrounding electrode. 100 % of the O_2 was detected at the gas flowrate of 5 l/min (Figure 5.11.4). The FTIR spectra showed only the presence of ozone produced by plasma. In the case

of argon and nitrogen, percentage of oxygen was decreasing to 0% at gas flow 5 l/min (Figure 5.11.4). In this case we did not observe a spectrum of any molecule except traces of CO_2. These results would indicate that during skin treatment by the discharge gas, mostly only this gas is present without any admixture of air. The oxygen monitor cannot detect oxygen with concentration lower than 0.1%. The ratio of N_2:O_2 in the atmosphere is 3.73. We concluded that the concentration of air during the treatment of skin in the case of argon, nitrogen or oxygen is less than 0.5%. On the other hand, the air microplasma discharge produced several molecules and we could detect ozone, NO_2, N_2O, CO, CO_2.

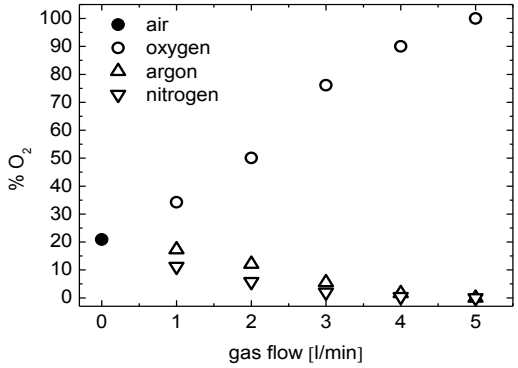

Figure 5.11.4: Evolution of the percentage of oxygen between the sample and the electrode with increasing gas flow F1through the microplasma electrode.

6.1.2.2 Optical emission spectroscopy of plasma discharges

A plasma plume was observed in the air by an optical emission spectrometer placed approximately 2 mm from the end of the plasma nozzle (without any sample). Several argon lines were detected; the emission of these lines should come from excited atoms generated by electron collisions. The emission of these lines induced the presence of electrons; therefore plasma was present near the end of the plasma jet nozzle. Consequently, we hypothesize that the plume of plasma jet could be formed by an electric field generated by the electrodes and the configuration of the plasma jet. In the case of microplasma electrode, the setup in Figure 5.11.5 was used. MgF_2 window was placed 1 mm from electrode. The window simulated skin sample. Signal integrated from the whole surface of the electrode was focused into the fiber.

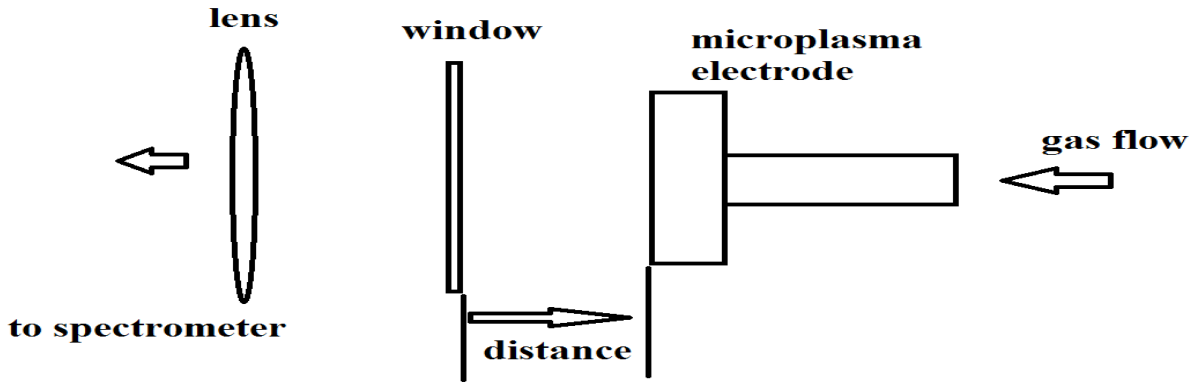

Figure 5.11.5: Set-up for measurement of optical signal from the whole surface of microplasma. All parallel beams are focused to the fiber by lens.

Comparison of emission spectra of plasma jet and microplasma is shown in Figure 5.11.6 and Figure 5.11.7. The emission spectrum of the plasma jet shows higher signal from nitrogen species (2^{nd} positive system in Figure 5.11.6) and oxygen species (atomic emission lines Figure 5.11.7) that can be due to higher amount of air in the discharge. Oxygen emission is almost not present in microplasma. OH emission is comparable in both spectra that come from moisture in the air. It is possible to see only emission from zero vibrational level of nitrogen. This fact indicates a low vibrational temperature. Vibrational temperature expresses ability how reactive species are in discharge. The higher vibrational temperature the easier is to dissociate molecule and create radicals. Simulation of OH(a-X) system in LIFBASE [1] shows vibrational temperature in the range 1300 – 1500 K. It means that 94 – 95 % of molecules in OH(a) state are in vibrational level $v = 0$. Rotational temperature is around 300 K in the case of microplasma and 500 K in the case of plasma jet. Rotational temperature is very often in equilibrium with translation temperature, but it is not always the case of OH(a-X) emission. The temperature of plasma in plasma jet is higher than in microplasma but as we can see in the next section, it does not reach 500 K. The higher rotational temperature of OH(a-X) system can be caused by energy transfer from Ar metastable states.

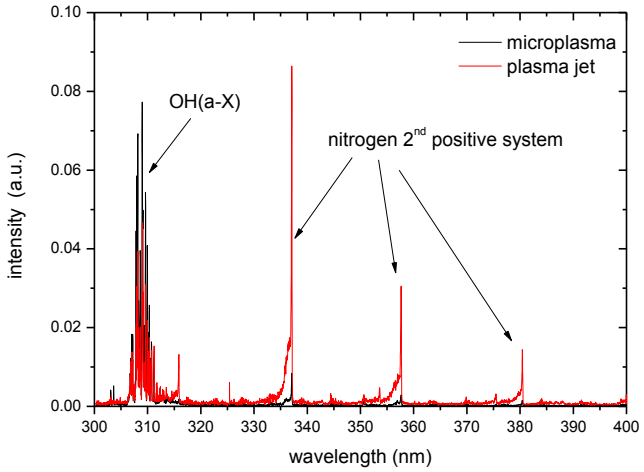

Figure 5.11.6: UV emission of plasma jet and microplasma in Ar gas.

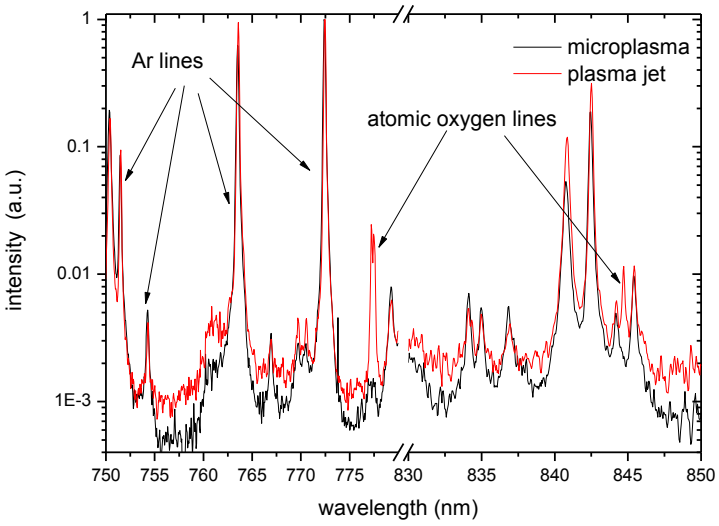

Figure 5.11.7: Visible emission of plasma jet and microplasma in Ar gas.

6.1.3 Temperature effect of the plasma on the skin

Plasma temperatures greater than 45°C can disqualify the plasma source from clinical use because of burning of the skin. The plasma jet heated the skin sample to a relatively high temperature up to 60°C, as shown in Figure 5.11.8 and Figure 5.11.10, which is not suitable for treatment in vivo. High temperatures can cause improvement of skin permeability by changing the structure of lipids in stratum corneum [2], and these changes are reversible up to 75°C [3].

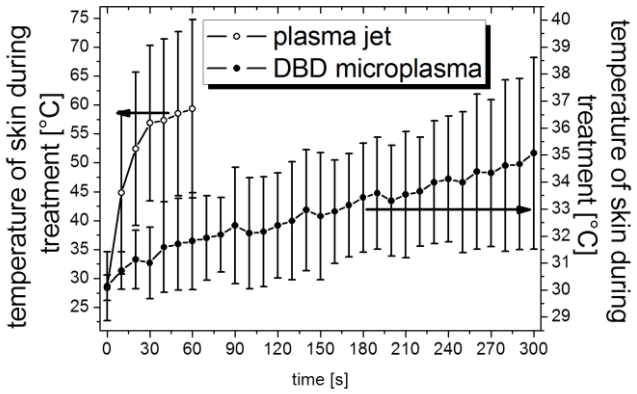

Figure 5.11.8: Evolution of skin temperature during treatment by plasma.

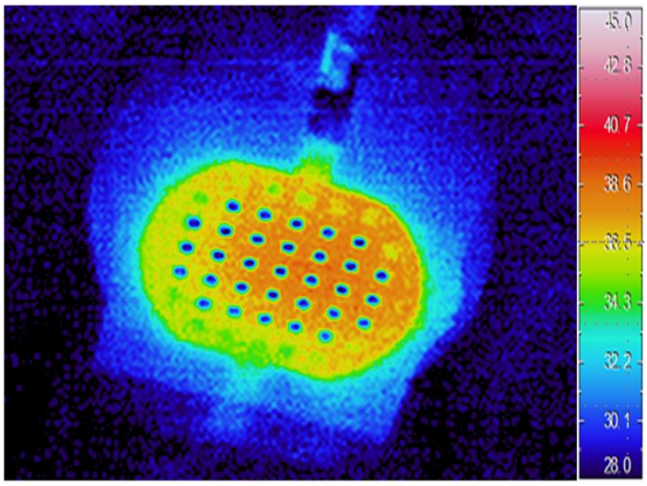

Figure 5.11.9: Distribution of temperature on electrode of microplasma barrier discharge after 5 minutes of discharge. Achieved temperature of electrode was below 40°C.

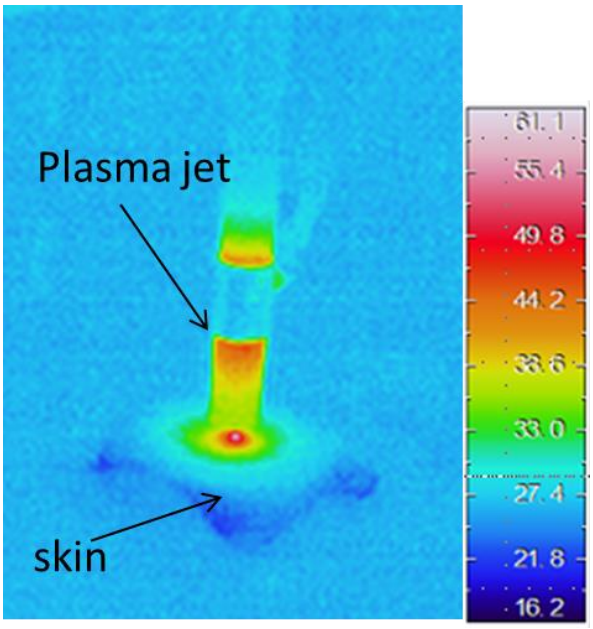

Figure 5.11.10: Treatment of skin by plasma jet (after 60 s).

However, some damage could be inflicted upon keratinocytes. On the other hand, the skin temperature after treatment of microplasma dielectric barrier discharge was not elevated to a temperature higher than 40°C (Figure 5.11.8). Because of the small distance between the skin and the electrode of the microplasma dielectric barrier discharge, the electrode temperature was measured after 5 minutes of discharge for confirmation of the correct value (Figure 5.11.9). This temperature is close to the temperature of the skin measured during treatment by microplasma dielectric barrier discharge; it is suitable for treatment of human skin, but also when drug was applied 1 – 2 min after treatment, the temperature decreased. It suggests that in both cases, temperature had no influence on drug penetration.

6.2 Interaction of plasma and skin surface

6.2.1 Motivation

Skin adhesion to substances or patches is very important for application of cosmetic formulation or transdermal drug delivery. Skin adhesives in wound protection represent a large market [4]. The skin is usually very hydrophobic, so creams have to be lipophilic or they have to be composed of substances which change properties of the skin surface. Wet or unclean skin may be is more hydrophilic and clean and dry skin as mostly lipophilic [5]. On the other hand, some parts of the skin can be hydrophilic because of presents of fatty acids from sebum or sweat. This is the case of forehead and opposite – lipophilic is forearm [6]. In

the case of transdermal patches, surface energy of the adhesive must be equal to or less than that of the adherent (the skin in our case). Flow of drugs through the skin can be described by equation

$$\boldsymbol{J = D_{SC}\frac{C_S}{h_{SC}}} \qquad (16)$$

where J is the flow of the drug, D_{SC} is the diffusion coefficient through the stratum corneum, C_S is concentration of the drug in the solution and h_{SC} is the thickness of stratum corneum. The evolution of the concentration of the drug can be expressed by Figure 6.2.1.

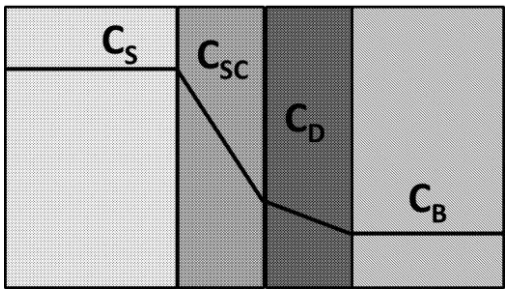

Figure 6.2.1: Evolution concentration evolution of the drug. Constant concentration C_S is in the solution applied on the skin, linearly decreasing in stratum corneum – C_{SC}, linearly decreasing in dermal layer C_D (less steep) and constant in blood stream C_B.

Surface properties of the skin can be investigated by measuring of contact angle of the water droplets. Small amount of liquid can be spread on the surface of solid and form a drop. Angle between surface and surface of droplet is called contact angle. When some molecules are dissolved in liquid they can move towards solid surface and their concentration can be higher at the interface than in the bulk of the liquid. This phenomenon is called adsorption [7]. Adsorption can occur on different interfaces, but pharmaceutically the most important is liquid/solid interface. It means that, if we can increase skin ability to adsorb molecules, we can increase the concentration of drug close to surface of stratum corneum and also drug flow through the skin as it is described by equation (16). If contact angle of solution can reach a certain critical value, it can be absorbed by skin [8]. Water contact angle showed that vehicles with higher skin wettability increased the contact of the drug with skin surface and therefore increased drug flow through the skin. Absorption of drug through the skin is affected by partition coefficient of the drug between the formulation and the skin surface. So the skin contact with drug during the application period is necessary [9]. In the next part, we will characterize surface properties of the skin by measurement of water contact angle after microplasma treatment of the skin.

6.2.2 Preparation of samples

Pig skin of Yucatan micropig from Charles River Japan, Inc. (Yokohama, Japan) was used for investigating of the influence of the plasma treatment. The pig skins were stored at −20 °C in a freezer before the experiment. At first, the fat layer of the skin was removed by using a knife, then it was cut and soaked at 4 °C in phosphate buffered saline (PBS) for 3 h, and then after a bath in 60 °C PBS for 1 min, the epidermal layer of a thickness of 200 mm was peeled by using tweezers. Finally, the skin sample was cut to 10×15 mm or 5×15 mm pieces and attached to plastic sheet by using double-sided tape. Samples were dried 2-3 days if we used dry skin or used immediately if we investigated hydrated skin.

6.2.3 Contact angle

We measured contact angle of skin samples treated by microplasma using different gasses.

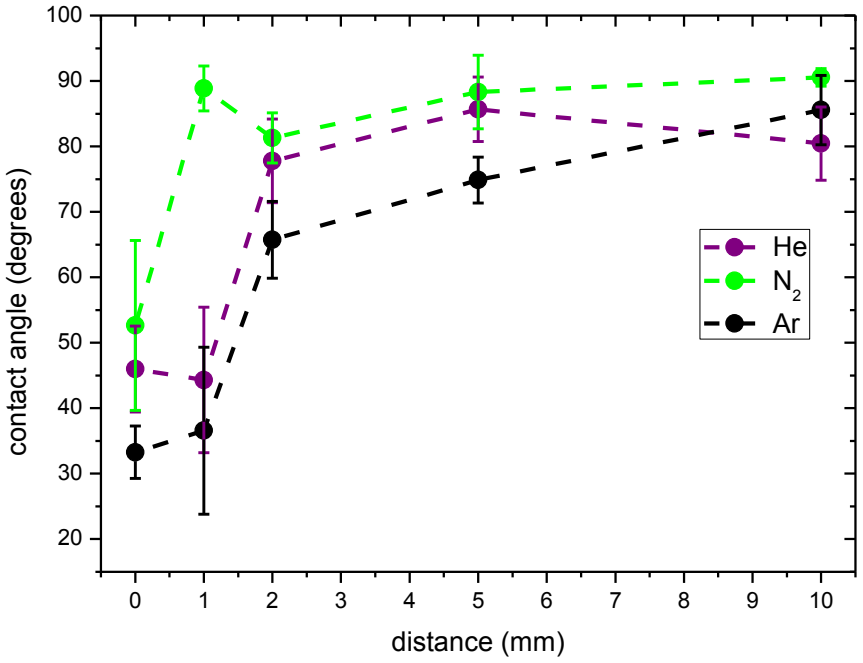

Figure 6.2.2: Water contact angle on the skin after 5 minute of microplasma treatment using helium, nitrogen and argon. The skin was placed in different distances from the electrode.

Figure 6.2.2 shows water contact angle of the skin after 5 minutes of treatment by microplasma dependent on distance from electrode. Water contact angle of untreated skin is in range of 80° – 110° [10]. Contact angle depends very strongly on hydration of the skin,

which will be possible to see in the next figures. After argon plasma treatment, water contact angle reached value around 35° when skin is on surface of electrode or 1 mm from electrode. We cannot say that the skin surface is only more hydrophilic, but more correctly, it is functionalized. This means that plasma created active bonds on surface by breaking of some previous bonds or by adsorption of oxygen, nitrogen groups. This effect is strongly reduced when distance from electrode increased. Figure 6.2.2 indicates that argon microplasma can affect the skin surface even in higher distance than 1 mm. On the other hand, in the case of helium microplasma, changes are possible observe in distance less than 2 mm. Helium plasma is relatively easy to ignite even at low voltage, as well as argon, so the reason why helium is less effective than argon can be weight of helium ions which are much lighter than argon and etching effect and breaking bonds is less significant. Effect of nitrogen microplasma is observable only when skin is in contact with electrode, probably because of much harder ignition and smaller dimension of plasma. At higher distances, only reduced amount of active particles which can survive outside of plasma can react with the skin. The same effect was observed in the case of oxygen or air microplasma (not in figure).

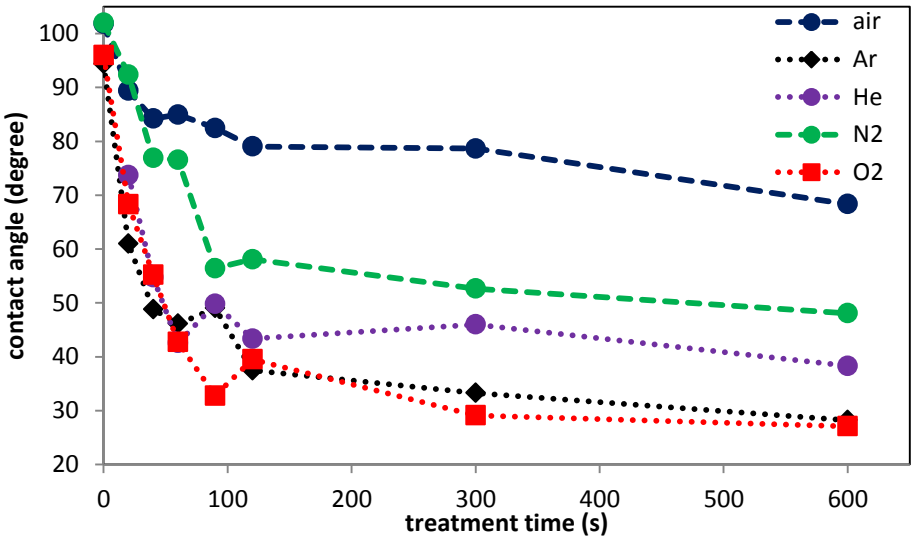

Figure 6.2.3: Evolution of water contact angle for different treatment times and gasses when the skin is in contact with electrode.

Figure 6.2.3 shows water contact angle depending on microplasma treatment time and used gas when the skin was in contact with electrode. Effectivity of the skin treatment is the worst in the case of air plasma followed by nitrogen, helium and very similar for argon and oxygen. The water contact angles were measured prior to plasma treatment. The procedure of plasma treatment was following:

Skin sample was treated 20 s by plasma and then water contact angle was measured. When water droplets were removed from skin, skin was treated again by 40 s followed by measurement of water contact angle. This procedure was repeated for times 60 s, 90 s, 120 s, 300 s and 600 s.

After treatment of 90 – 120 s, water contact angle is decreasing very slightly. After the final treatment of 600 s, the skin samples were put table in laboratory at normal conditions (pressure 1 bar, room temperature (not regulated)). In certain times, contact angles were measured again to observe ageing of the skin and returning to the original state. Figure 6.2.4 shows ageing of skin after argon microplasma treatment. Ageing can be fit by equation:

$$\boldsymbol{CA(t) = A + B\left[1 - exp\left(-\frac{t}{t_B}\right)\right] + C\left[1 - exp\left(-\frac{t}{t_C}\right)\right] = A + F1 + F2} \qquad (17)$$

where *CA(t)* is the contact angle changing in time *t*, constant *A* represents the contact angle at the beginning (just after treatment), t_B is characteristic time of increasing of function *F1*, t_C is the characteristic time of increasing of function *F2*, *B* and *C* are the constants characterizing amplitude of the increasing. The increase of water contact angle is characterized by "fast" and "slow" ageing.

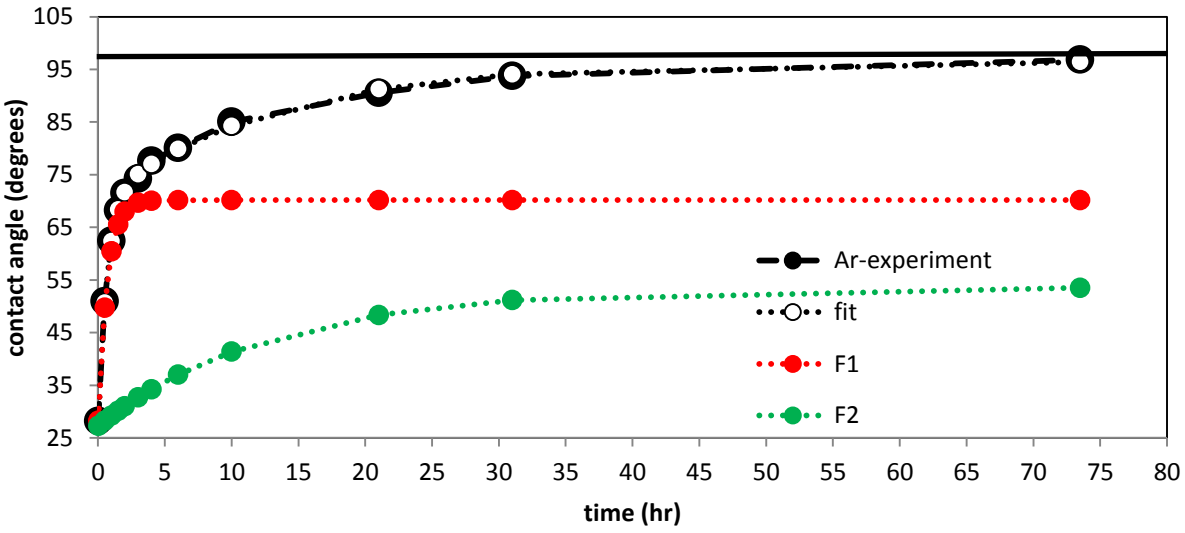

Figure 6.2.4: Ageing of the properties of the skin treatment characterized by water contact angle. Fit of ageing by linear combination of F1 and F2 function.

Fast ageing time is reverse correlated with contact angle and the smaller is the contact angle is the longer time t_B is. Time t_B delays from several minutes up to approximately 1 hour. Slow ageing has no correlation with water contact angle but time t_C is very different in dry

samples in comparison with hydrated samples. t_C delays from 10 to 15 hours in dry samples but more than 30-40 hours in hydrated samples. That is the reason why we suppose that F2 function is caused by drying of the skin.

We compared microplasma treatment of hydrated and dry skin samples in Figure 6.2.5 (skin sample is in direct contact with microplasma electrode) and Figure 6.2.6 (skin sample is 1 mm from microplasma electrode. Skin samples were treated by the same procedure as in Figure 6.2.3. Measured water contact angle of hydrated skin samples is close to 65° (in Figure 6.2.5) and 85° (in Figure 6.2.6). After microplasma treatment of hydrated skin, water contact angle increased probably because of water evaporation. The temperature of oxygen plasma is higher than argon plasma, so increase of water evaporation and also contact angle by heating is more significant. As a result we can observe very different behavior of hydrated and dry sample. In the case of argon, heating of the sample is not very high, so higher evaporation happens at first seconds and after that water contact angle decreases similarly to the dry sample as well. A similar behavior can be noticed if the distance of sample from electrode is 1 mm (in Figure 6.2.6).

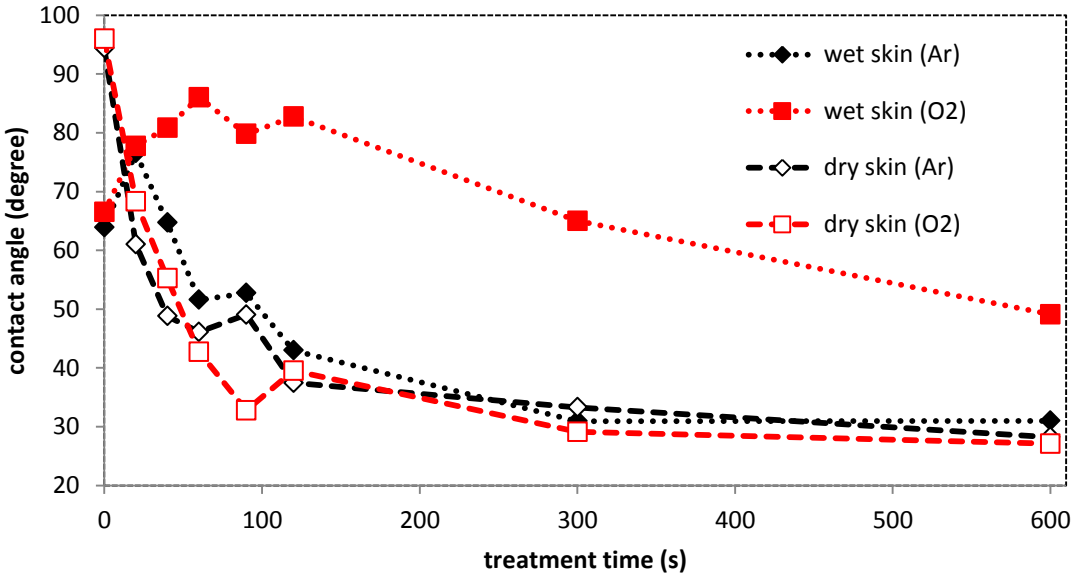

Figure 6.2.5: Comparison of evolution of water contact angle for different treatment times for argon and oxygen gasses. Dry and wet skin samples were used when the skin was in the contact with microplasma electrode.

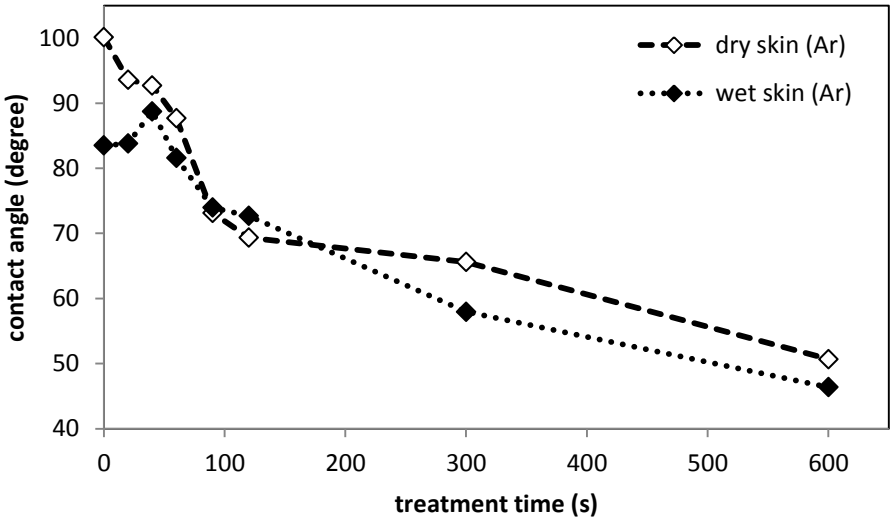

Figure 6.2.6: Comparison of evolution of water contact angle for different treatment times for argon and oxygen gasses. Dry and wet skin samples were used when the skin was 1 mm from the surface of microplasma electrode.

Structure of electrode determined how the surface properties of the skin will change. Figure 6.2.7 shows that it is not uniform. If the sample is treated repeatedly, it is not in the same position against electrode and properties of the skin are more and more uniform. How strong is this effect, it is shown in Figure 6.2.8. The skin sample that was treated by argon microplasma for example 30 s until water contact angle did not reach constant value.

Figure 6.2.7: The skin covered by water layer after microplasma treatment shows clearly patterns of electrode where the effect of plasma is the strongest.

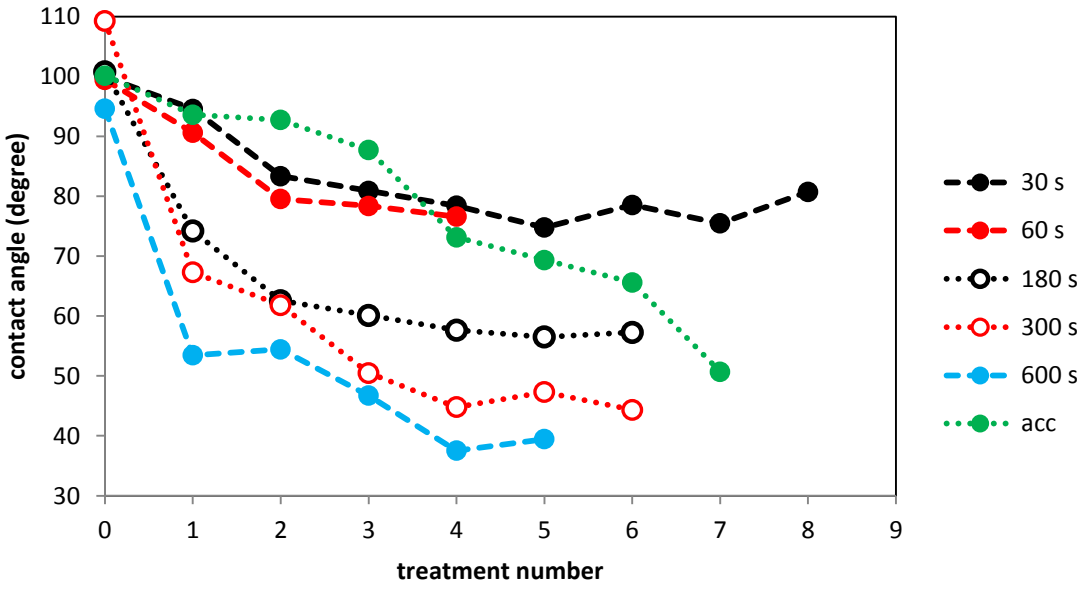

Figure 6.2.8: dry skin 1 mm from electrode. Treatments are accumulated with the same treatment time except „acc“ where time is changed 20, 40, 60, 90, 120, 300, 600s.

6.2.4 X-ray photoelectron spectroscopy

Analysis of the skin surface was done by XPS to confirm if the ratio of surface elements was changed. Skin samples treated from distance 1 mm by helium and argon microplasma indicate higher concentration of oxygen and nitrogen atoms with respect to other samples (Figure 6.2.9 – values were normalized).

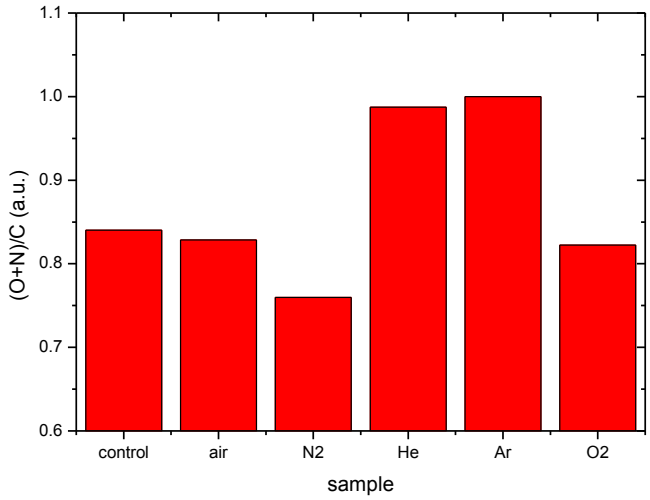

Figure 6.2.9: Normalized ratio of concentrations of oxygen and nitrogen to carbon after 5 minutes of microplasma treatment of the skin at distance 1 mm from electrode for different discharge gasses.

When the skin samples were in contact with the electrode, all microplasma treated samples contained more oxygen and nitrogen atoms than non-treated sample (control). It seems that Figure 6.2.10 could indicate correlation between water contact angles of Figure 6.2.3, but helium and mainly air microplasma treatment break away from this dependency.

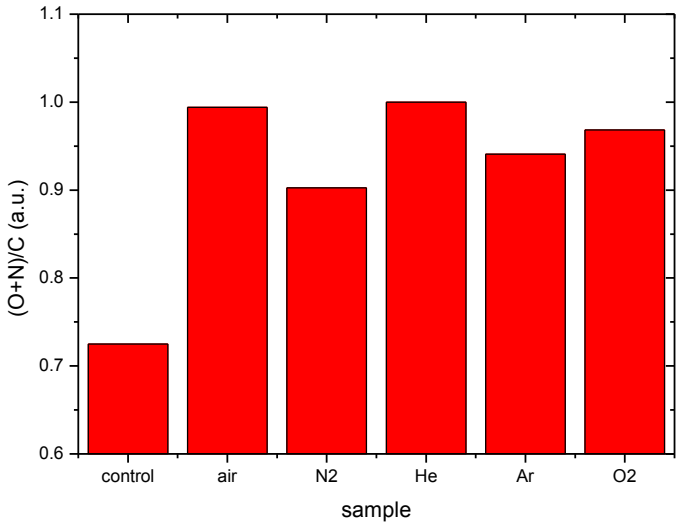

Figure 6.2.10: Normalized ratio of concentrations of oxygen and nitrogen to carbon after 5 minutes of microplasma treatment of the skin when the skin is in contact with electrode for different discharge gasses.

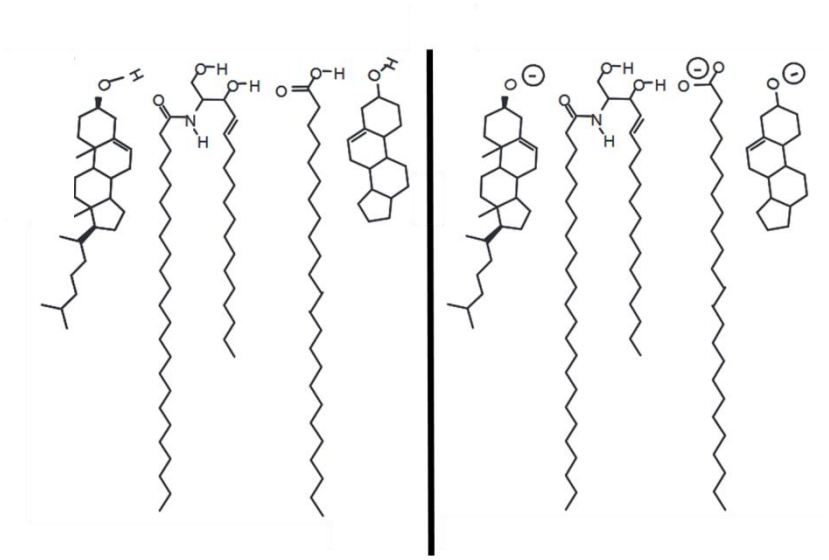

Figure 6.2.11: Molecules can form ions after plasma treatment [11] at the surface of the skin. After that water contact angle will decrease.

Oxygen and nitrogen content is one of the factors which has influence on contact angle, but the most probably not the only one. Plasma treatment can cause not only

incorporation of new oxygen and nitrogen atoms, but also can create some free bonds – dehydrogenated free bonds that make surface more wettable for water molecules (Figure 6.2.11). Surface of polymers have some freedom and molecules on the surface can be oriented differently than in the bulk material. The short range mobility of molecules can have major influence on surface properties of the skin [12]. It is also possible that the reorientation of the molecules at the surface has a dominant effect, too.

6.2.5 Histological observation of the skin section

Plasma particles can etch skin surface and reduce thickness of stratum corneum. Histological skin section can show us how effective is the etching. The layer of stratum corneum of non-treated skin in Figure 6.2.12A has thickness close to 30 μm. After 10 s treatment by plasma jet, thickness decreased to 20 μm, 18 μm after 30 s of treatment and 10 μm after 60 s of treatment (Figure 6.2.13). The skin treated 60 s by plasma jet is shown in Figure 6.2.12B, adhesion of stratum corneum layer is reduced in the whole skin. On the other hand, microplasma treated skin is much less damaged and no reducing of adhesion is observed (Figure 6.2.12C). Skin etching by microplasma is saturated after 60 s at thickness of 15 μm (Figure 6.2.13). Third layer of stratum corneum is the strongest barrier. Third layer has thickness of 1/5 of whole thickness of stratum corneum. It is 6 μm in our case. Thickness can have influence on transdermal delivery in the sense of higher flow but it does not help too much to overcome skin barrier. Very high temperature can seriously damage the skin. Skin after plasma jet treatment with gas temperature close to 200°C is shown in Figure 6.2.14. Heat damage is characterized by changing color of the whole thickness skin and also by melting of some parts of the skin.

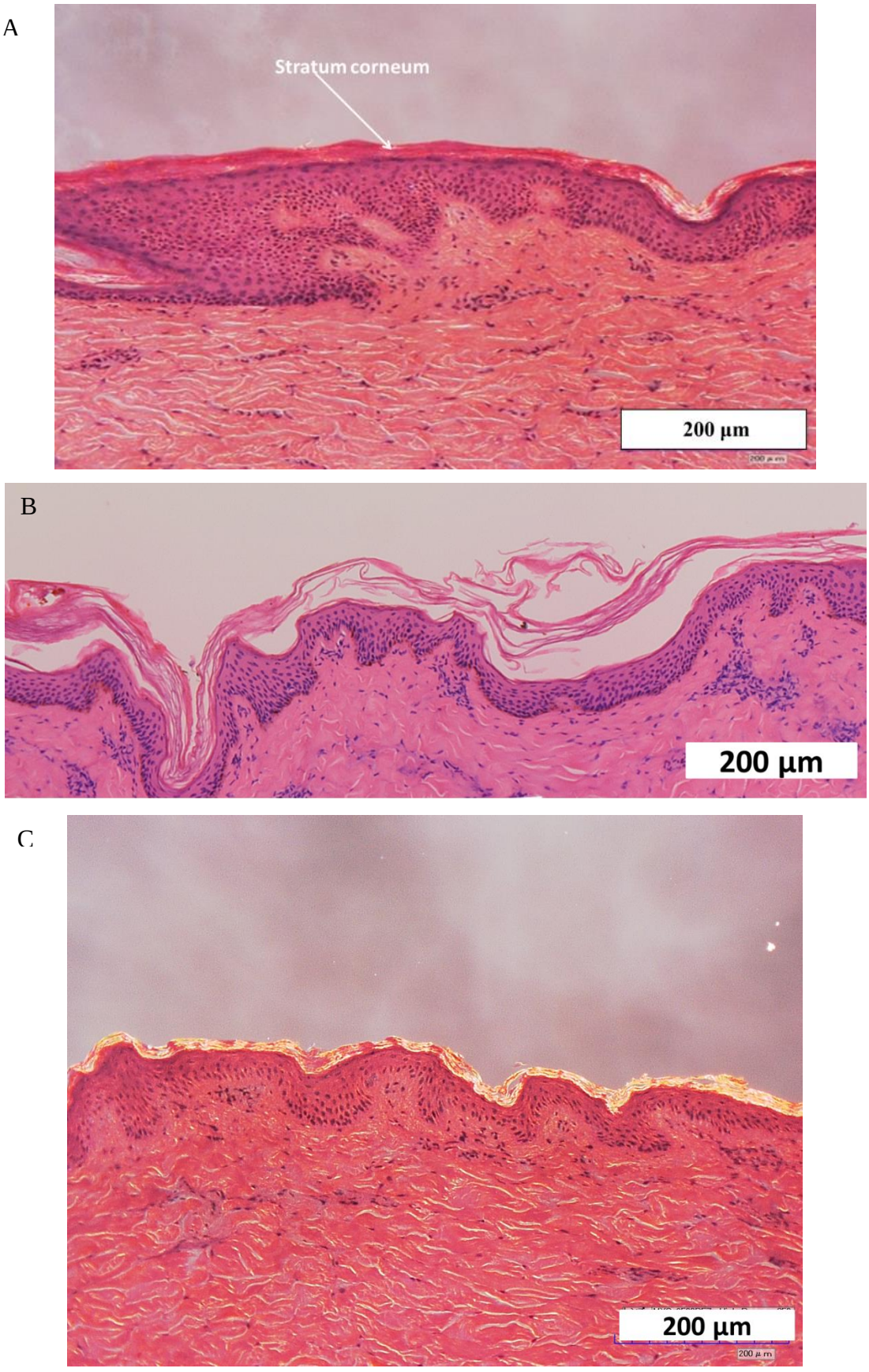

Figure 6.2.12: Histological cross sections of the skin A:nontreated skin B: skin treated by plasma jet for 60 s.

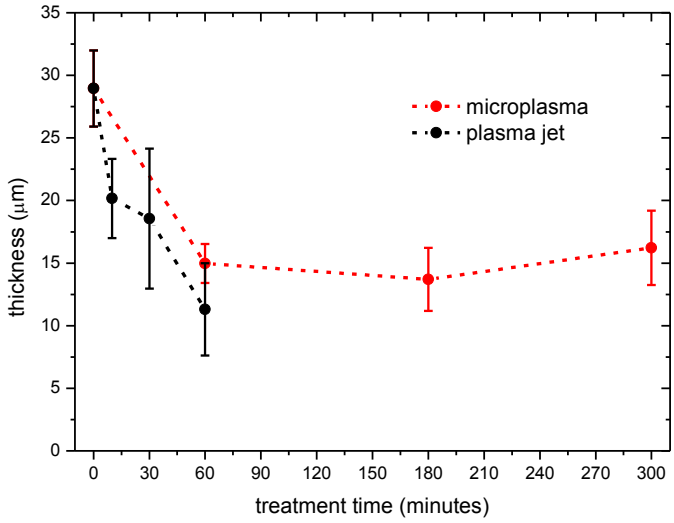

Figure 6.2.13: Thickness of stratum corneum depending on treatment time by plasma jet or microplasma.

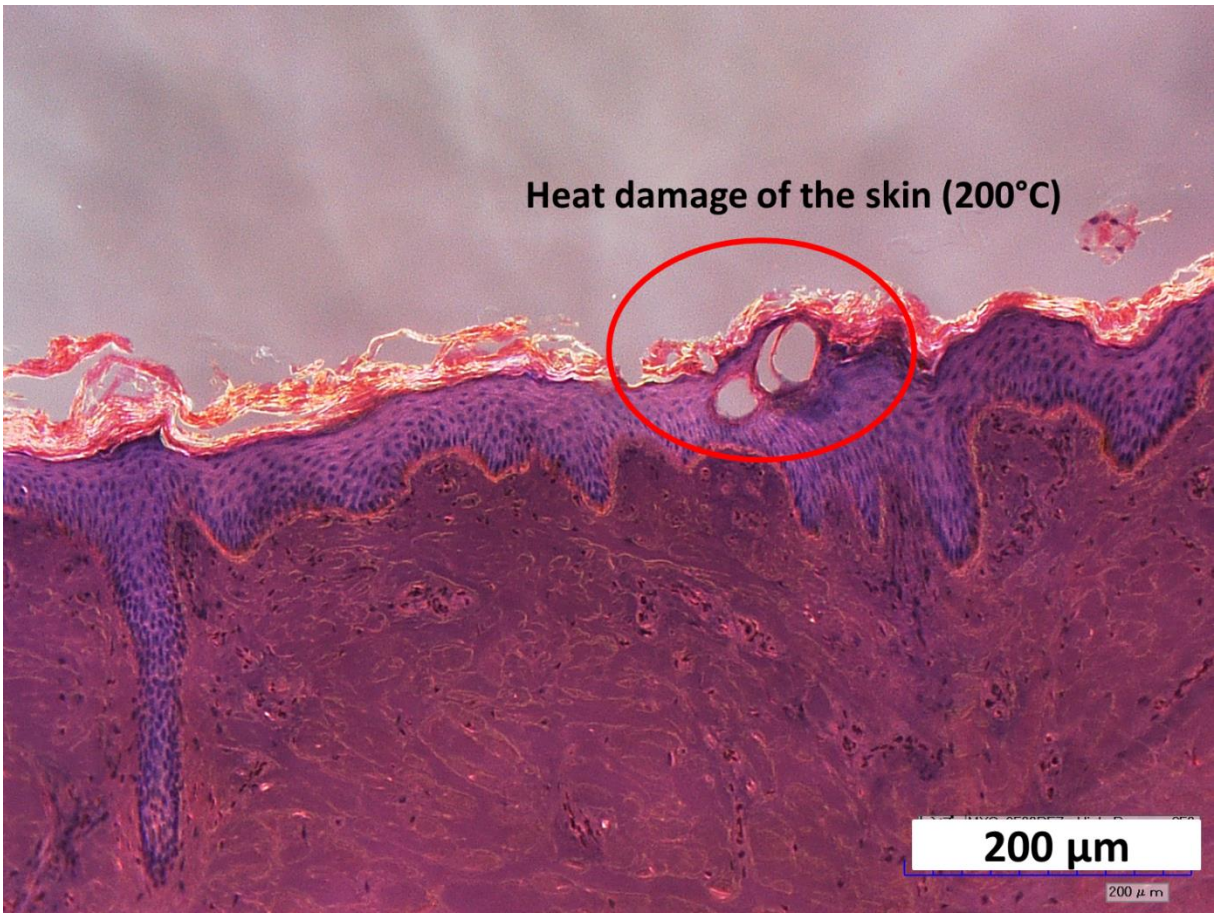

Figure 6.2.14: Heat damage to the skin after plasma jet treatment with temperature of plasma of 200°C.

6.2.6 Conclusion

Plasma treatment of the skin reduces the water contact angle by functionalization of the skin surface. The most effective is using Ar plasma. Microplasma has very low dimensions, so samples have to be very close to the surface of electrode. Ar microplasma offers low temperature plasma and also the ability to treat skin from higher distance than using other gases. Time of recovery of the skin surface is relatively fast and it can take from several minutes up to 1.5 hours. This time is in inverse correlation with the contact angle. Skin roughness has a minor effect on the water contact angle because the skin is not a flat surface. A much higher effect than change of roughness after treatment has the homogeneity of treatment of the skin surface. Plasma treatment creates free bonds and they are oxidized, which is proved by XPS measurement. However, this is not the only process which increases water contact angle. Reorientation of molecules of the skin can be a dominant effect. Skin can be etched by plasma. Plasma jet can cause more damage to the skin and decrease thickness of stratum corneum to 10 μm during 60 s while microplasma to 15 μm during 60 s. Microplasma etching effect is saturated after 60 s. Plasma did not etch the strongest layer of the skin.

6.3 Plasma treatment of lipids

6.3.1 Motivation and sample preparation

The skin and stratum corneum is composed of many atoms and molecules such as lipids, water, proteins, and amino acids, Sodium or Potassium. Interpretation of changes of these molecules after plasma treatment can be difficult. We chose several lipids to reduce this problem and to make it as simple as possible for analyzing. Lipids such as stearic acid, erucic acid, cholesterol, ceramide C4 were as model lipids of lipid membrane in the stratum corneum.

Stearic acid, erucic acid, cholesterol and ceramide C4 were in form of wax or powder. Sample was put on aluminum foil on the heater and heated to the temperature above melting point until samples changed to liquid state. Liquid sample was placed to cold metallic holder until lipid solidified. Sample had round shape with diameter approximately 5 mm. Prepared samples were treated by argon microplasma discharge 5 minutes at distance of 0.5 – 1 mm from surface of electrode. Samples prepared by this way were investigated by XPS, RAMAN or FTIR-ATR spectroscopy before and after plasma treatment.

6.3.2 Stearic acid

Stearic acid (Figure 6.3.1) is a saturated carboxylic acid composed of 18 carbon atoms, 36 hydrogen and 2 oxygen atoms ($C_{18}H_{36}O_2$). Melting temperature is in the range 69 – 71 °C and boiling temperature is 361°C. It is one of the lipids present in stratum corneum.

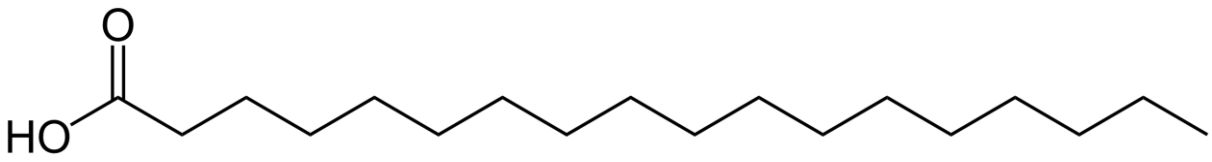

Figure 6.3.1: Chemical structure of Stearic acid.

6.3.2.1 X-ray photolectron spectroscopy of Stearic acid

Concentration of elements

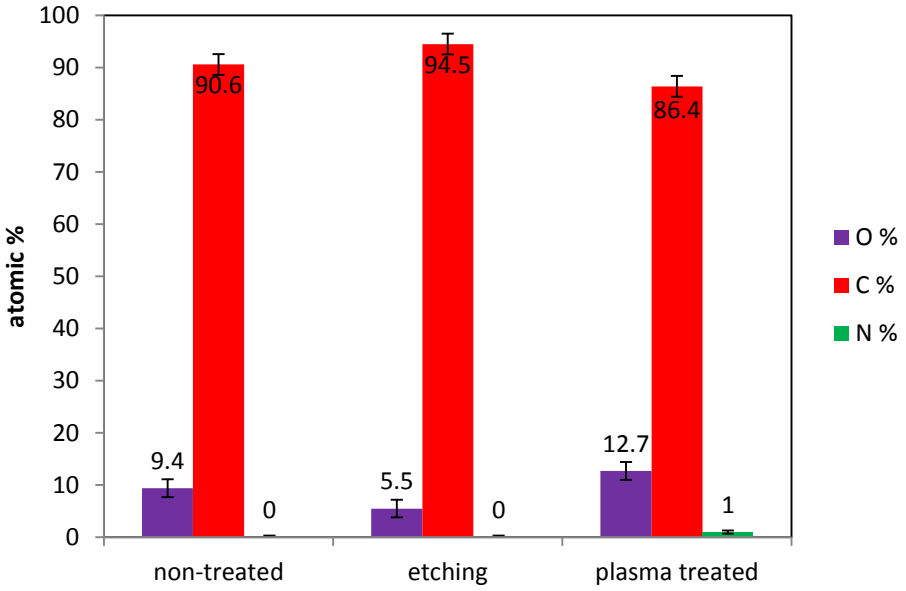

Figure 6.3.2: Concentration of elements in Stearic acid sample before any treatment (non-treated), after Ar ion etching in vacuum in ESCA chamber and after Ar microplasma treatment.

Concentration of elements based of chemical composition of stearic acid (excluding hydrogen atoms) is 10% of oxygen and 90% of carbon. Elemental composition determined by XPS measurement determined 9.4 ± 1.7% of oxygen and 90.6 ± 2% of carbon (Figure 6.3.2). Ar etching in vacuum chamber caused decrease of oxygen concentration to 5.5 ± 1.7% (94.5 ± 2% of carbon atoms) in Stearic acid. Microplasma treated stearic acid was oxidized and nitrated. Oxygen concentration increased to 12.7 ± 1.7% and nitrogen concentration from 0% to 1% ± 0.3%. We suppose that the amount of carbon is constant and no significant amount of

carbon from air contaminated sample. Under this assumption, we normalized measured XPS spectra of carbon, oxygen and nitrogen to area under the carbon peak (after subtraction of background). After that, all spectra were normalized to the area under carbon peak of non-treated sample. Carbon spectra (Figure 6.3.3) was possible to fit by four peaks (C-C/C-H, C=O, O=C-N, O=C-OH) in the case of Ar microplasma treated stearic acid and by 3 peaks (C-C/C-H, C=O, O=C-OH) in the case of non-treated stearic acid and stearic acid etched by Ar ions under low pressure.

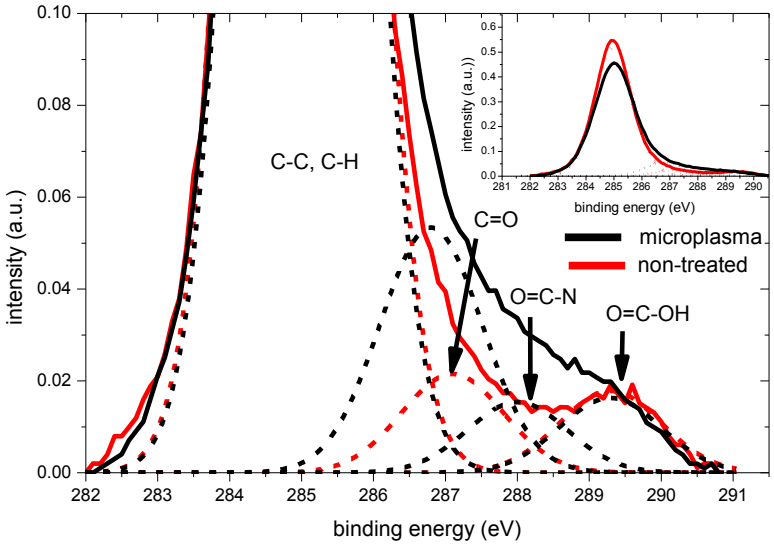

Figure 6.3.3: Carbon spectra of non-treated stearic acid (solid red line) and fitted peaks (dashed red lines) or microplasma treated stearic acid (solid black line) and fitted peaks (dashed black lines).

Non-treated samples should be composed only from O=C-OH functional group and hydrocarbon chain. However, C=O functional group of ketones can be observed in spectrum. It means that purity of stearic acid was low or some chemical changes happened during sample preparations. The sample was heated to approximately 90°C prior to other measurements to be melted and solidified, but the process of creation of ketones (hydrocarbons only with C=O group) requires temperature more than 200°C and presence of catalyst [13]. Areas of functional groups of carbon spectra normalized to whole carbon area of the sample are described in Figure 6.3.4. Etching of stearic acid didn't change concentration C-C, C-H bonds but only decrease of oxygen containing groups. On the other hand, microplasma treatment decreased number C-C, C-H and increased mostly C=O functional groups and also groups with incorporated nitrogen. Figure 6.3.4 also shows that non-treated

stearic acid contained 6.4% of oxygen in carboxylic bonds (O=C-OH) instead of 10%, meaning purity 64% (95% declared by producer).

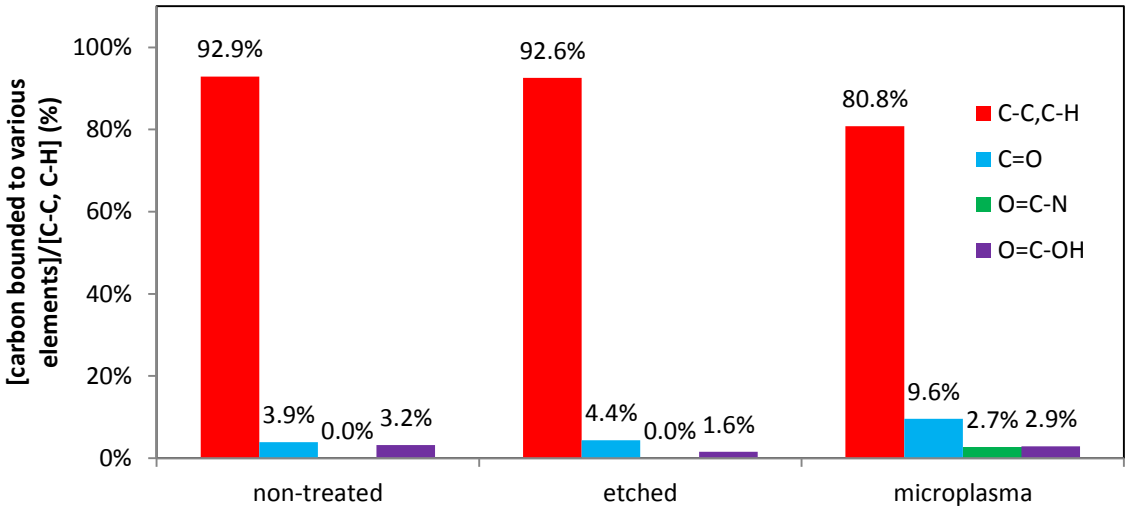

Figure 6.3.4: Percentage of functional groups in non-treated, etched and plasma treated sample normalized to carbon peak area of non-treated sample.

Presence of nitrogen was confirmed in carbon spectra by O=C-N at position 288 eV in microplasma treated sample and also in nitrogen spectrum.

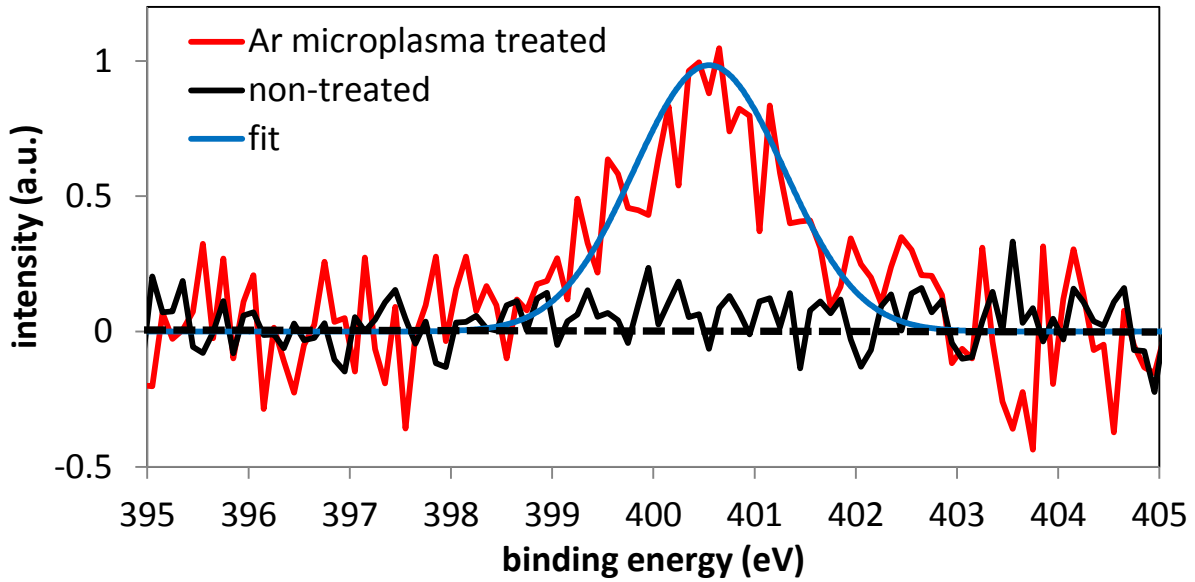

Figure 6.3.5: XPS spectra of non-treated Stearic acid and 5 min treated by Ar microplasma. (Gaussian fit with FWHM = 1.75 eV is at position 400.6 eV).

As it is seen in Figure 6.3.5, nitrogen peak is observed at position 400.5 eV with FWHM of 1.75 eV. Typical position of C-N and O=C-N peaks is 399 – 401.1 eV and 399.8 – 400.9 eV, respectively [14].

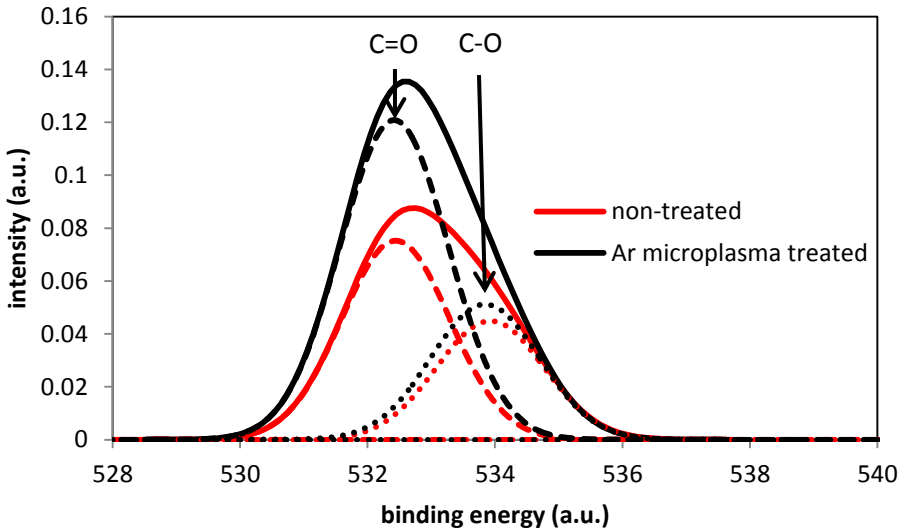

Figure 6.3.6: Oxygen spectra of non-treated and Ar microplasma treated stearic acid with dashed and dotted fit peaks.

Oxygen spectrum also confirmed higher presence C=O (Figure 6.3.6). Oxygen spectrum is composed of 60% of O=C-OH and 40% of C=O what agrees with carbon spectrum. Figure 6.3.7 shows the percentage of C-O and C=O bond normalized to amount in non-treated sample using oxygen spectra.

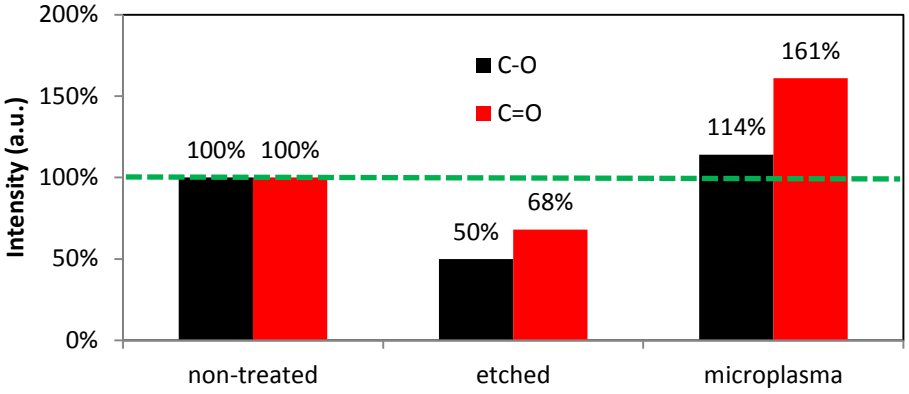

Figure 6.3.7: Change of concentration C-O and C=O functional groups of non-treated, etched and Ar microplasma treated stearic acid.

Comparison of Figure 6.3.7 and Figure 6.3.4 shows that Ar^+ etching removed –OH group from stearic acid. As C=O bonds decrease less than C-O, it means that some C=O from carboxylic group is removed, but some can create ketones. Ar microplasma treatment creates ketones by breaking C-H or C-C bonds and by reaction of atmospheric oxygen. Amount of C-O bonds increased only slightly.

Plasma treatment of stearic acid in Ar gas and in the mixtures Ar+10%O_2 and Ar+10%H_2 was investigated in DC discharge of work of Bernadelli *et al.* [15]. They found out that the surface is preferentially etched in discharge zone and grafted on post-discharge zone (zone without electrons and charged particles and chemically active species). Etching was the most effective in mixture of Ar+10%O_2 probably because of chemical sputtering and less effective in Ar and Ar+10%H_2 discharge. In our case, Ar ions were effective for etching which can be a question of the used power. At low temperature (up to 45°C), carboxylic group (-COOH) is removed prior to breaking C-C and C-H and functionalization process starts at higher temperatures (~60°C) and production of volatile products, such as alcohols, ketones, acids or esters, during discharge treatment is realized by Ar+10%O_2 [16]. However, it was not confirmed by our measurements. In the post-discharge zone, etching of stearic acid occurs by atomic oxygen which breaks C-C bonds [17]. Functionalization is done by grafting OH group to hydrocarbon chain and C=O can be formed after longer treatment by oxidation of grafted OH and carboxylic functional group was not changed. Analysis of products created after plasma treatment showed the presence of carboxylic acids with shorter chains [17]. Noel et al. [18] investigated treatment of stearic acid in microwave Ar-N_2 and Ar-O_2 atmospheric post-discharge. They also confirmed higher etching rate by in Ar-O_2 mixture than Ar-N_2 and formation shorter chain carboxylic acids. On the other hand C=C bonds were produce more in Ar-N_2 post-discharge. The presence of nitrogen was confirmed in both discharges by mass spectrometry but only by observing short chain ions such as CN, HCN, NH etc.

6.3.2.2 *FTIR spectroscopy of Stearic acid*

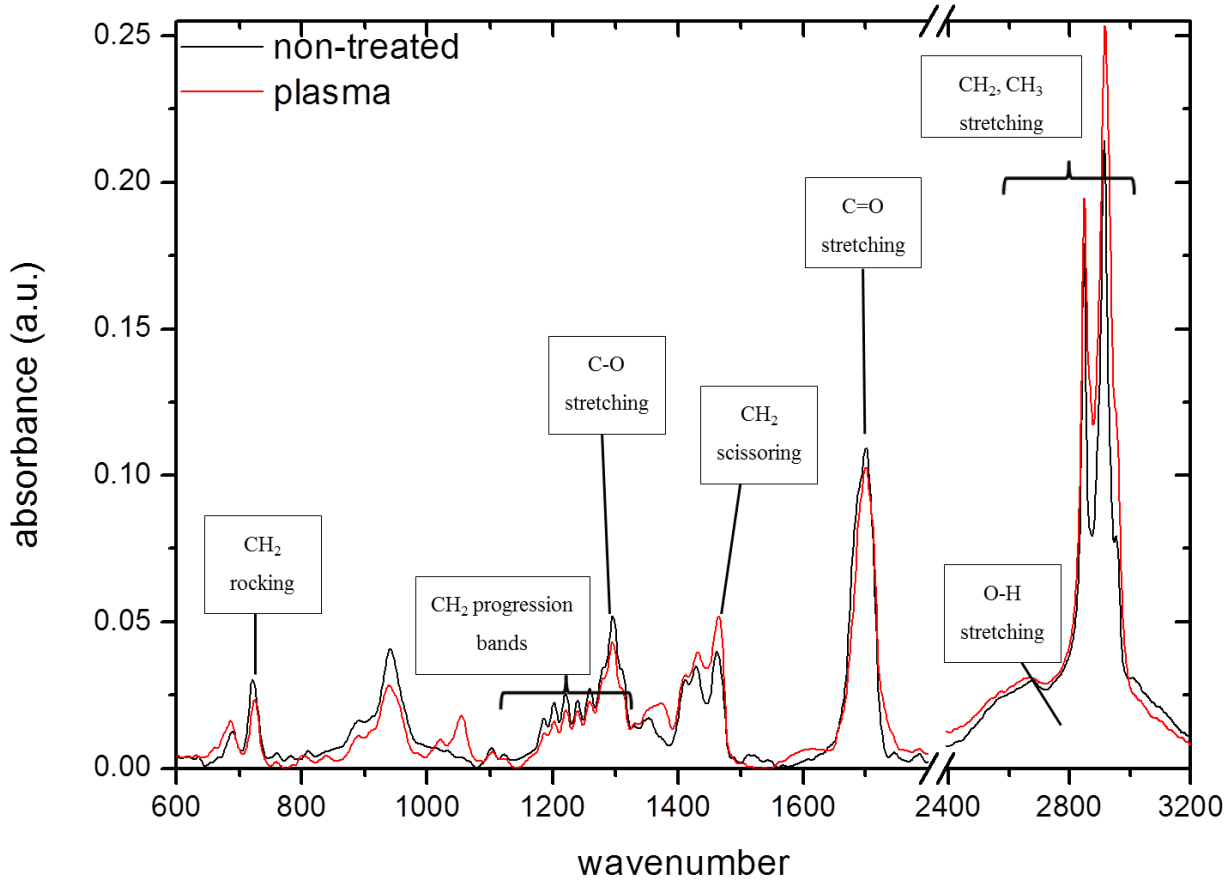

Figure 6.3.8: FTIR spectrum of 5 minutes Ar microplasma treated and non-treated stearic acid.

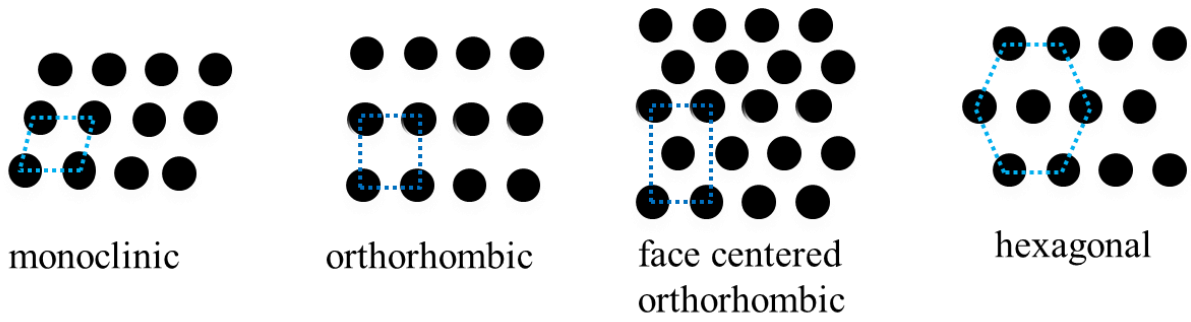

Figure 6.3.9: Possible packing of lipid molecules in lipid matrix.

Methylene rocking vibration at 720 cm^{-1} can characterize lateral packing structure of hydrocarbon chains. Orthorhombic packing (Figure 6.3.9) characterize splitting of CH_2

rocking peak into two bands near 720 cm^{-1} and 730 cm^{-1}. As the temperature is increasing, orthorhombic structure can go through the hexagonal to liquid. During this process, band at 730 cm^{-1} is approaching to the 720 cm^{-1} and finally it will disappear. This phenomenon can be explained by expansion of lattice and loosening of the structure. However, heating is not the only one method to change structure. It was shown by Zhang et al. [19] that the presence of impurities can increase the lattice dimension. They compared polyethylene lattice with halogen impurities. As the number of the impurities increased, the distance between the above-mentioned split bands decreased. If the peak is near 717 cm^{-1}, it would be evidence of triclinic organization. Peak intensity increases in direction from liquid organization through hexagonal and orthorhombic to triclinic [20]. Intensity ratio can indicate crystallinity [21]. Doublet is visible for less than 40°C. Non-treated stearic acid is clearly composed of 2 peaks. However, because of low resolution we fixed one peak at 720 cm^{-1} as its position is not changing too much. The second peak appeared at 728.5 cm^{-1}. After plasma treatment of stearic acid, this band was moved to the lower wavenumbers to the 726.9 cm^{-1} (Figure 6.3.10), what indicates increase of lattice dimensions. Ratio of absorbance (A_{730}/A_{720}) was changed from 0.76 to 1.75.

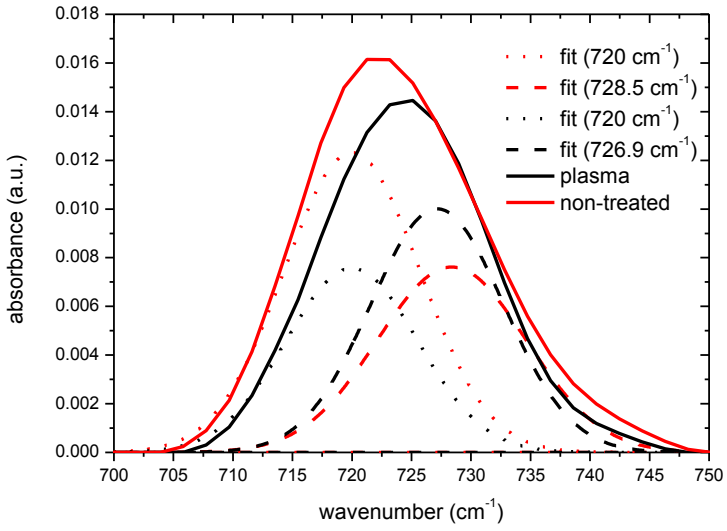

Figure 6.3.10: CH_2 rocking band. Black line represents experimental spectrum of microplasma treated stearic acid and red line represents non-treated stearic acid sample.

The presence of progression bands (from 1185 cm^{-1} to 1350 cm^{-1}) also indicates the presence of orthorhombic packaging. Progression bands come from wagging progression of CH_2 bands in the "trans" conformation. When alkyl chains are disordered, wagging decrease

and peaks are replaced by other bands present in different conformation of alkyl chain [22, 23]. The number of the progression bands is $N/2$, where N is the number of CH_2 bands. Another band characterizing structure is scissoring CH_2 split band at 1463 cm^{-1} and 1472 cm^{-1}, bands are approaching and finally, they are replaced by one band in 1464 cm^{-1} in hexagonal and liquid packing. Progression bands are still present in stearic acid sample before and after plasma treatment. Distance 9 cm^{-1} of scissoring band decrease to 6.7 cm^{-1} after plasma treatment. Figure 6.3.11 shows C=O stretching band non-treated and plasma treated sample. It is clear that C=O band is composed of several peaks A1-A6. This area is sensitive to hydrogen bonding. Peak lower than 1700 cm^{-1} is typical for H-bonded dimers and peaks at higher wavenumbers are characteristic for monomers or interaction between H-atoms is weaker what can be caused higher distance between molecules. Absorbance of peaks at higher wavenumbers is higher after plasma treatment than in non-treated sample.

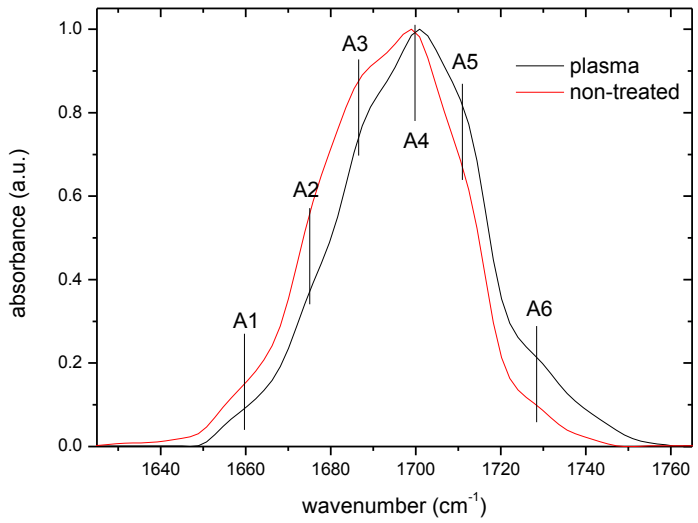

Figure 6.3.11: C=O stretching band before and after 5 minutes Ar microplasma treatment.

All these results indicate increase of lattice dimension.

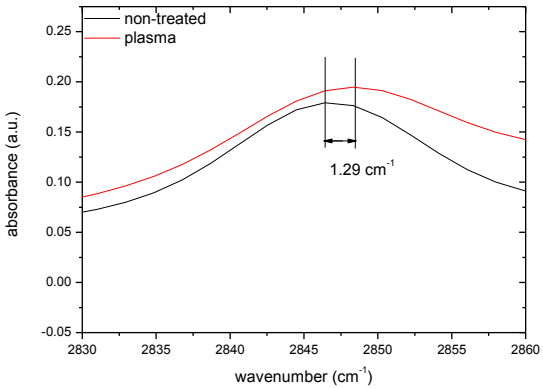

Figure 6.3.12: CH_2 symmetric stretching band before and after 5 minutes Ar microplasma treatment.

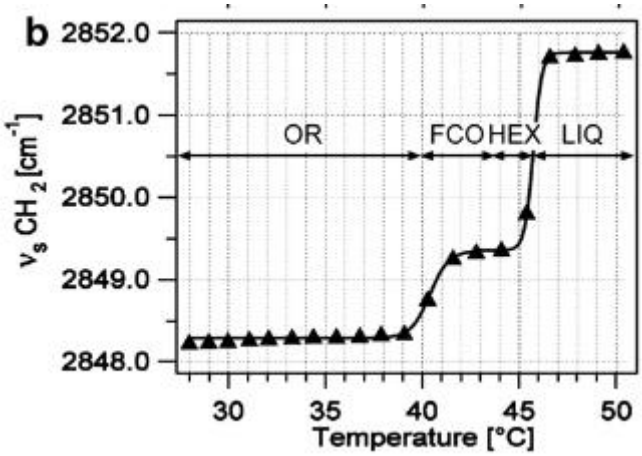

Figure 6.3.13: Position of CH_2 symmetric stretching band at different temperatures and characterized by organization structure (OR-orthorhombic, FCO-faced centered orthorhombic, HEX-hexagonal, LIQ-liquid).

Conformation of hydrocarbon chain can be characterized by CH_2 symmetric stretching is moved from 2846.7 to 2848.1 cm^{-1}. This value still indicates orthorhombic packing.

6.3.3 Erucic acid

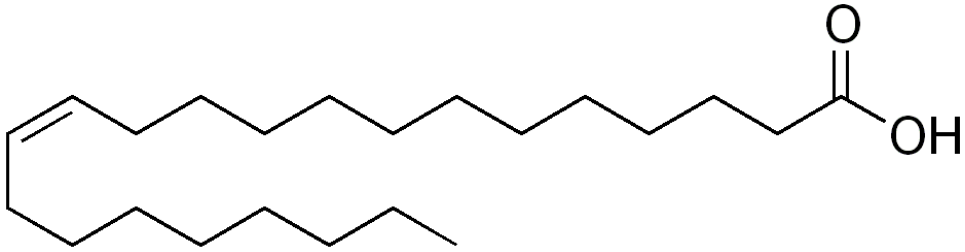

Figure 6.3.14: Erucic acid structure.

Erucic acid (Figure 6.3.14) is a monounsaturated carboxylic acid composed of 22 carbon atoms, 42 hydrogen atoms and 2 oxygen atoms ($C_{22}H_{42}O_2$). Melting temperature is 33.8°C and boiling temperature is 381.5°C. All unsaturated skin carboxylic acids have low melting temperature. Plasma treatment of erucic acid can cause melting and evaporation of sample.

6.3.3.1 X-ray photolectron spectroscopy of Erucic acid

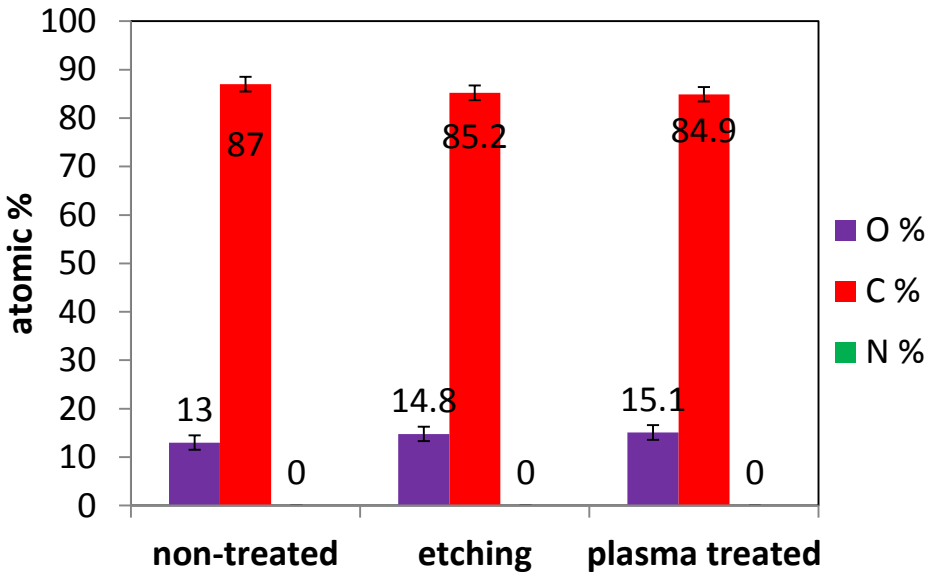

Figure 6.3.15: Concentration of elements in ereucic acid sample before any treatment (non-treated), after Ar ion etching in vacuum in ESCA chamber and after Ar microplasma treatment.

Concentration of elements based of chemical composition of erucic acid (excluding hydrogen atoms) is 8%. Elemental composition determined by XPS measurement determined 13% ± 2% of oxygen and 87% ± 2% of carbon (Figure 6.3.15). Ar etching in vacuum chamber caused decrease of oxygen concentration to 14.8% ± 2% (85.2% ± 2% of carbon atoms) in erucic acid. Oxygen concentration increased to 15.% ± 2%.

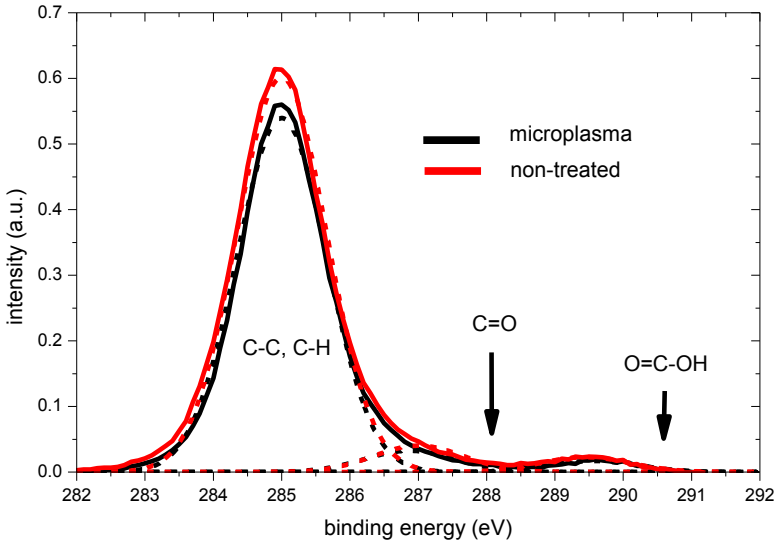

Figure 6.3.16: Carbon spectra of non-treated erucuc acid (solid red line) and fitted peaks (dashed red lines) or microplasma treated erucic acid (solid black line) and fitted peaks (dashed black lines).

Erucic acid is sensitive to air and can be easy oxidized by atmospheric oxygen what can explain its higher oxygen concentration. All XPS spectra were normalized area under the carbon peak (after subtraction of background). Carbon spectra (Figure 6.3.16) was possible to fit by three peaks (C-C/C-H, C=O, O=C-OH). According Figure 6.3.17, erucic acid is composed of 6.8% of carboxylic oxygen, meaning 85% possible purity (more than 85% according producer). Rest of oxygen present in sample can belong to oxidation of molecule. Normalization of carbon spectra of non-treated erucic acid (Figure 6.3.17) shows that etching of sample by Ar ions causes breaking some C-C/C-H bonds in vacuum chamber. Decrease of C-C/C-H bonds and also sum of all bonds equal to 88.5% proves it. On the other hand, number of C=O and O=C-OH bonds increases. There is low pressure without any air in the ESCA chamber. Increase of oxygen bonds can be explain by melting of erucic acid during Ar ion bombardment and free oxygen radical can diffuse in sample from inside to outside and be caught by free bond on surface. Serious changes can be detected by a change of color from white to transparent after ion bombardment.

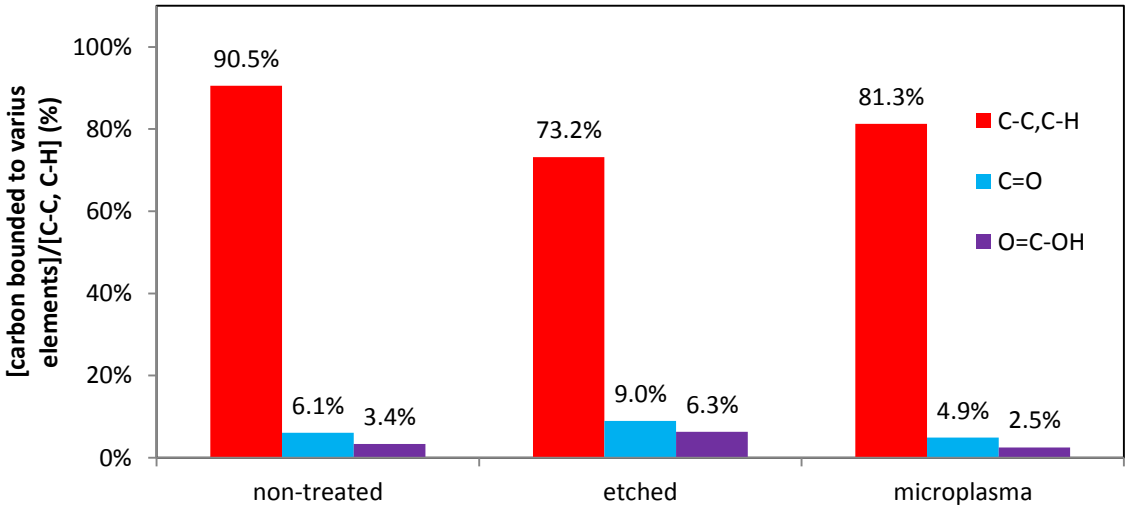

Figure 6.3.17: Percentage of functional groups in non-treated, etched and plasma treated sample normalized to carbon peak area of non-treated sample.

Plasma treatment of erucic acid breaks C-C/C-H, C=O, O=C-OH bonds what is observed by decrease of percentage of carbon peak. The difference of concentration of other functional groups is less than 1.5% which is within statistical error. The evidence that concentration oxygen containing functional groups are similar with non-treated and plasma treated samples can be seen in Figure 6.3.18. The intensities of both lines are similar with higher decrease of C-O from O=C-OH group.

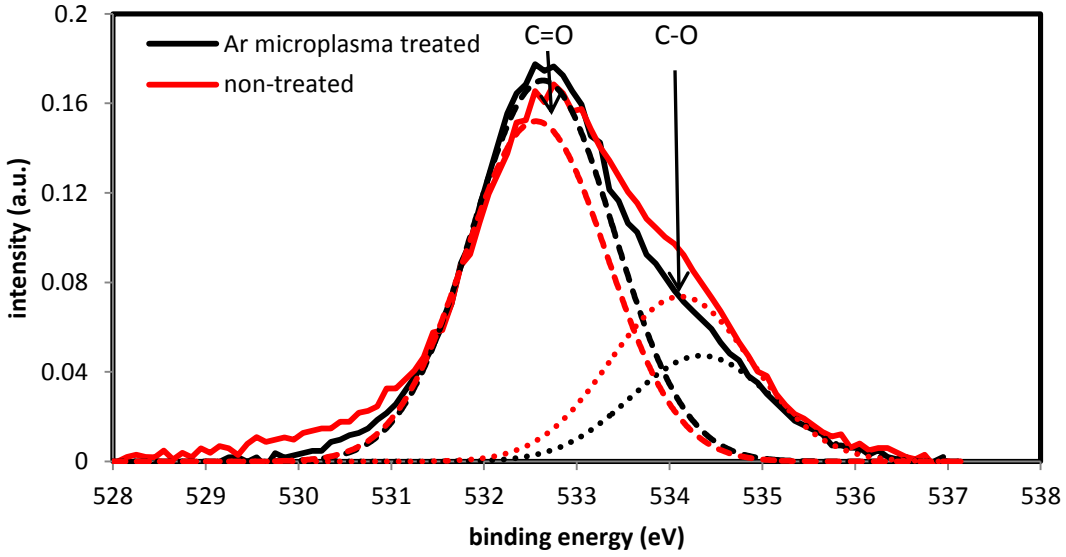

Figure 6.3.18: Oxygen spectra of non-treated erucic acid (solid red line) and fitted peaks (dashed red lines) or microplasma treated erucic acid (solid black line) and fitted peaks (dashed black lines).

6.3.3.2 *FTIR spectroscopy of Erucic acid*

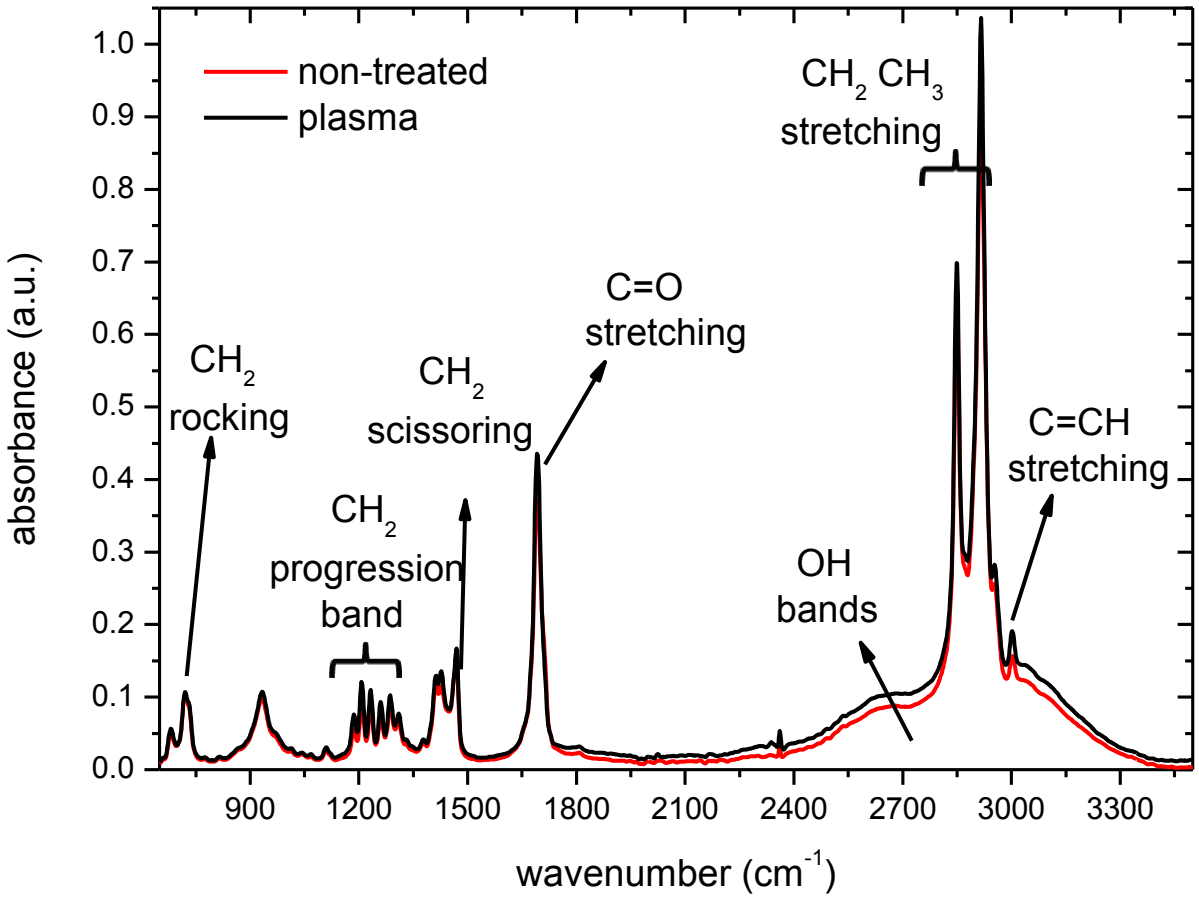

Figure 6.3.19: FTIR spectrum of 5 minutes Ar microplasma treated and non-treated erucic acid.

FTIR spectrum indicate also orthorhombic packing because of presence of progression bands and doublet of CH_2 rocking with distance 13.6 cm^{-1} before plasma treatment and 13.3 cm^{-1} after plasma treatment. CH_2 scissoring doublet change distance from 6.9 cm^{-1} to 6.1 cm^{-1}. Position of symmetric CH_2 stretching was changed from 2849.3 cm^{-1} to 2849.7 cm^{-1}. Changes are not as significant as in the case of stearic acid what can be caused by the fact that a lot of molecules are evaporated during plasma treatment.

6.3.4 Cholesterol

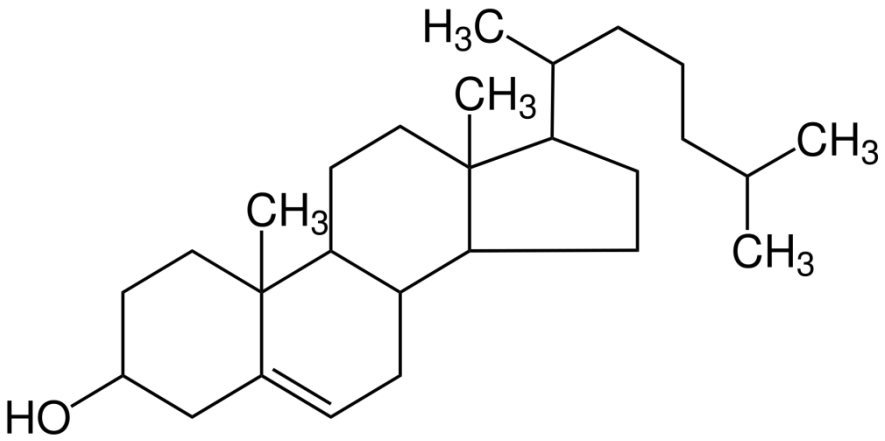

Figure 6.3.20: Structure of cholesterol.

Cholesterol (Figure 6.3.20) is an important lipid of lipid membranes composed of 27 carbon atoms, 46 hydrogen atoms and 1 oxygen atom ($C_{27}H_{46}O$). Melting temperature is 148-150°C and boiling temperature is 360°C. According chemical formula, cholesterol is composed of 3.6% of atomic oxygen when only oxygen and carbon are taken in account.

6.3.4.1 X-ray photolectron spectroscopy of Cholesterol

The concentration is higher when it is determined by XPS which is an evidence of oxidation (Figure 6.3.21).

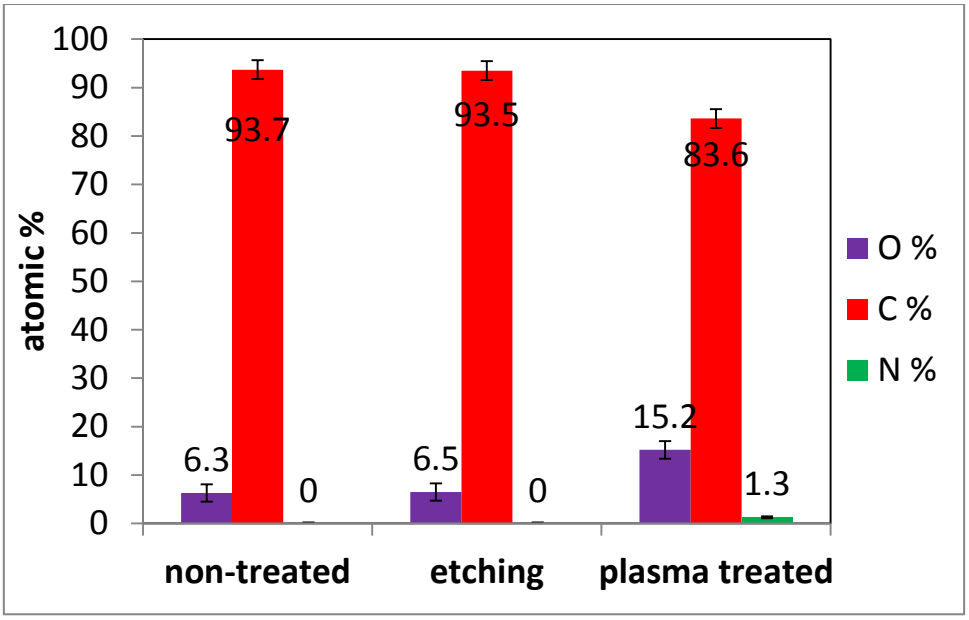

Figure 6.3.21: Concentration of elements in cholesterol sample before any treatment (non-treated), after Ar ion etching in vacuum in ESCA chamber and after Ar microplama treatment.

Etching by Ar ions did not cause changes in elemental composition. Microplasma treatment induced breaking carbon bonds and nitration of cholesterol molecule (Figure 6.3.21). Carbon spectra can be fitted by four peaks (C=C, C-H/C-C, C-O/C-N, C=O/O=C-OH) (Figure 6.3.22).

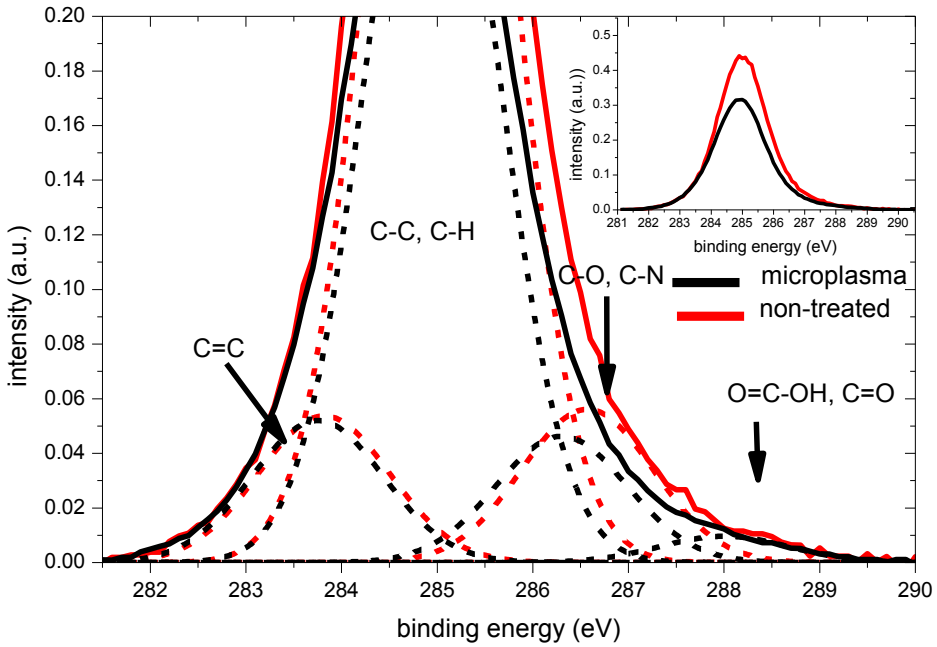

Figure 6.3.22: Carbon spectra of non-treated cholesterol (solid red line) and fitted peaks (dashed red lines) or microplasma treated cholesterol (solid black line) and fitted peaks (dashed black lines).

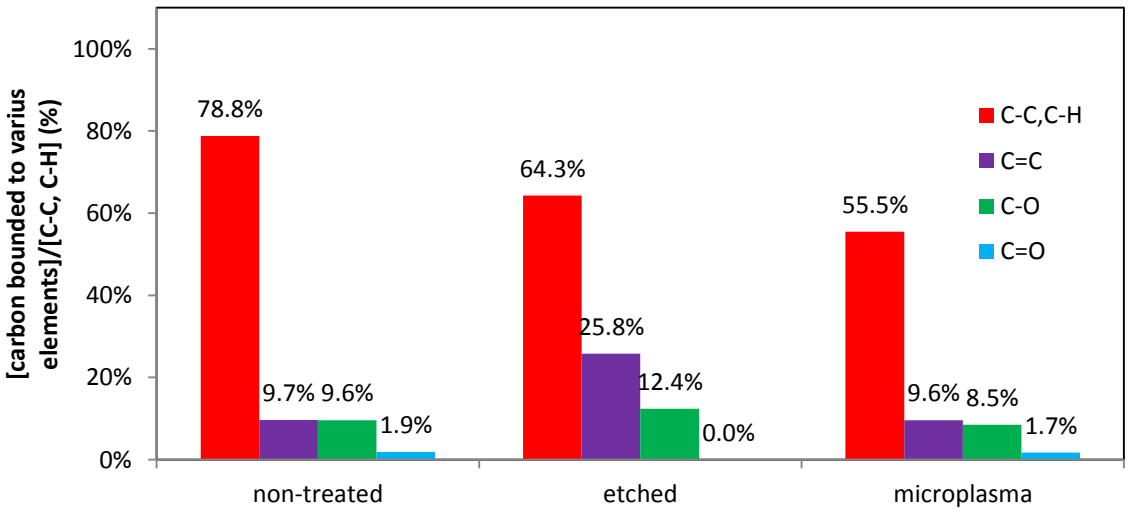

Figure 6.3.23: Percentage of functional groups in non-treated, etched and plasma treated sample normalized to carbon peak area of non-treated sample.

Decrease of C-C/C-H bonds and increase of C=C bonds can be observed by etching of cholesterol by Ar ions (Figure 6.3.23). Main difference between non-treated cholesterol and microplasma treated sample is in concentration of C-C/C-H bonds. This phenomenon induces breaking of these bonds as other bonds are comparable with non-treated sample. Oxygen spectra confirms this behavior, but in addition carboxylic groups O=C-OH are produced (Figure 6.3.24, Figure 6.3.25).

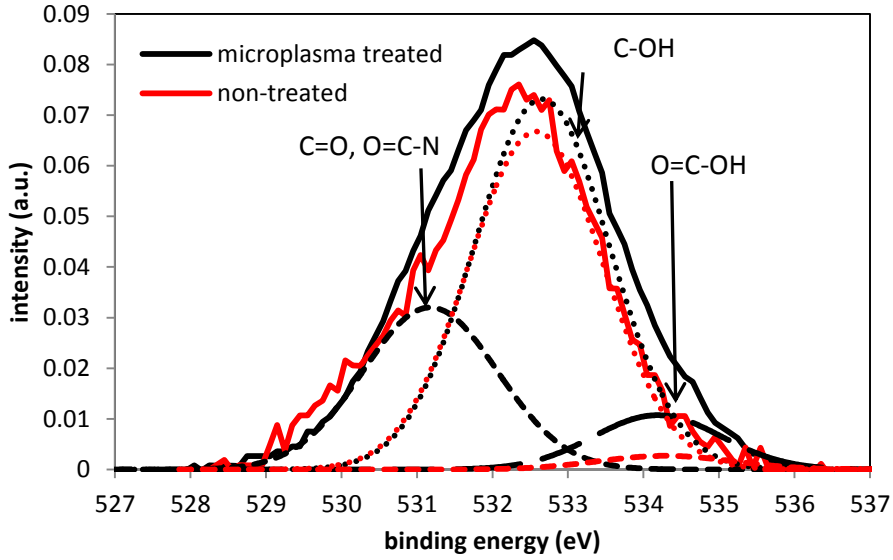

Figure 6.3.24: Oxygen spectra of non-treated cholesterol (solid red line) and fitted peaks (dashed red lines) or microplasma treated cholesterol (solid black line) and fitted peaks (dashed black lines).

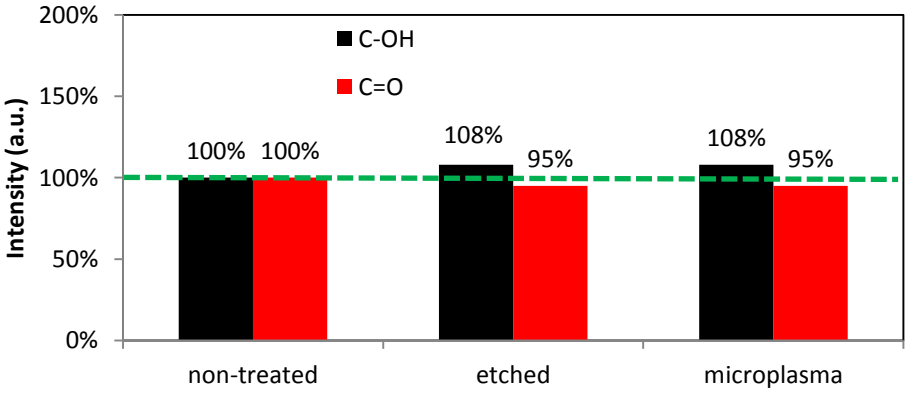

Figure 6.3.25: Change of concentration C-O and C=O functional groups of non-treated, etched and Ar microplasma treated cholesterol.

Nitrogen spectra show new peaks after plasma treatment. One at 400 eV and another at 401.5 eV with FWHM equal to 1.75 eV (Figure 6.3.26). The first one can belong to O=C-N

(399-401.1 eV) or C-N (399.8-400.9 eV) bonds and another one to $C=NH^+$ (401.2-401.9 eV) or $C-NH^+$ (401.4-402.1 eV).

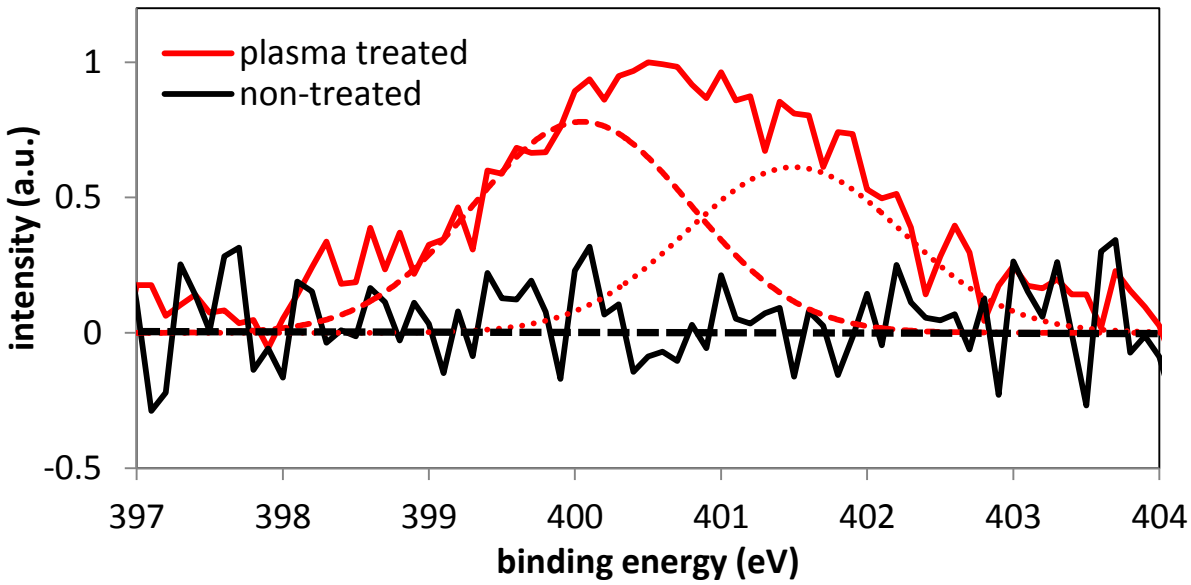

Figure 6.3.26: XPS spectra of non-treated cholesterol and 5 min treated by Ar microplasma. (Gaussian fit with FWHM = 1.75 eV is at position 400 eV and 401.5 eV).

6.3.4.2 FTIR spectroscopy of Cholesterol

FTIR spectrum shows practically no structural changes. The most of changes are visible in C=C stretching band and C-C stretching band in aromatic ring what can indicate destruction of aromatic ring causing increase of CH_2 bands. Figure 6.3.27 also shows a decrease of the thickness of OH band meaning weaker hydrogen bonding between molecules. In addition, a very small amount of C=O bands belongs to acid group (COOH).

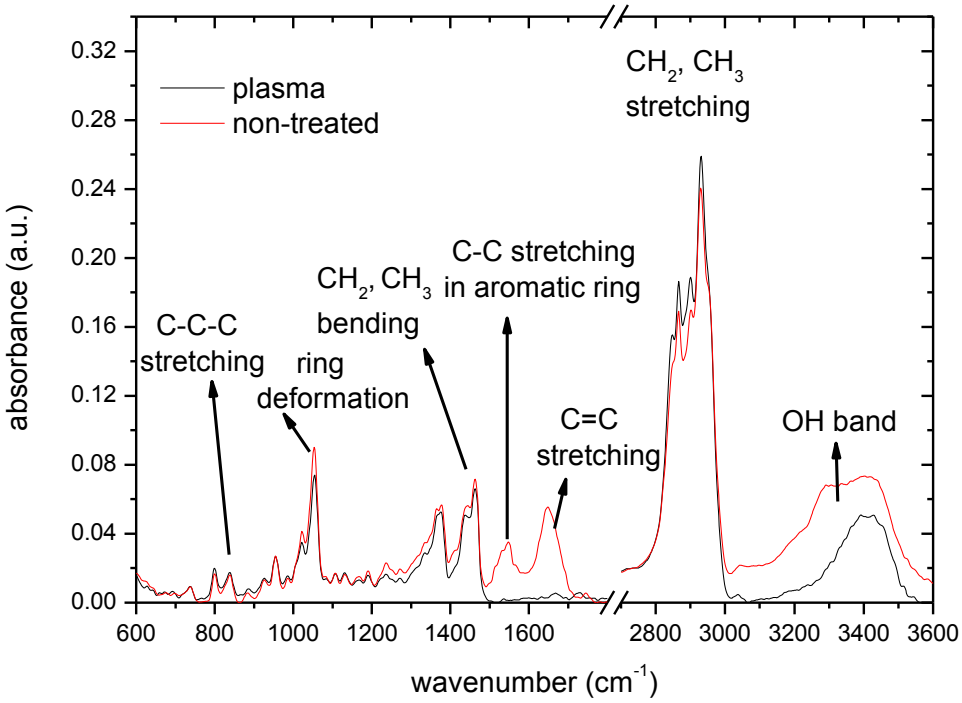

Figure 6.3.27: FTIR spectrum of 5 minutes Ar microplasma treated and non-treated cholesterol.

6.3.5 Ceramide C4

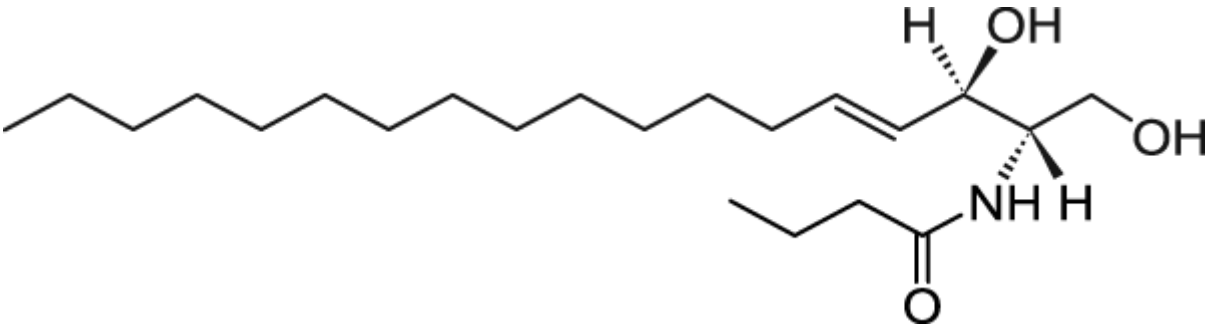

Figure 6.3.28: Structure of ceramide C4.

Ceramide C4 (Figure 6.3.28) is model ceramide used in our experiments. Ceramides are main part of lipid membranes. It is composed of 22 carbon atoms, 43 hydrogen atoms, 3 oxygen and 1 nitrogen atom ($C_{22}H_{43}NO_3$). Melting temperature is 64-67°C. According to the chemical formula, ceramide C4 is composed of 11.5% of atomic oxygen and 3.8% of atomic nitrogen, when only oxygen, carbon and nitrogen are taken in account.

6.3.5.1 *X-ray photoelectron spectroscopy of Ceramide C4*

The concentration is higher when it is determined by XPS which is an evidence of oxidation (Figure 6.3.29).

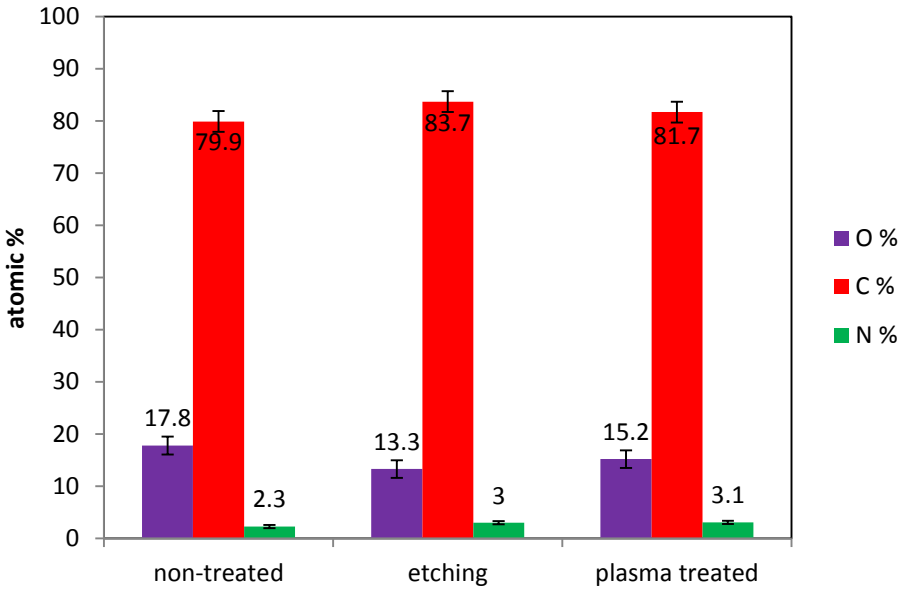

Figure 6.3.29: Concentration of elements in ceramide C4 sample before any treatment (non-treated), after Ar ion etching in vacuum in ESCA chamber and after Ar microplasma treatment.

Figure 6.3.29 and also Figure 6.3.30 shows that there are no huge changes in the elemental composition of ceramides.

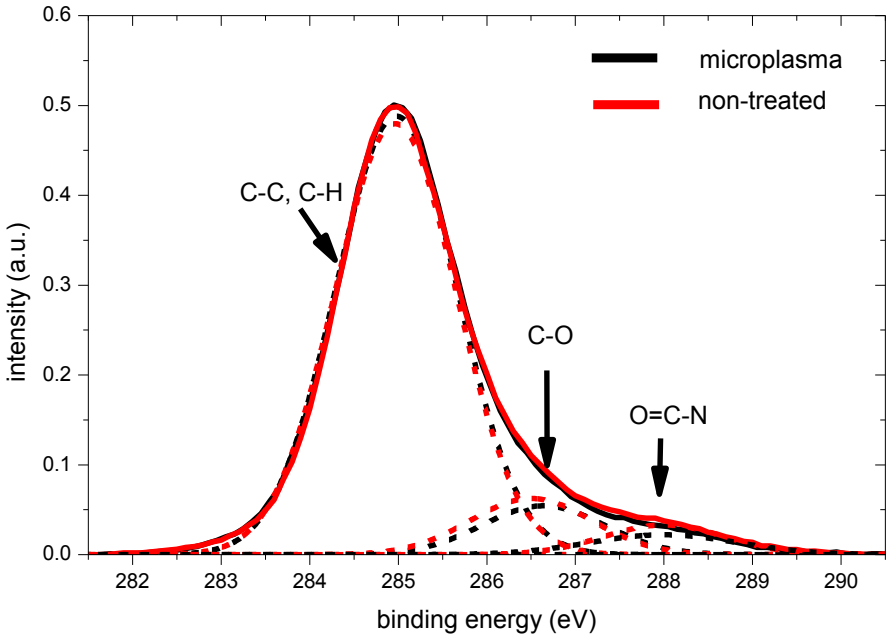

Figure 6.3.30: Carbon spectra of non-treated ceramide C4 (solid red line) and fitted peaks (dashed red lines) or microplasma treated ceramide C4 (solid black line) and fitted peaks (dashed black lines).

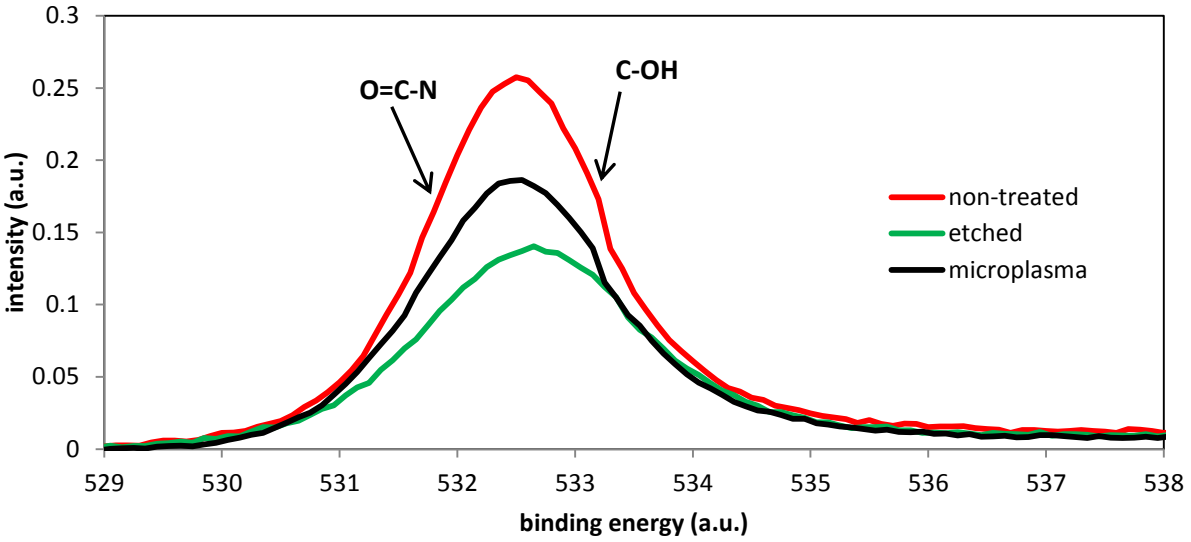

Figure 6.3.31: Oxygen spectra of non-treated ceramide C4 (red line), etched ceramide C4 (green line) and microplasma treated cholesterol (black line).

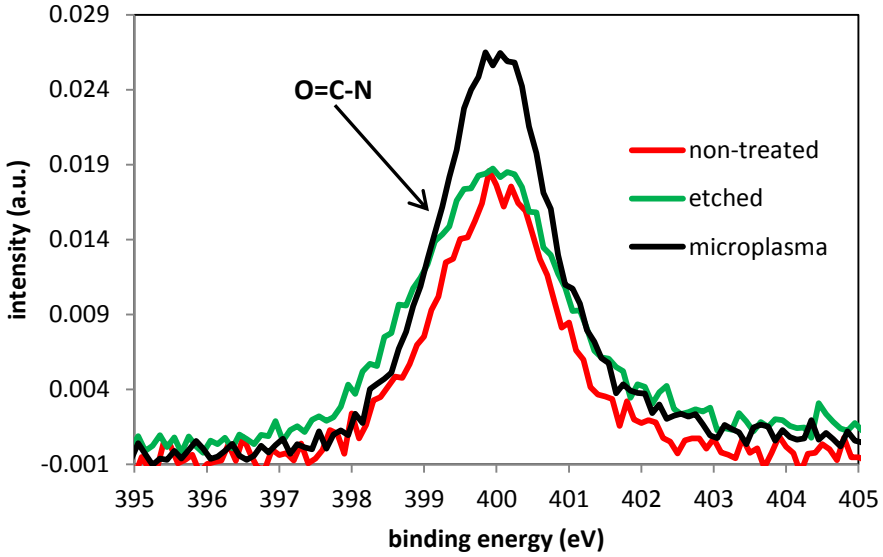

Figure 6.3.32: Nitrogen spectra of non-treated ceramide C4 (red line), etched ceramide C4 (green line) and microplasma treated cholesterol (black line).

More detailed view to nitrogen (Figure 6.3.31) and oxygen (Figure 6.3.32) spectra shows decrease oxygen bonds by etching and also by microplasma treatment of ceramide C4 and increase nitrogen bonds C-N by microplasma treatment. The oxygen bonds are difficult to distinguish because there are very close to each other. N-C=O can be found in range of (531.1 – 532.2) eV and C-O in range of (532.4 – 533.6) eV.

6.3.5.2 *FTIR spectroscopy of Ceramide C4*

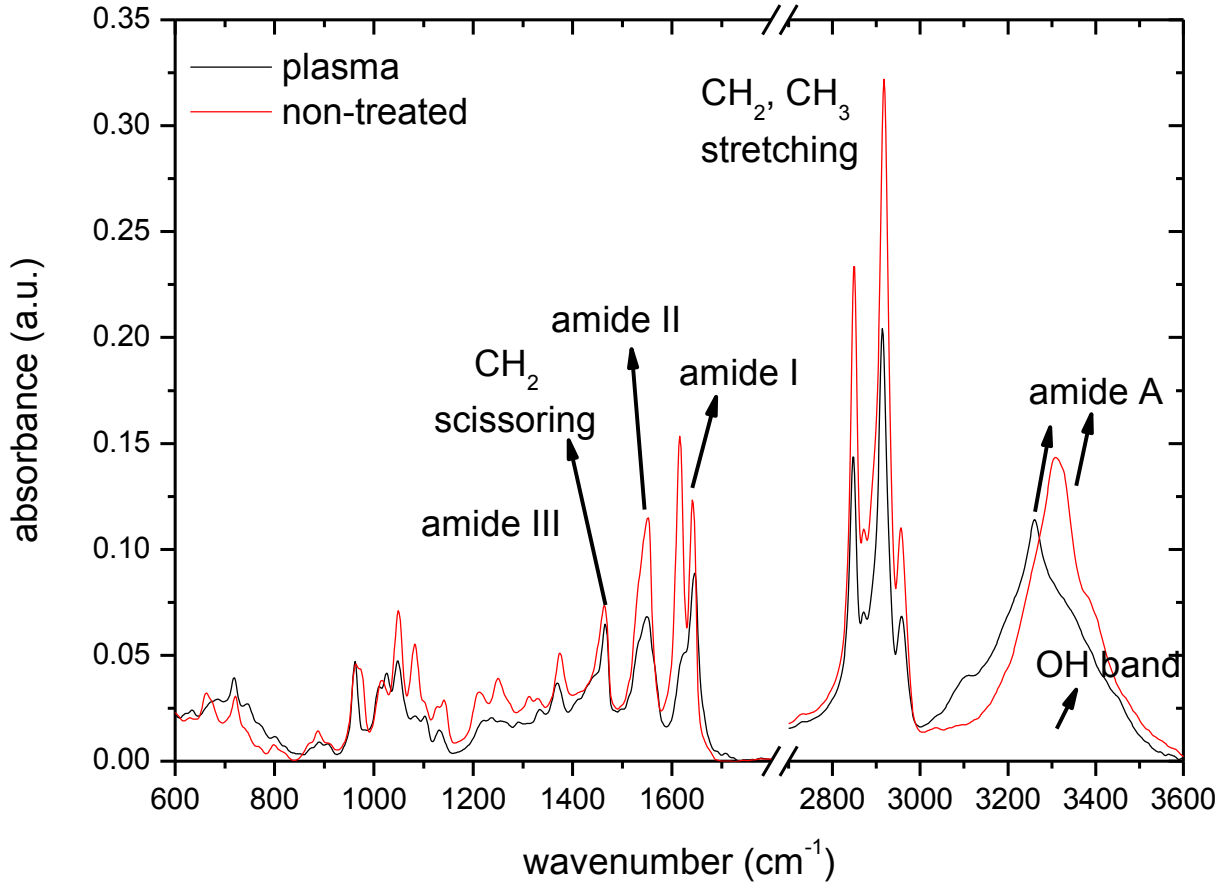

Figure 6.3.33: FTIR spectrum of 5 minutes Ar microplasma treated and non-treated ceramide C4.

FTIR spectra show significant changes of ceramide after plasma treatment. The position change of NH stretching vibrations in Amide A indicates hydrogen bonding interactions. Amide I band was split into 2 peaks, after treatment of plasma, the second peak decreased. Similar effect was observed in the work of Moore [24] during increasing of the temperature. CH_2 rocking band is shifted from orthorhombic to triclinic organization. Band was shifted from 720 cm^{-1} to 718 cm^{-1}. Similarly, symmetric stretching band is shifted from 2849.5 cm^{-1} to 2847.5 cm^{-1} indicating more solid organization.

6.3.6 Conclusion

Etching by Ar ions was effective in decreasing of C-C and C-H bonds in the case of erucic acid and also in the cholesterol with cyclic structure. When C-C, C-H bonds decrease, the number of carbon bonded to oxygen by single bonds increase (number of oxygen double bonds decrease). On the other hand, C-C and C-H bonds of ceramide and stearic acid were very stable to etching by argon ions but the number of carbons bonded to oxygen decreased.

Plasma treatment of lipids decrease number of C-C and C-H bonds about 10 % in the case of stearic acid and erucic acid and 25% in the case of cholesterol. The number of oxygen and nitrogen bonds increased (erucic acid had no nitrogen bonds.). In the case of ceramide, number of C-C, C-H bonds was not changed, but the number of oxygen bonds was decreased.

The structure of stearic acid and erucic acid was orthorhombic with increase of lattice after plasma treatment. Cholesterol and ceramide was structurally more seriously changed after plasma treatment but no increase of lattice, as observed.

6.4 Plasma treatment of the skin

6.4.1 Motivation and sample preparation

Pig skin of Yucatan micropig from Charles River Japan, Inc. (Yokohama, Japan) was used for investigating of the influence of the plasma treatment. The pig skins were stored at −20 °C in a freezer before the experiment. At first, the fat layer of the skin was removed by using a knife, then it was cut and soaked at 4 °C in phosphate buffered saline (PBS) for 3 h, and then after a bath in 60 °C PBS for 1 min, the epidermal layer of a thickness of 200 mm was peeled by using tweezers. Finally, the skin sample was cut to 3×3 mm^2 attached to plastic sheet by using double-sided tape. FTIR-ATR observation allows us to investigate structure changes of the skin after plasma treatment. Comparison with heating and UV irradiation will help us to isolate some phenomena and assigned them to certain processing of the skin.

6.4.2 FTIR spectroscopy of plasma treated skin

6.4.2.1 Effect of plasma jet treatment time

Prepared skin samples were treated gradually by Ar plasma jet and their spectra were measured by FTIR-ATR spectrometer after total treatment of 0, 10, 30, 60, 120, 420 and 900 s. Skin temperature evolution during treatment where measured by thermocamera and it is depicted in Figure 6.4.1. The reason why this temperature is lower than in chapter 6.1.3 is that

skin has much lower dimension and heat is transferred to the base under sample. Another reason can be also the lower amount of water in the skin.

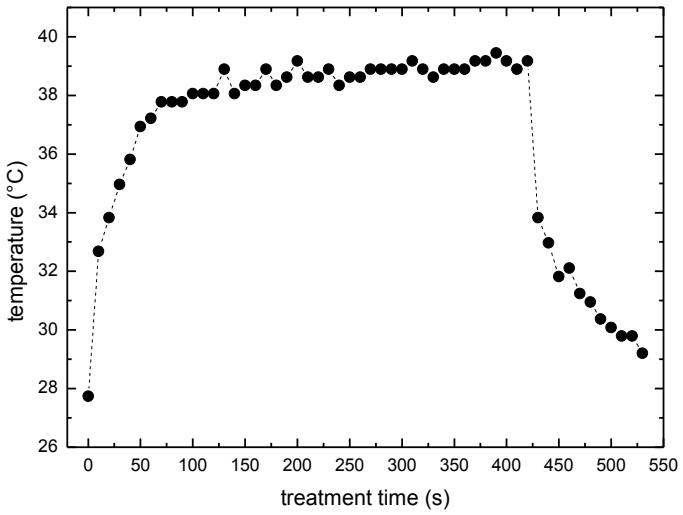

Figure 6.4.1: Temperature evolution of the skin sample treated 420 s by Ar plasma jet.

Water OH bands

Figure 6.4.2 shows typical ATR-FTIR spectra of stratum corneum layer (white line). The spectrum is overlapped by many vibrational bands and the analysis is not simple. A huge part of the spectrum is covered by OH bands coming from liquid water present in the epidermal layer (green line in Figure 6.4.2). To subtract these bands, spectrum of distilled water was measured. This spectrum was scaled in such a way that after subtraction, zero spectrum was achieved in the range (1800 – 2000 cm^{-1} and 3400 – 4000 cm^{-1}). Resulted spectrum (blue line in Figure 6.4.2) was analyzed further. According scaling factor, we were able to detect relative changes of water content in stratum corneum. Plasma jet treatment caused a decrease of water content in stratum corneum to approximately 30% of initial value. This value was saturated between 120 and 420 seconds of treatment (Figure 6.4.3). There are two reasons of increased water evaporation after plasma treatment of the skin. The first one is heating of the sample. The second one is an increase of the permeability of the stratum corneum [25].

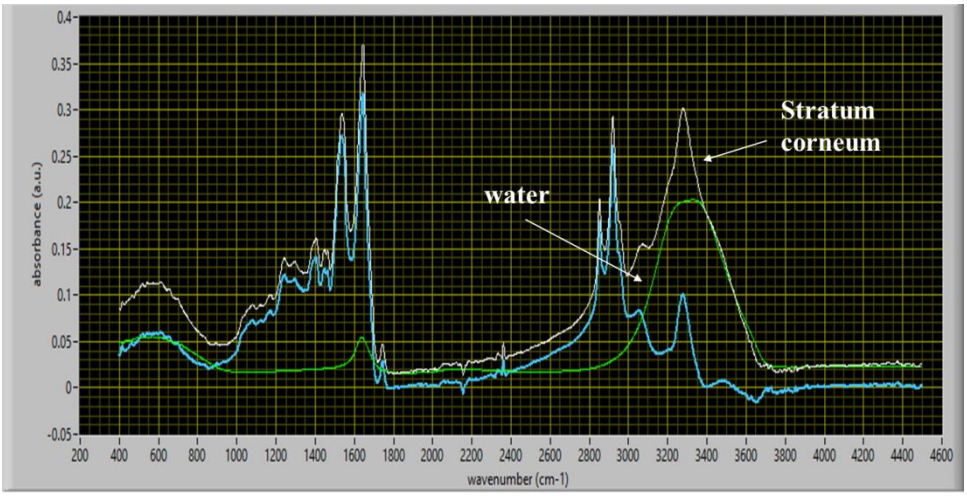

Figure 6.4.2: Spectrum of stratum corneum (white), spectrum of water (green), stratum corneum spectrum after substraction of water.

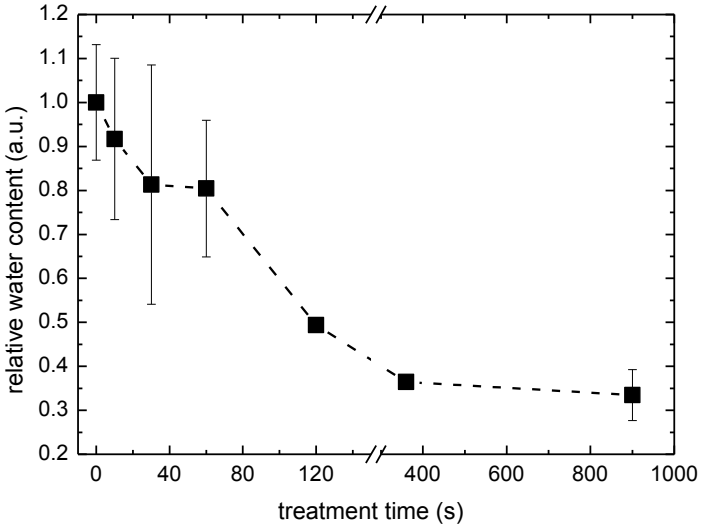

Figure 6.4.3: Relative water content in stratum corneum during plasma treatment.

Methyl CH_3 and Methylene CH_2 bands

Bandwidth and absorbance determined by area of the vibrational bands depicted by Figure 6.4.4 were analyzed. Lipids of the stratum corneum are characterized by methylene symmetric and asymmetric stretches at 2850 cm^{-1} and 2920 cm^{-1} and methyl asymmetric stretches at 2955 cm^{-1} (Figure 6.4.4A). Methyl symmetric stretches vibration comes from proteins. These bands were analyzed by Gaussian fit. To increase the precision of the fit, the 2^{nd} derivation of the spectra was also fitted. Second derivation was scaled to have

approximately the same effect on result as spectrum (Figure 6.4.4B). Asymmetric stretching band of CH_2 was simulated by three Gaussian peaks (Figure 6.4.4A).

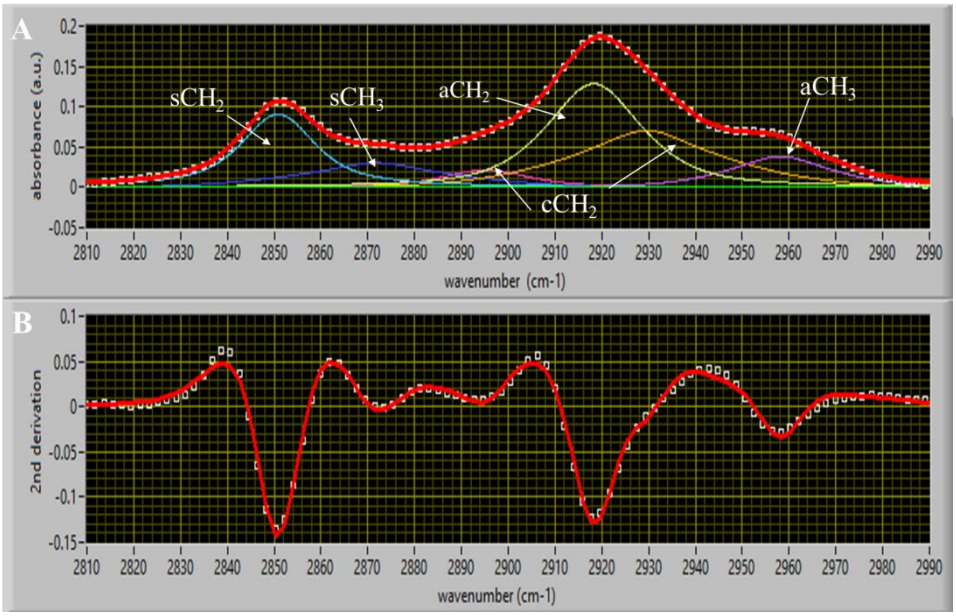

Figure 6.4.4: Simulation of methyl and methylene symmetric and asymmetric stretches of CH_3 and CH_2.
A: Experimental spectrum (white points) with simulated spectrum (red). Resolved peaks are sCH_2 (symmetric stretches vibration of CH_2), aCH_2 (asymmetric stretches vibration of CH_2), sCH_3 (symmetric stretches vibration of CH_2), aCH_3 (symmetric stretches vibration of CH_3), two components of cCH_2 (two components of the **as**ymmetric stretches vibration of CH_2),
B: The second derivation of experimental spectrum (white points) and the second derivation of simulated spectrum (red).

Absorbance of all bands decreased which induced the extraction of lipids as it is shown in Figure 6.4.5. We could also observe the change of bandwidth which is connected with the structural changes of lipids. Bandwidth of asymmetric methylene stretching band increased from 16 cm^{-1} to 19 cm^{-1} and symmetric methylene stretching band increased 14.7 cm^{-1} to 16.5cm^{-1}, as it is shown in Figure 6.4.6. In the case of the bandwidth and also absorbance, saturation effect was achieved after 120 s of the skin treatment.

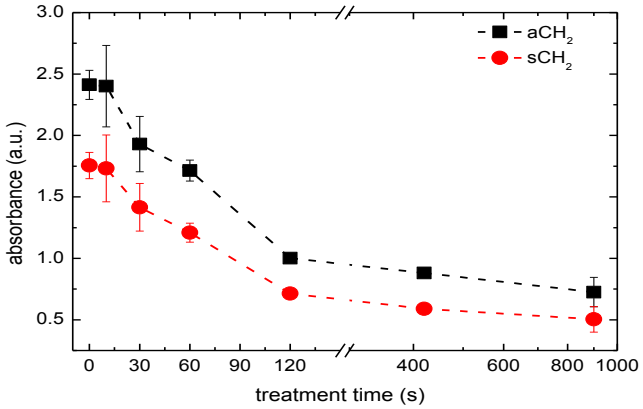

Figure 6.4.5: Absorbance of methyl and methylene symmetric and asymmetric stretches of CH_3 and CH_2. sCH_2 is the symmetric stretches vibration of CH_2, aCH_2 is the asymmetric stretches vibration of CH_2, sCH_3 is the symmetric stretches vibration of CH_2, aCH_3 is the symmetric stretches vibration of CH_3.

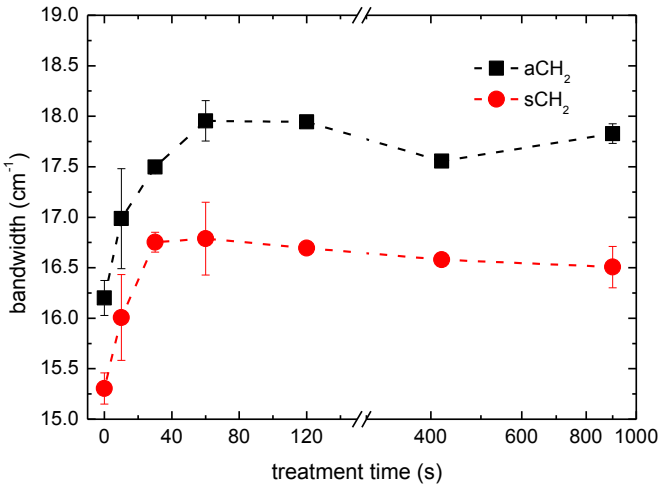

Figure 6.4.6: Bandwidth of methyl and methylene symmetric and asymmetric stretches of CH_3 and CH_2. sCH_2 is the symmetric stretches vibration of CH_2, aCH_2 is the asymmetric stretches vibration of CH_2, sCH_3 is the symmetric stretches vibration of CH_2, aCH_3 is the symmetric stretches vibration of CH_3.

The ratio of symmetric stretching band of CH_2 and CH_3 can give us information about the chain length of the skin lipids. Absorbance ratio of these bands sCH_3/sCH_2 indicates sharp decrease of chain length till 120 s of treatment time and further the ratio is changed only very slightly (Figure 6.4.7.). Absorbance of symmetric bands gives information about skin lipids and asymmetric stretching band gives information about proteins. Their ratio correlates with stratum corneum thickness and the ratio is saturated after 120 s. This saturation showed that etching process was stopped by this time (Figure 6.4.7).

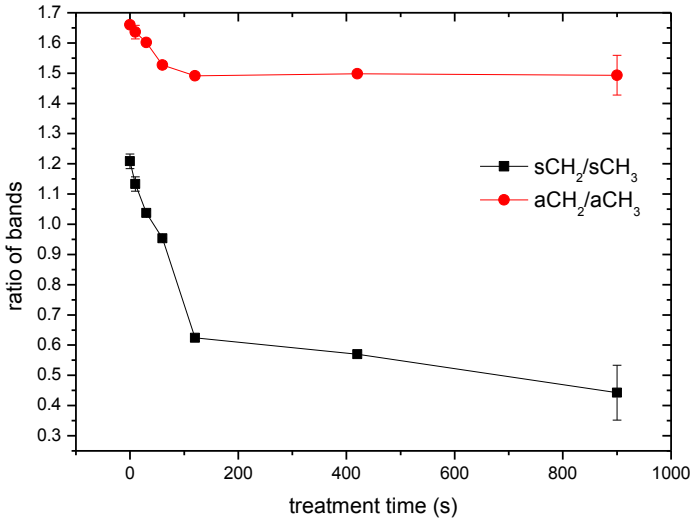

Figure 6.4.7:The ratio of methyl and methylene symmetric and asymmetric stretches of CH_3 and CH_2. sCH_2 is the symmetric stretches vibration of CH_2, aCH_2 is the asymmetric stretches vibration of CH_2, sCH_3 is the symmetric stretches vibration of CH_2, aCH_3 is the symmetric stretches vibration of CH_3.

We did not observe relevant shift of symmetric CH_2 band indicating change of fluidity of lipid bilayer (Figure 6.4.8).

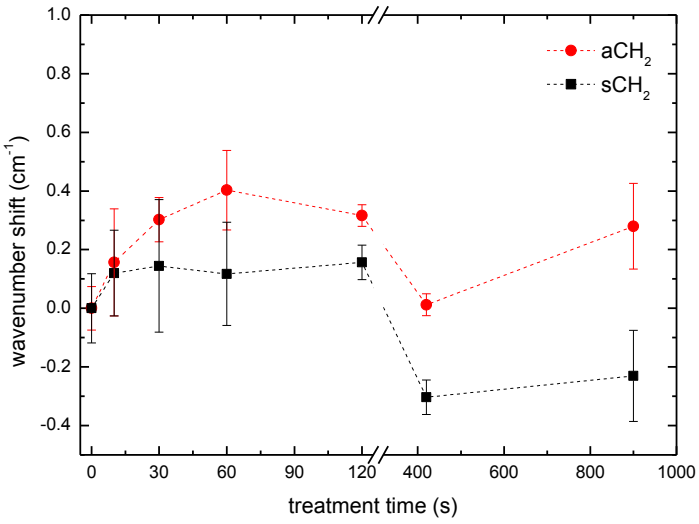

Figure 6.4.8: Wavenumber shift of methyl symmetric sCH_3, methylene symmetric sCH_2 and methyl asymmetric aCH_3, methylene asymmetrica sCH_2 .

C=O stretching vibrational bands

Position of C=O stretching band strongly depends on structure of molecule and it can be found from 1600 cm^{-1} to 1780 cm^{-1}. C=O stretching bond at 1744 cm^{-1} belong to ester

bonds [26] and near 1710 cm^{-1} to fatty acids and also to skin sebum. Sebum is composed from glycerides, free fatty acids, wax esters, squalene, cholesterol esters and cholesterol [27]. These sebum molecules were partially extracted/decomposed by plasma treatment (Figure 6.4.9). On other hand, absorbance of fatty acid is increasing. This can be caused by hydrolysis of esters and it seems that after 120 s of treatment, fatty acids are decomposed, too.

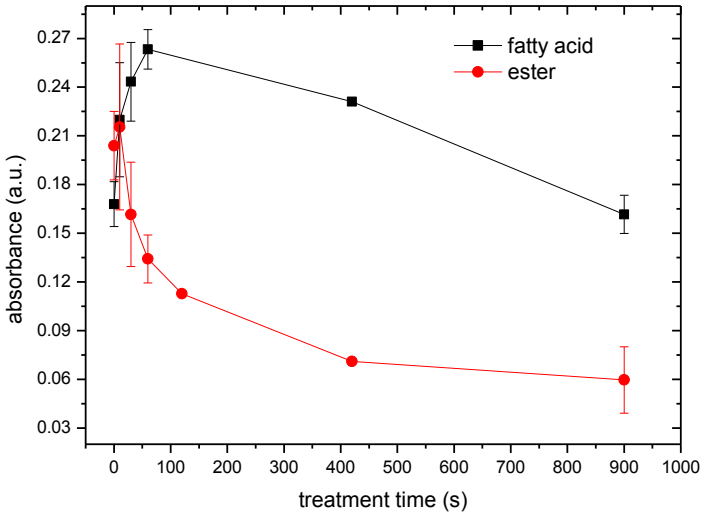

Figure 6.4.9: Evolution of absorbance of ester C=O stretching band and fatty acid C=O stretching band.

6.4.2.2 UV effect

To investigate the effect of UV radiation, we irradiated skin samples through the borosilicate glass (BK7), PEN film or MgF_2 glass. Transmittance through these materials is shown in Figure 6.4.10. We also used lamp with emission at 254 nm and another lamp with emission at 365 nm. UV A radiation has range 315-400 nm and it is assigned to radiation through the borosilicate glass (BK7) and lamp with emission at 365 nm. UVB radiation has range 280-315 nm it is assigned to radiation of lamp at 254 nm. UVC radiation has range 100-280 nm and it is assigned to radiation through the MgF_2 glass. Radiation through the PEN film is assigned to visible radiation. Changes of bandwidths of asymmetric stretching band after 1 minute of irradiation by plasma jet are shown in Figure 6.4.11. We can suppose that irradiation of sample by visible light or by UVA should have almost no effect. However, results shows that neither UVB nor UVC have no effect on structure of the skin lipids during so short time of irradiation. Also Figure 6.4.12 shows no change of fluidity or lipid chains after UV irradiation.

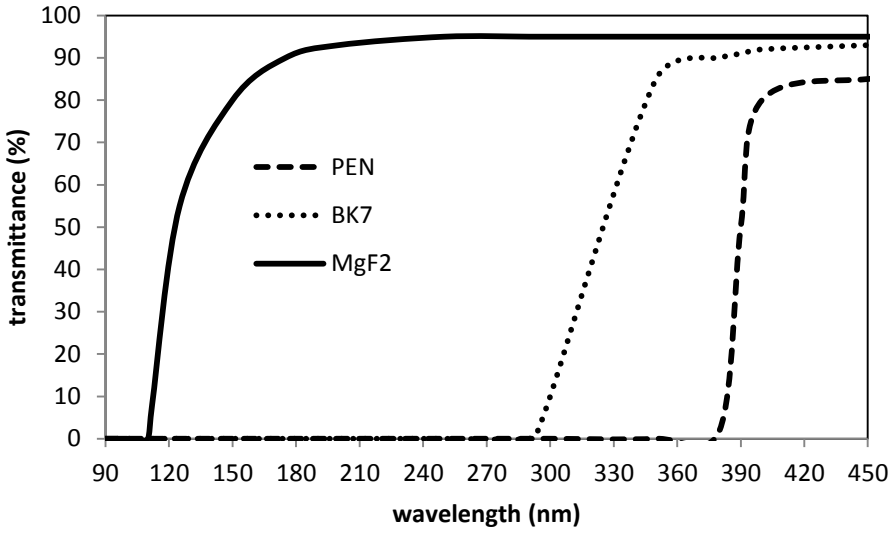

Figure 6.4.10: Transmittance of PEN film, BK7 – borosilicate glass and MgF_2 glass.

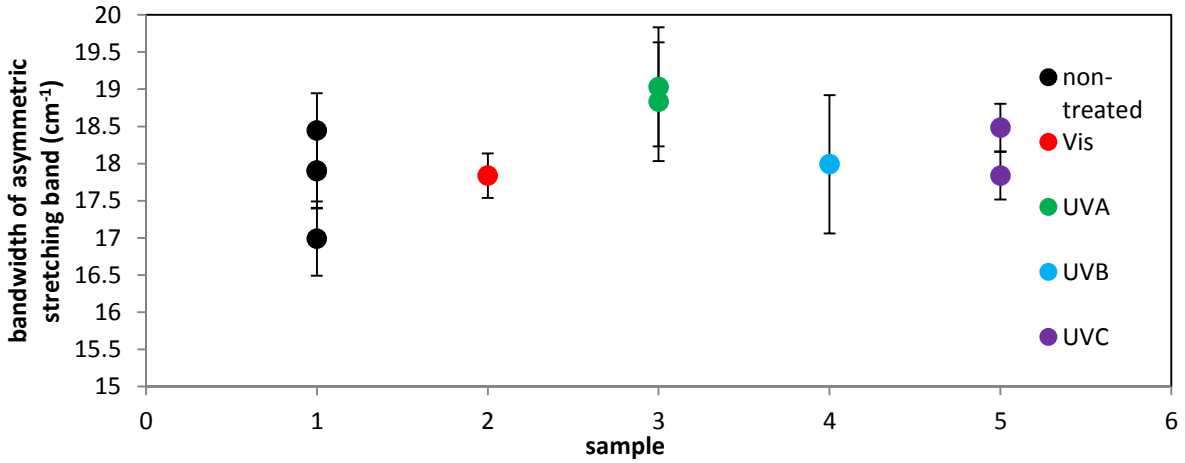

Figure 6.4.11: Bandwidth of asymmetric stretching CH_2 band after 1 minute irradiation by visible light, UVA, UVB, and UVC light.

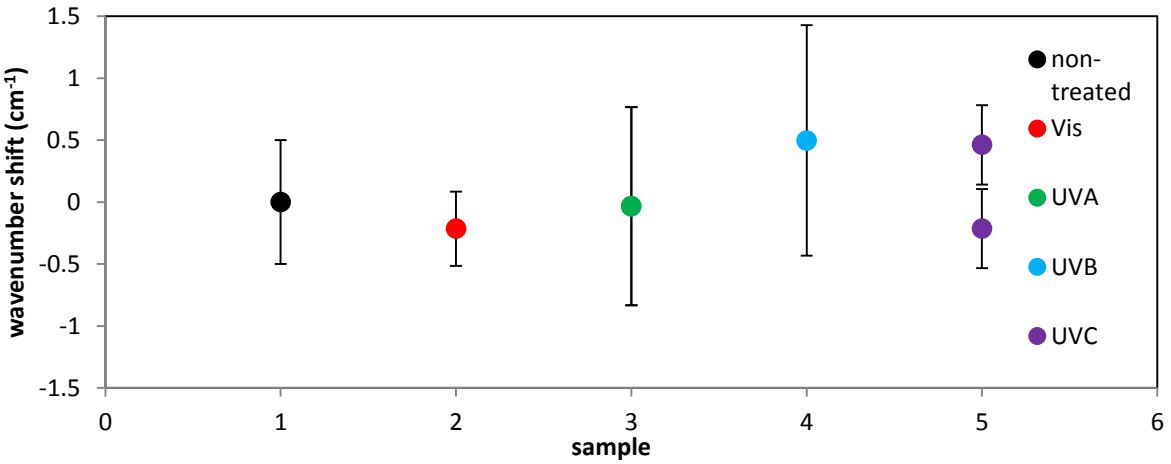

Figure 6.4.12: Change of wavenumber shift of symmetric and asymmetric CH_2 stretching bands by microplasma.

6.4.2.3 Heat effect

During plasma treatment of the skin, not only UV light could have some effect, but also the heat generated by plasma. Figure 6.4.13 shows how the temperature of skin was changed for different voltages applied to plasma jet. When 3.2 kV or 4 kV are applied, temperature of skin will reach 40°C or 45°C, respectively. But at 7 kV, it is already 90°C. After plasma treatment, the temperature will decrease to the initial value approximately after 100 s.

.

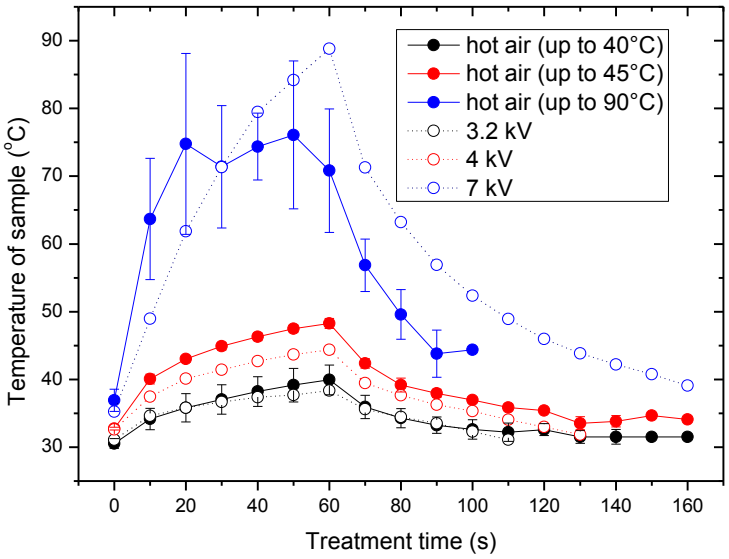

Figure 6.4.13: Temperature of the skin heated by fan hot air or plasma jet with different voltages.

To eliminate effect of plasma, we used hot air of a fan to increase temperature of the skin sample to simulate condition during plasma treatment. Observation of ratio CH_2/CH_3 of

stretching bands demonstrated that this ratio did not change. We can conclude that heating of sample did not etch of stratum corneum neither break C-H bonds (Figure 6.4.14).

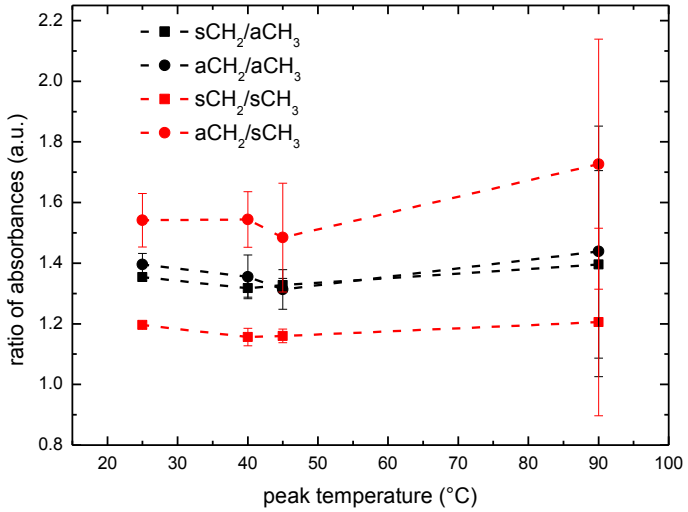

Figure 6.4.14: Ratio of methyl and methylene symmetric and asymmetric stretches of CH_3 and CH_2. sCH_2 is the symmetric stretches vibration of CH_2, aCH_2 is the asymmetric stretches vibration of CH_2, sCH_3 is the symmetric stretches vibration of CH_2, aCH_3 is the symmetric stretches vibration of CH_3.

However, absorbance of lipid CH_2 band decreased linearly with increase of peak temperature (Figure 6.4.15). Also bandwidth increased, but it is almost constant till 45°C (Figure 6.4.16).

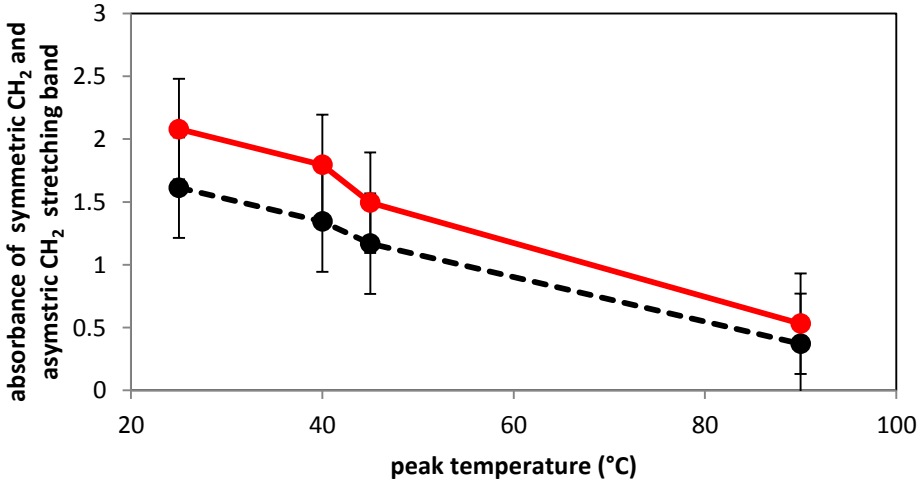

Figure 6.4.15: Absorbance of methylene symmetric (black line) and asymmetric (red line) stretches of CH_2 at different peak temperatures.

More dramatic increase happened at peak temperature 90°C. It is known that heating of skin can increase bandwidth of CH_2 bands and it is explained by the increase of space in lipid bilayer and molecules have more space with any type of rotation which is connected with the bandwidth. An increase of bandwidth to 90°C can be caused by serious damage.

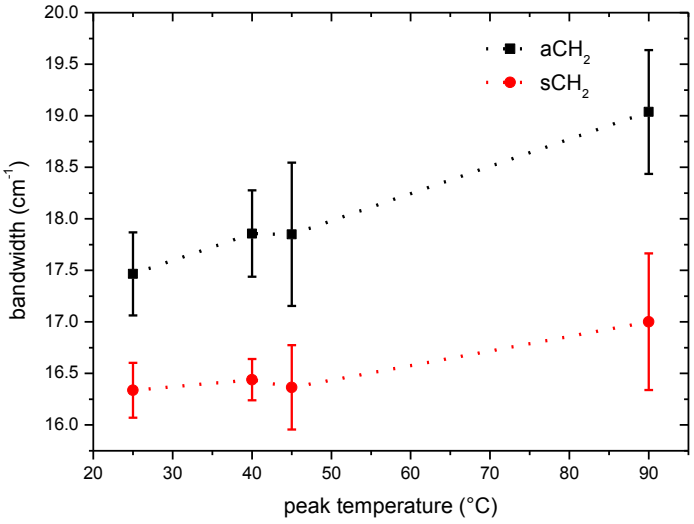

Figure 6.4.16: Bandwidth of methylene symmetric (red line) and asymmetric (black line) stretches of CH_2 at different peak temperatures.

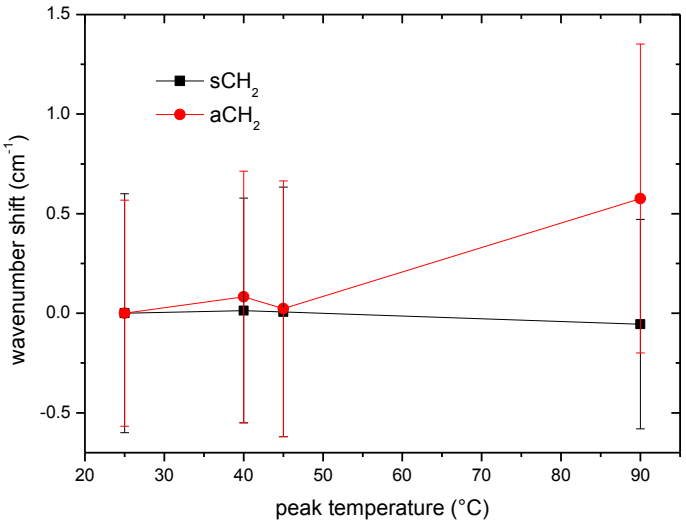

Figure 6.4.17: Wavenumber shift depending on peak temperature.

However, we did not notice any change of fluidity which can be shown by change of the wavenumber (Figure 6.4.17). Fluidity of lipids chains can be increased by heating but when temperature decrease, fluidity decreases, too.

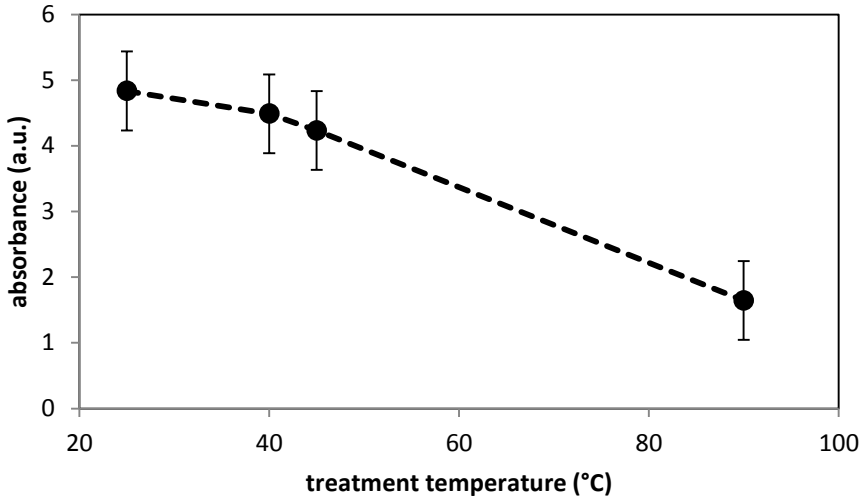

Figure 6.4.18: Absorbance of Amide A N-H stretching band at different peak temperatures.

Amide A band (at 3280 cm^{-1}) comes from the N-H stretching of proteins. This band is insensitive to protein conformations and exclusively depends on N-H bond which allows us to determine protein concentration from absorbance of the band [28]. The position of Amide A depends on the strength of hydrogen bonds [29]. According to Olsztynska-Janus *et* al., when N-H is involved in the hydrogen bond, N-H stretching vibration can be shifted to lower wavenumbers. A decrease of absorbance demonstrate a decrease of the number of N-H in amide (C=O)-NH structure and probably decomposition of proteins.

6.4.2.4 *Effect of sample distance from electrode*

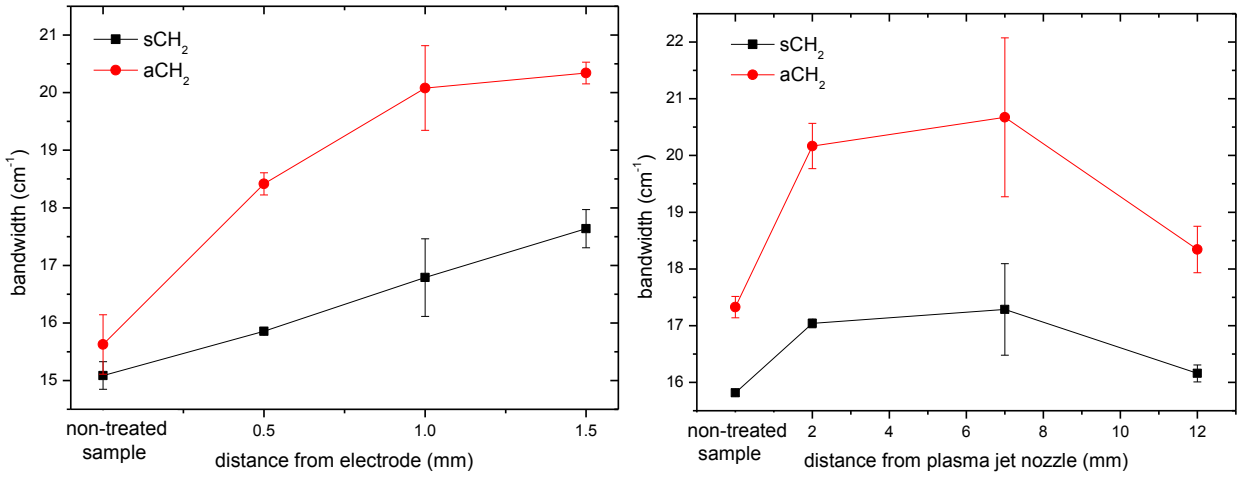

Figure 6.4.19: Change of bandwidth of symmetric and asymmetric CH_2 stretching bands by microplasma (left) treatment and plasma jet (right) treatment at various distances.

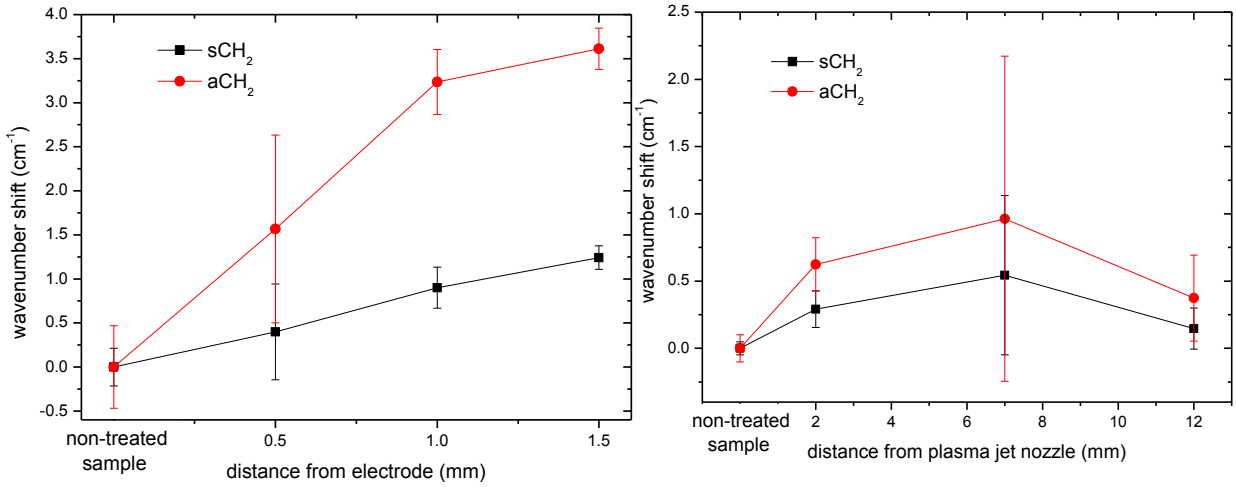

Figure 6.4.20: Change of wavenumber shift of symmetric and asymmetric CH_2 stretching bands by microplasma (left) treatment and plasma jet (right) treatment at various distances.

Skin samples were treated at 0.5, 1 and 1.5 mm by microplasma and treated by plasma jet at distance 2 mm (in the plasma), 7 mm (at the edge of plasma) and 12 mm (outside of plasma). Figure 6.4.19 left shows an increase of the bandwidth of symmetric and asymmetric CH_2 stretching bands with distance from electrode. Increase of bandwidth means increase of space between lipid chains. Plasma jet treatment caused increase of bandwidth, too, but it is independent on distance while sample is in contact with plasma. When the samples is outside of plasma of plasma jet, the bandwidth does not change or only minimal

change happened, as seen in Figure 6.4.19 (right). Figure 6.4.20 demonstrates the change of the wavenumber of symmetric and asymmetric CH_2 stretching bands after microplasma and plasma jet treatment. Change of wavenumbers indicates change of density of lipid chains. Qualitative dependence is the same like in Figure 6.4.19. The reason why the wavenumber shifts and bandwidth increased can be higher concentration of air in plasma with increasing distance between sample and microplasma electrode. Microplasma can change fluidity of the skin more than plasma jet.

6.4.2.5 Principle component analysis

For the principle component analysis of second derivation of FTIR spectra of non-treated samples, microplasma treated samples at 0.5 mm, 1 mm, 1.5 mm and plasma jet treated samples at 2 mm, 7 mm and 12 mm were prepared. We used FTIR spectra from 1400 cm^{-1} to 4000 cm^{-1}.

The wavenumber was used as parameter of the samples. Score plot shows clear difference between microplasma and plasma jet treated samples. Non-treated samples used for plasma jet and microplasma treatment are also separated probably because they were prepared in different days (Figure 6.4.21). In Figure 6.4.21 only values indicated peak in second derivation spectra was used. Graph also shows clear difference between plasma treated and non-treated samples (Figure 6.4.22). Loading plot (Figure 6.4.23) can show us parameters which can change together. Loading plot shows that changes in proteins and lipids occur independently. Also esters and carboxylic acids of sebum change independently.

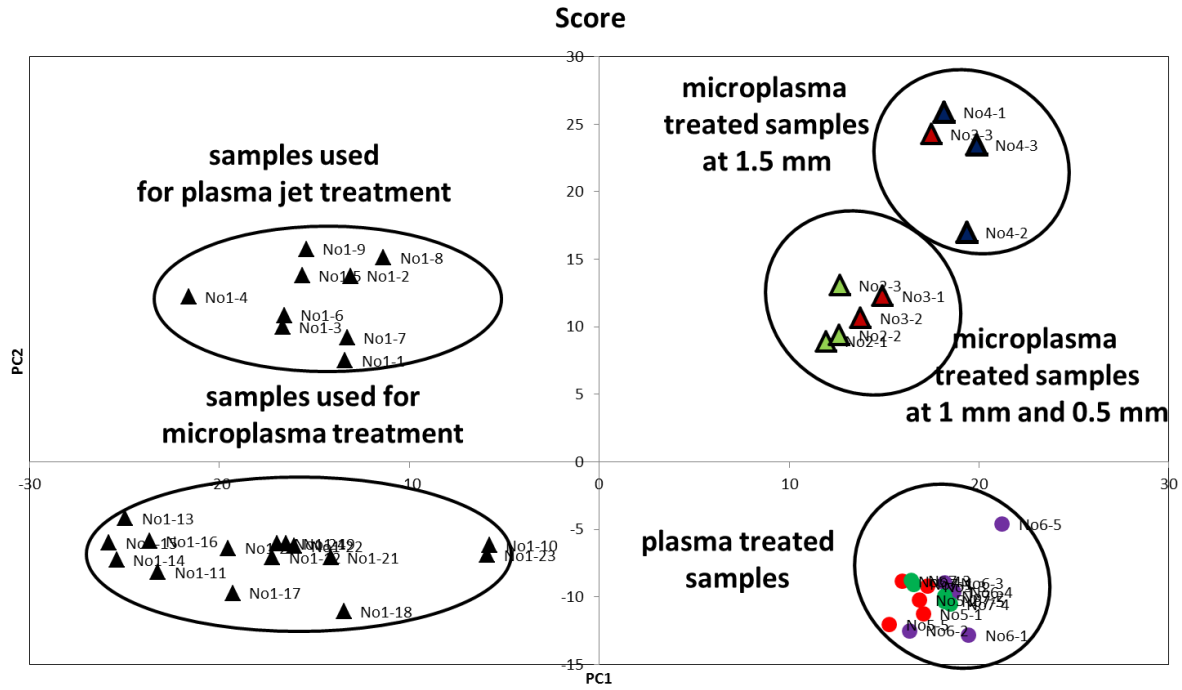

Figure 6.4.21: Score plot: black triangles – non-treated samples, red circles –plasma jet treatment at 2 mm, violet circles – plasma jet treatment at 7 mm (edge of plasma), green circles – plasma jet treatment at 12 mm (outside of plasma), green triangles – microplasma treatment at 0.5 mm, red circles – plasma treatment at 1 mm, blue circles – microplasma treatment at 1.5 mm.

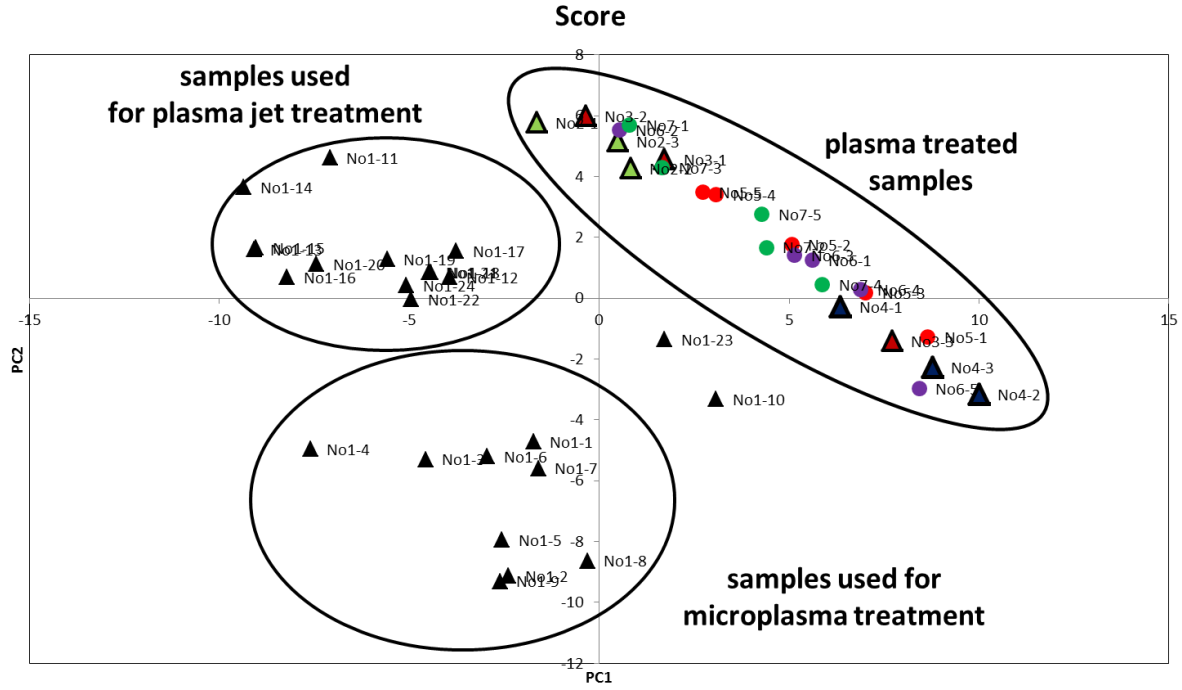

Figure 6.4.22: Score plot: black triangles – non-treated samples, red circles –plasma jet treatment at 2 mm, violet circles – plasma jet treatment at 7 mm (edge of plasma), green circles – plasma jet treatment at 12 mm (outside of plasma), green triangles – microplasma treatment at 0.5 mm, red circles – plasma treatment at 1 mm, blue circles – microplasma treatment at 1.5 mm.

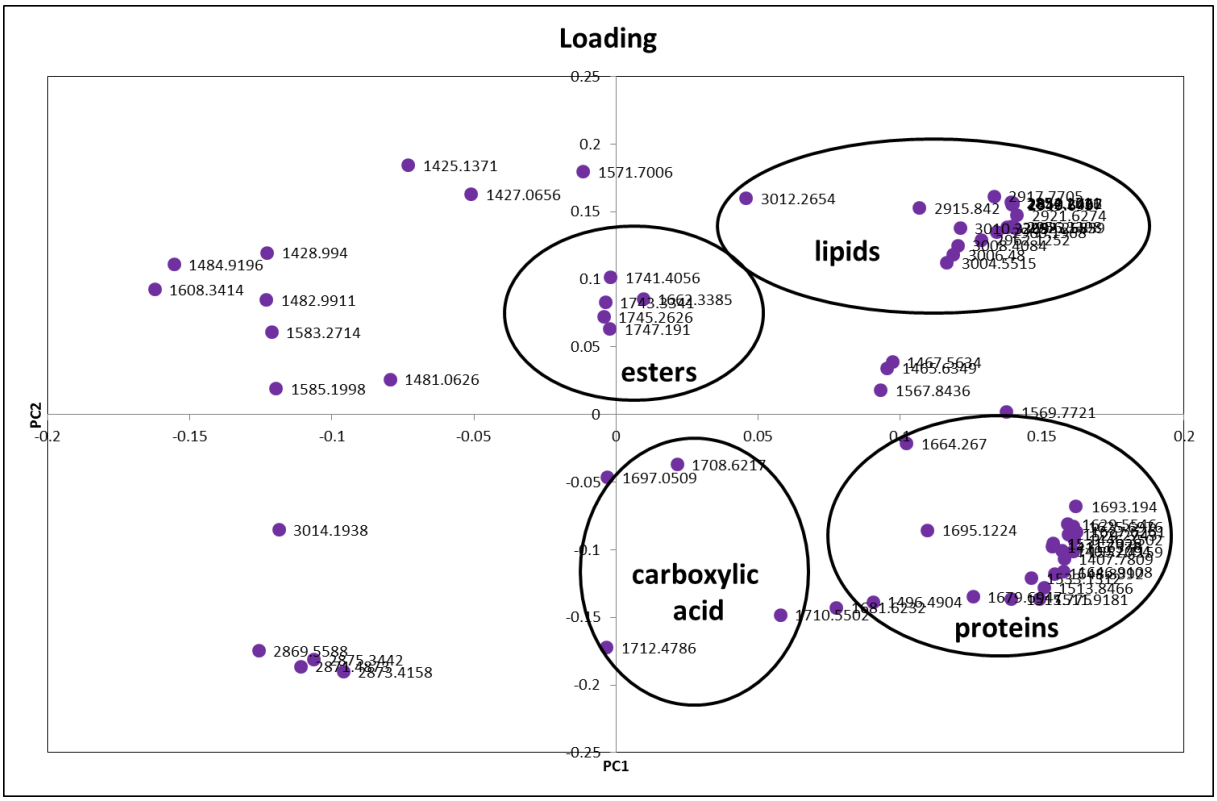

Figure 6.4.23 Loading plots describing FTIR peaks which depends to each other.

6.4.3 Transmission electron microscopy

Full thickness (dermal + epidermal layer) skin was cut to ultra-thin sheets by ultra-microtome to observe lamellar structure of lipid matrix. This matrix can be observed as bright lines with dark space in between. Bright lines represent lipid tail and dark space represents hydrophilic heads [30]. Unaltered lipid lamellae are shown in Figure 6.4.24.

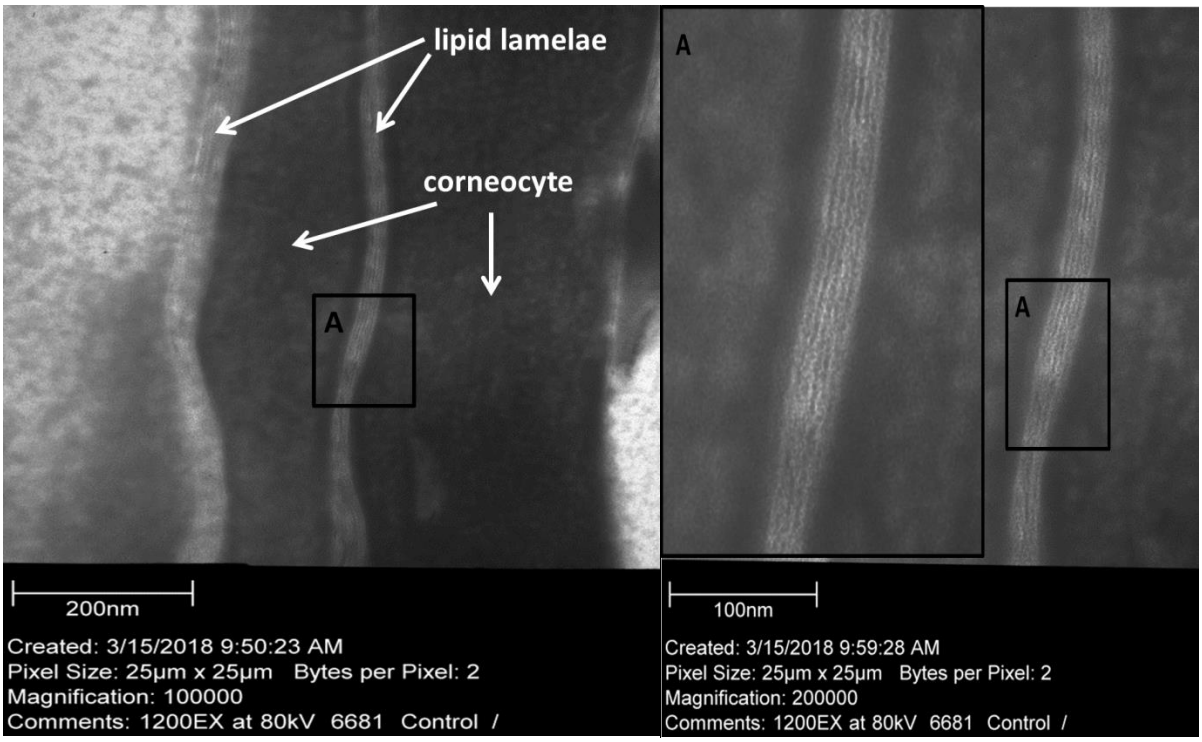

Figure 6.4.24: Lipid lamellae of untreated skin sample with detail in A.

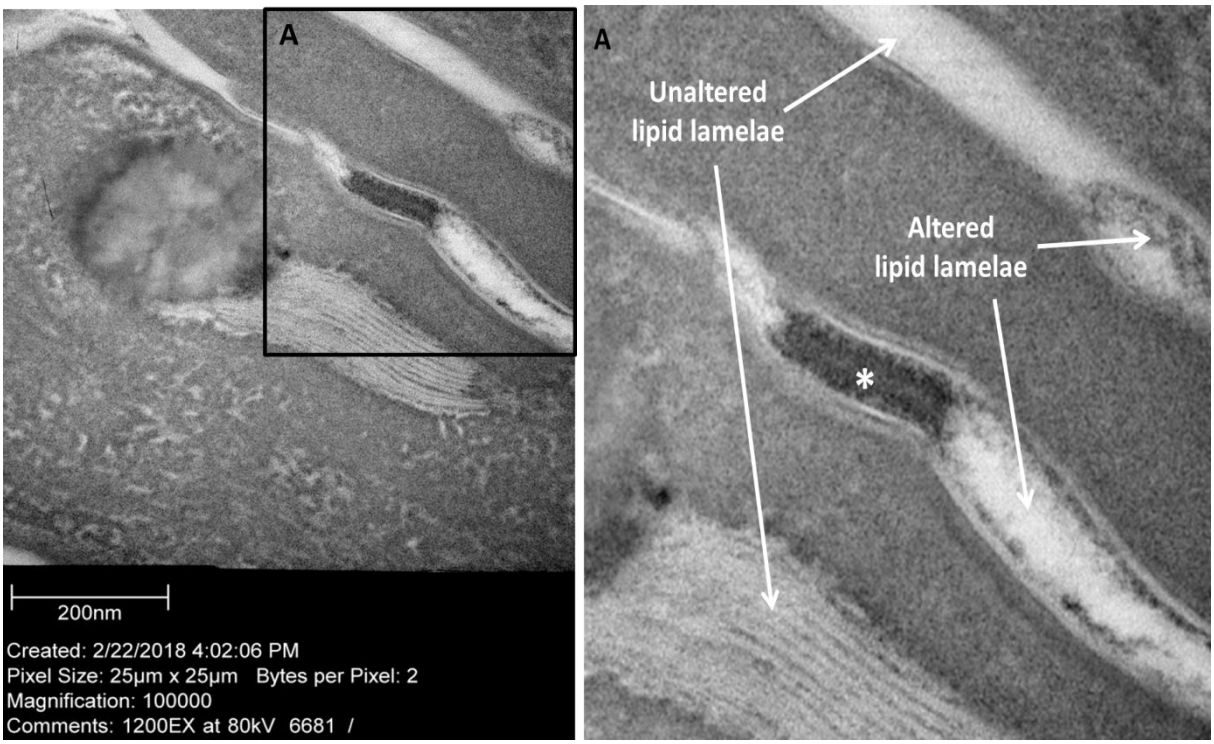

Figure 6.4.25: Lipid lamellae of microplasma treated skin sample with detail in A. Asterix – space without lipid lamelae.

Lipid lamellae of microplasma treated skin shows disturbed areas (non-homogeneous) of lipid membrane with lacunar space along corneocytes and also extracted lipids in “asterix” space in Figure 6.4.25. The skin was treated 5 minutes by argon microplasma.

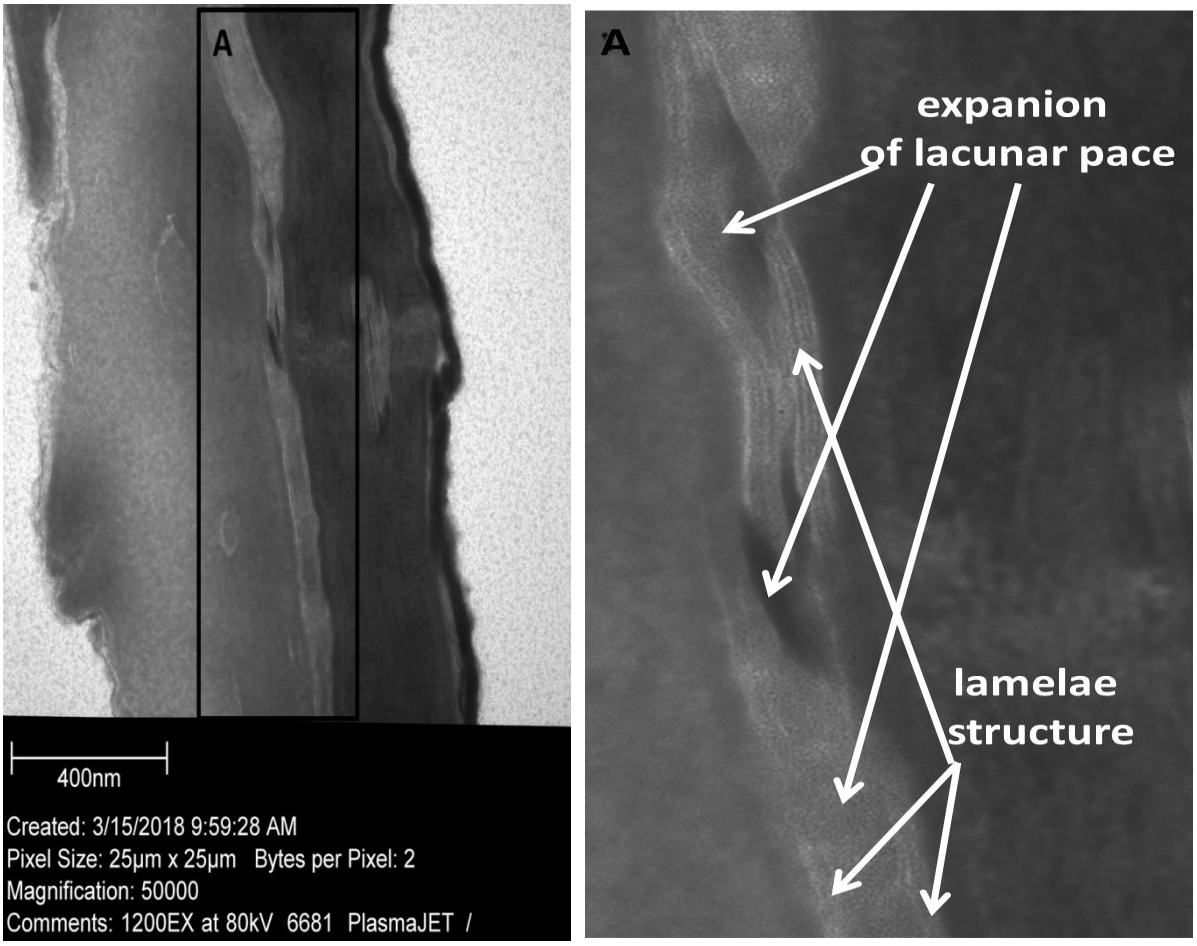

Figure 6.4.26: Lipid lamellae of plasma jet treated skin sample with detail in A.

Figure 6.4.26 shows lipid lamellae after 60 s argon plasma jet treatment. Lamellar structures are visible along the cornecytes but there is an expanding lacunar space between lamellae, splitting lamellar arrays. A similar effect is also visible during hydration of skin which can also alter lipid membranes [31].

6.4.4 Conclusion

FTIR-ATR spectroscopy of plasma treated skin showed that the plasma increases the space in lipid bilayer that is indicated by an increase of bandwidth. Etching of stratum corneum was confirmed. Extraction of lipids and breaking lipid chain was observed by a decrease of absorbance and by ratio symmetric CH_2 and asymmetric CH_3 band, respectively. Changing lipid structure was not observed. These effects could not be due to UV irradiation.

However, some changes can be realized by heating of skin, such as decrease of absorbance of lipid bands or increase of space in lamellar structure of lipids but these changes are not so significant like in the case of plasma treatment. Observation of lipid lamellae of pig skin by plasma jet confirmed spots with increased lamellar space. In the case of microplasma treatment, we could observe areas with lipid extractions and altered lipid lamellae.

6.5 Permeability of plasma treated skin

6.5.1 Motivation and sample preparation

Pig skin of Yucatan micropig from Charles River Japan, Inc. (Yokohama, Japan) was used for investigating of the influence of the plasma treatment. The pig skins were stored at −20 °C in a freezer before the experiment. At first, the fat layer of the skin was removed by using a knife, then it was cut and soaked at 4 °C in phosphate buffered saline (PBS) for 3 h, and then after a bath in 60 °C PBS for 1 min, the epidermal layer of a thickness of 200 mm was peeled by using tweezers. Finally, the skin sample was cut to 15×15 mm and placed inside of Franz cell which will be described later. We observed evaporation of water through the skin which is light molecule and can offer us some insight to the processes inside of the skin after treatment. Heavy drug, such as Cylosporine A, allows to see if plasma treatment of the skin is sufficient for drug delivery.

6.5.2 Trans-epidermal water loss

Measurement of trans-epidermal water loss is direct measurement of barrier function of the skin. The skin was placed in a Franz cell (Figure 6.5.3). The acceptor compartment was filled by distilled water. Water can be evaporated through the skin “membrane” that serves as a membrane. The donor compartment was empty. TEWL was measured after treatment during 3 days in the donor compartment by attachment of the TEWL probe. Figure 6.5.1 shows amount of water evaporation during several hours after Ar microplasma treatment when electrode was 1 mm from skin sample. We compared argon microplasma treatment with treatment by air, nitrogen, helium and control (non-treated sample). Argon microplasma treatment shows the highest evaporation delaying several hours. High evaporation at the beginning is due to moisture in the skin. This result confirms the results of chapter 6.2.3 where only argon and helium could make significant changes on the surface of the skin. Higher evaporation indicates altered lipid membrane, in our case caused only by Argon microplasma treatment.

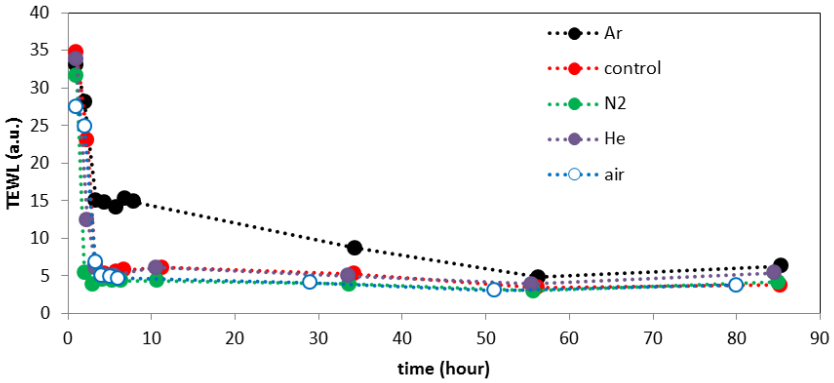

Figure 6.5.1: Trans-epidermal water loss measured by TEWL probe during several hours after microplasma treatment.

We also tested repeated treatment of the skin after treatment of Argon microplasma (Figure 6.5.2). Again, at the beginning we could observe high evaporation because of moisture in the skin. High evaporation of water delayed longer time in the case of Ar microplasma treatment than in the case of the control (non-treated) sample. When the amount of water decreased to the low level, we treated sample by microplasma again and we observed that the increase of the evaporation was delayed by 2 hours. It indicates that repeated effect of plasma can be reached.

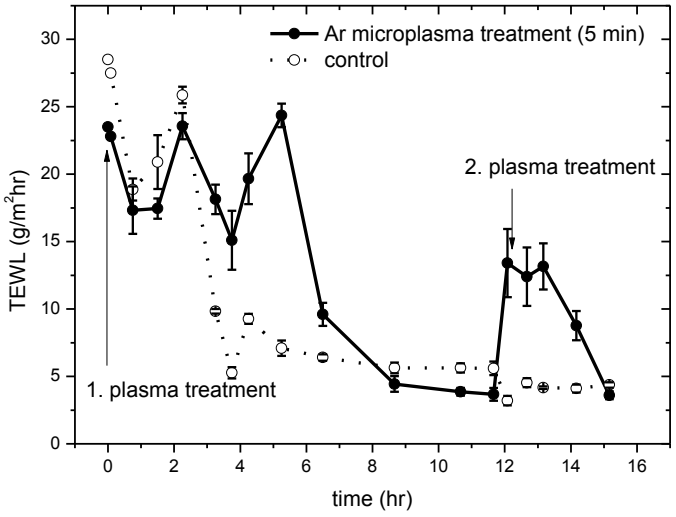

Figure 6.5.2: Trans-epidermal water loss measured by TEWL probe during several hours after microplasma treatment in comparison with non-treated sample.

6.5.3 Permeability and HPLC of Cyclosporine A

Permeability of drug Cyclosporine A was determined using Franz cell experiment. Effect of plasma jet and also microplasma will be compared.

6.5.3.1 Cyclosporine A

Cyclosporine A is a lipophilic drug with a molecular weight of 1,203 Da ($g \cdot mol^{-1}$) and a molecular formula of $C_{62}H_{111}N_{11}O_{12}$ [32]. It is a cyclic undecapeptide. As it is known, cyclic molecules and also molecules with molecular weights higher than 500 Da are difficult to deliver to the body through the skin [33].

6.5.3.2 Cyclosporine A diffusion in Franz cell

The permeability of skin was investigated by Franz diffusion cell. The procedure is illustrated in Figure 6.5.3. The skin sample was used as a membrane between the receptor and donor compartments. The diffusion area was equal to 1.65 cm^2. The donor compartment was filled by 0.5 mL of a solution of Cyclosporine A in propylene glycol with a concentration of 10 mg/mL. The receptor compartment with a volume equal to 10 mL was filled by a solution of PBS and ethanol with a ratio of 70:30 (vol/vol). The Franz cell was kept in a water bath at 37°C with constant stirring. The 0.5 mL of solution in the receptor compartment was removed for analysis of content of Cyclosporine A at determined times. This volume was replaced by a new solution of PBS/ethanol (70:30 = vol/vol). Ethanol increased the solubility of Cyclosporine A in PBS and it was used from 10% to 33% in previous studies [34, 35, 36].

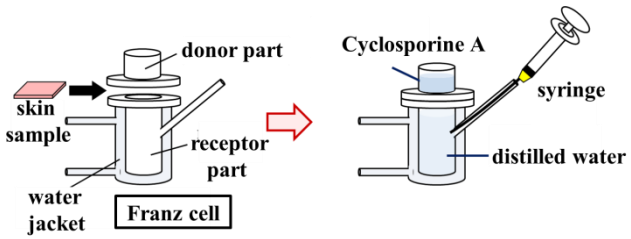

Figure 6.5.3: Procedure of drug permeability with a Franz diffusion cell.

6.5.3.3 *Measurement concentration of diffused Cyclosporine A by HPLC*

The amount of Cyclosporine A that penetrated through the skin was measured by using a High Performance Liquid Chromatograph (HPLC) LC-2010AHT (Shimadzu). The mobile phase consisted of acetonitrile/water = 70/30. The flowrate was set to 1 mL/min. A column Lichropsher 5 μm RP-18 100 Å with dimensions of 150 mm × 4.6 mm was used as a stationary phase. The column temperature was set to 60°C. Cyclosporine A was detected at 210 nm with a retention time of 11.4 minute.

6.5.3.4 *Permeated amount of the drug and the drug flow*

We determined the amount of drug that penetrated by both plasma sources, and also the drug flow during the time while the drug solution was placed on the skin. At first, skin samples were treated by a plasma jet or microplasma dielectric barrier discharge, and then the drug solution was applied on the skin. Also, diffusion of skin sample without any treatment was observed as a control sample. The accumulated amount of drug which diffused through the skin versus time is shown in Figure 6.5.4. Any penetration of Cyclosporine A during 24 hours was not observed when the skin was not treated by plasma. Dependency of the amount of penetrated drug was very similar for plasma jet and microplasma dielectric barrier discharge. The average amount of drug the penetrated after 24 hours was 14 μg in the case of microplasma dielectric barrier discharge, and 12.5 μg in the case of plasma jet.

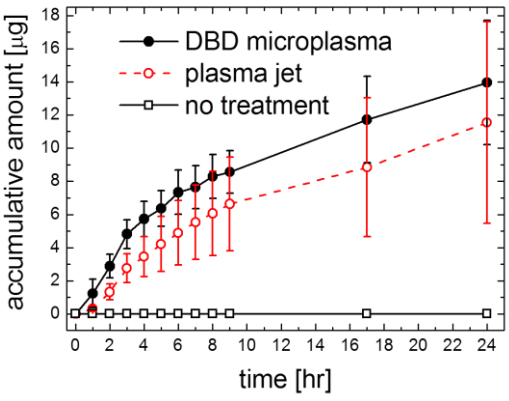

Figure 6.5.4: Accumulative amount of penetrated Cyclosporine A through the epidermal layer of the pig skin (four samples were used for microplasma dielectric barrier discharge treatment and five samples for plasma jet treatment).

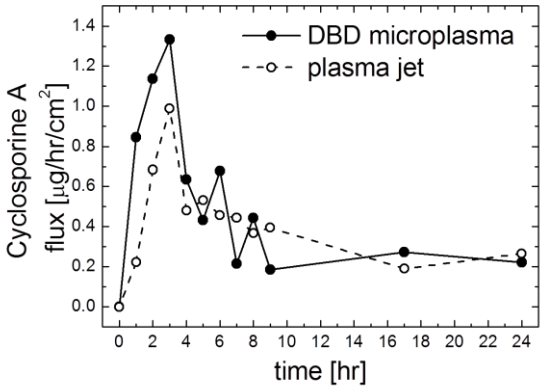

Figure 6.5.5:Evolution of rate of drug delivery through the epidermal layer of the pig skin (four samples were used for microplasma dielectric barrier discharge treatment and five samples for plasma jet treatment).

Figure 6.5.5 shows the flux of drug through the skin during 24 hours. The shape of the curve of drug concentration in the blood is given by the shape of the drug flux curve. The flux is not constant and a maximum of flux was achieved 3 hours after application of solution with Cyclosporine A with a value equal to 2 $\mu g \cdot h^{-1}$ in the case of microplasma dielectric barrier discharge and 1.5 $\mu g \cdot h^{-1}$ in the case of plasma jet. Comparison of the non-treated control sample with the sample treated by plasma indicates that the plasma changed the character of stratum corneum (upper layer of skin). An increase of drug flux later followed by a decrease of flux shows that this change was only temporal.

Several methods have been used for investigation of the permeability of skin for Cyclosporine A. Very often, mice or rat skins were used which has a higher permeability than pig or human skin. Wang *et al.* [37] investigated the permeability of mice skin by chemical enhancers, a tape striping method [38], and iontophoresis. Approximately 2 μg of Cyclosporine A was penetrated during 24 hours when 1% of azone was used as a chemical enhancer, 3.5 μg in the case of 30 stripes by tape, and 4.5 μg by iontophoresis. After using multiple pulses in electrophoresis, 3.45 μg penetrated through rat skin after 12 hours in Wang *et al.*`s study [39]. Lecithin vesicular carriers made it possible to penetrate 1.88 μg of Cyclosporine A through mice skin during 24 hours in Guo *et al.* [40]. All of these methods were less effective than plasma treatment followed by application of Cyclosporine A. A higher permeated amount was observed when ultrasound combined with chemical enhancers was used, where 7.5 μg penetrated through the rat skin after 30 min of exposure [41]. Chemical enhancers alone such as Sodium Laurilsulfate allowed penetration of only 2.75 μg [42] during 12 hours. Using Organogels was also effective for drug permeation where 20 – 40

μg of Cyclosporine A was delivered through rat skin [43]. The most effective was anodal iontophoresis using a current density 0.57 mA/cm^2 and 5 hour application; a drug flux of 10 μg·h^{-1}cm^{-2} was achieved through human epidermis.

6.5.3.5 Approach to increase the drug flow

Maximal drug flow was determined by the drug concentration in the solution placed on the skin. The flux of a drug *J* through the skin can be expressed as follows

$$J = \frac{DPC_0}{h} = K_p C_0, \tag{18}$$

where *D* is the diffusion coefficient of the drug, *P* is the partition coefficient skin/vehicle, C_0 is the concentration of the drug applied on the skin, *h* is the thickness of the skin, and K_p is the permeability coefficient given by [44]

$$\frac{1}{K_p} = \frac{1}{K_{SC}} + \frac{1}{K_{ep}} + \frac{1}{K_D}. \tag{19}$$

K_{SC} is the permeability coefficient of stratum corneum, K_{ep} is the permeability coefficient the epidermal layer, and K_D is the permeability coefficient of the dermal layer. The permeability coefficient is a function of diffusion, the thickness of the layer, and the partition coefficient. The difference between diffusion in stratum corneum and other layers is usually 3 – 4 orders [45]. The thickness of dermal layer is 2 – 3 mm [46] and thickness of stratum corneum is 20 μm. If we suppose that the partition coefficient between vehicle-stratum corneum is lower than the partition coefficient of the epidermal-dermal layer or stratum corneum-epidermal layer, then these values are related as shown below

$$K_{SC} \prec K_{ep}, \tag{20}$$

$$K_{SC} \prec K_D \tag{21}$$

and

$$\frac{1}{K_p} \approx \frac{1}{K_{SC}}. \tag{22}$$

This latter relation indicates that stratum corneum plays a main factor in the determination of the permeability coefficient.

Equation (23) shows that the steady state flux of a drug through the skin can be controlled by the concentration of drug applied on the skin and by the permeability of stratum corneum. Though steady flux was not achieved, we can expect an improvement in the amount of penetrated drug by increasing the concentration of applied drug. In this experiment, 10 mg·mL^{-1} of Cyclosporine A in propylene glycol was applied on the skin. A maximal flux J_{max} can be achieved by using saturation concentration of drug C_{sat}:

$$J_{\max} = \frac{DPC_{sat}}{h} = K_p C_{sat}. \qquad (23)$$

The saturated concentration of Cyclosporine A in propylene glycol is 400 mg/mL, 260 mg/mL in polyethylene glycol, 200 mg/mL in ethanol, and 30 μg/mL in water [47]. The maximal possible flux of the drug is 40 times higher than was measured in the experiment. Propylene glycol is used as a solvent or co-solvent of drugs [48, 49] or as an enhancer in combination with other chemicals because of synergetic effects [48]. Propylene glycol can move the thermal transition representing skin lipids or protein-associated lipids to lower temperatures [50], but mini mal changes in lipid membrane of stratum corneum was found to be caused by propylene glycol itself [51]. In this series of experiments, we did not confirm any drug penetration for the control skin samples.

6.5.4 Conclusion

Plasma sources increased the permeability of skin in comparison with non-treated samples. Increased permeability was temporary and, after approximately 3 h, it started to decrease. No significant difference between plasma jet treatment and microplasma dielectric barrier discharge treatment was observed. We concluded that particles created in plasma are the main factors that increased the permeability of the skin. After 24 h of application of the drug, 14 μg of Cyclosporine A penetrated through the epidermal layer of skin after 5 min of microplasma dielectric barrier discharge treatment and 12.5 μg after 1 min of plasma jet treatment. Unlike microplasma dielectric barrier discharge, plasma jet discharge heated the skin up to 60 °C, which was not suitable for clinical applications, and some improvements are needed to ensure non-heating functionality. Experiment with trans-epidermal water loss shows that after argon microplasma treatment, evaporation of water delay longer time than the non-treated skin sample. That phenomenon indicate altered lipid barrier. However, after repeated plasma treatment, evaporation of water through the skin increases again. Tran-

epidermal water loss and also experiment with penetration of Cyclosporine A shows that plasma can increase of the skin permeability only temporally. According to Choi *et al.* [52], this window is opened for three hours. It seems that it is in agreement with our results where flux of the drug started to decrease after 3 hours. However, a small flow of Cyclosporine A was possible to observe. This behavior can mean that there are 2 processes which allow penetrating drug – short-term and long-term process. Choi says that short-term process is controlled reducing the expression of E-cadherin. Long-term process can be caused by changing fluidity and by decreasing of packing density of lipids which seem to be stable for longer time after plasma treatment. In this experiment we suppose that pig skin is comparable with human skin. It was shown that the histological and biochemical properties was similar to human skin [53, 54, 55, 56]. Content of stratum corneum glycosphingolipids and ceramides are similar in human and in domestic pig. Thickness of stratum corneum in pigs is 21 – 26 μm which is comparable to human skin [57]. The follicular structure of pig skin also resembles that of humans, with hairs extending deeply into the dermis. Pig skin is the most suitable model for human skin [58]. The problem with pigs is that it can grow to large size and it is be difficult to manipulate with them and that is the reason, why skin of other animals is used. Another solution is using miniature pigs. Usually, frozen skin is used and in this case, the stiffness of the skin decreases and energy needed for breaking stratum corneum increases in comparison with fresh skin [59].

6.6 Pharmacokinetics

6.6.1 Introduction to pharmacokinetics of Cyclosporine A

If seriously damaged organs are not possible to heal and restore them to their function, they must be transplanted. But immune reaction of the recipient can cause rejection of the organ by the body followed by death. Finding of immunosuppressive drugs helped to prevent rejection response. The immunosuppressive drugs reduce rejection and the action of the immune system but it can expose body to risk of an infection. Acute rejection can occur up to 3 months and chronic rejection occurs after this time. It means that the recipient has to take the immunosuppressive drugs during rest of his life with the transplanted organ. When Cyclosporine A was first used, the survival rate and number of transplantations increased [60]. The number of transplantations has increasing tendency also in Japan but not as dramatic as in other western countries. In 2015, 1661 kidney transplantations were realized, while 14

years ago (2001) it was only 705 [61]. Cyclosporine A is the main immunosuppressant for all kinds of organ transplantation but its use is associated with risk of nephrotoxicity, hypertension, hepatoxicity and neurotoxicity [62]. The main pathway of the administration of Cyclosporine A is intravenous or oral. Oral administration represents a very simple way but the bioavailability is low because of the metabolic effect of gastrointestinal tract. Two thirds of metabolic reactions of the drug are realized in gut and one third in liver [63]. Administration of the other drugs can increase or decrease metabolism of Cyclosporine A [63]. This complication always has to be kept in mind. Too high concentration of Cyclosporine can be followed by some side effects and in the extreme cases leads to death. On the other hand, lower concentration leads to the risk of rejection of the organ. During intravenous delivery, special assistant is needed. However, microneedles represent hope for the future. If microneedles are shorter than 0.5 mm, they are not painful. But redness of the skin can cause increased sensitivity to the sun in the place of administration [64]. For practical application, is important to know the concentration of drug delivered through the skin to the human blood. Cyclosporine therapy prevents rejection of transplanted organs. If the immune system of the recipient detects foreign antigens from a new organ, it causes an immune reaction and rejection of the new organ or death of the patient will occur. Cyclosporine therapy starts several hours before surgery and lasts several months with gradually decreasing concentration until rejection cannot occur. The therapeutic window for Cyclosporine A lies between 100 – 400 μg/L in blood [65]. This range can change a little depending on the transplanted organ. To achieve a therapeutic level of Cyclosporine A in blood for a longer time, higher initial concentrations than therapeutic are needed. Initial doses for oral delivery are 8 – 18 mg/kg/day or 3 – 6 mg/kg/day for intravenous delivery [65]. Ragab *et al.* [66] classified three categories of concentrations for renal transplantation: sub therapeutic range below 150 μg/L, therapeutic range between 150 to 300 μg/L, and toxic level with concentrations higher than 300 μg/L. Also, Cyclosporine peaks were classified as follows: therapeutic range below 800 μg/L, therapeutic range between 800 to 1000 μg/L, and toxic level with concentrations higher than 1000 μg/L.

According to Bauer [65], one month after transplantation, 2 hours after the dose, the recommended concentration is 1500 – 2000 μg/L in the case of renal transplant and 1000 μg/L in case of liver transplant. A two-compartment model is suitable for describing Cyclosporine A in the human body [65]. This model is used for estimation of drug

concentration in the blood in the next sections. The concentration in blood induced by transdermal delivery was compared with oral and infusion delivery [67, 68, 69].

6.6.2 Two-compartment model of Cyclosporine A

A two-compartment model was used for determination of the drug concentration in the blood. As the applied amount of Cyclosporine A is much higher than the penetrated amount, we can use an equation for intravenous infusion with drug flux determined by a diffusion experiment. The Drug flux is not constant, so we used a model of multiple infusions. The two-compartment model is illustrated in Figure 6.5.6. The shape of the curve of drug concentration in the blood is given by the shape of the drug flux curve (see Figure 6.5.5). We used the measured experimental data of drug flux which contains some errors and that is the reason why, except for the main peak at 3 hours, two smaller peaks appeared in our graphs (Figure 6.5.9 – Figure 6.5.12 shown later).

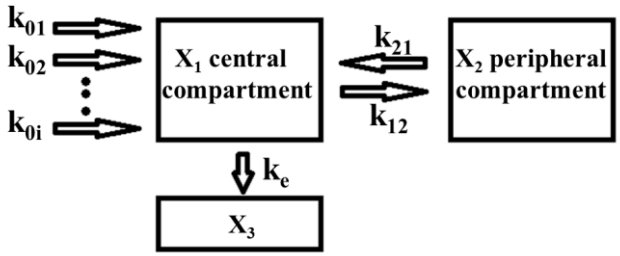

Figure 6.5.6: Diagram of the two-compartment model [67, 68, 69].

Variations in pharmacokinetics of Cyclosporine A between adults and children can be large [70]. We used data of Cremers et al.[71] for calculation of Cyclosporine A in blood of adults and Willemze et al.[72] in blood of children after infusion, oral delivery, and transdermal delivery (Table 1). Cremers et al.[71] investigated 60 adults with an average weight of 70 ± 15 kg. Willemze et al. investigated 17 children 1.8 – 16.1 years old with a weight range of 13 – 58 kg.

Table 4. Constants for two compartment model calculation of Cyclosporine A in blood.

	Ref. 71, adults weight 55 – 85 kg	Ref. 72, 1.8-16.1 years, weight 13 – 58 kg
k_a (h^{-1})	0.741	0.831
F	0.3 *[1]	0.386
V_1 (L/kg)	0.491	16.5 L *[2]
k_e (h^{-1})	0.559	0.625
k_{12} (h^{-1})	0.567	0.769
k_{21} (h^{-1})	0.149	0.265
*[1] taken from 65 *[2] independent of weight of patient		

6.6.2.1 Effective size of the treated area

We determined the minimal area suitable for the effective delivery of Cyclosporine A. The effective delivery is influenced by the amount of drug delivered per unit of time, and the time of the delivery of the therapeutic amount of the drug. The flux of the drug in our experiment is not sufficient for drug delivery for actual use in clinics. Adjustment of the drug concentration in blood can be done by adjusting the amount of applied drug to skin and by adjusting the size of the treated area of the skin. We used a flux with a saturated concentration applied to skin: 400 mg/mL in propylene glycol, so the measured flux was multiplied 40 times. In the experiment, the area that participated in penetration was determined by the area of Franz cell but would be given by the dimension of the electrode in clinical application.

The maximum amount of drug in blood occurred after 3 hours of drug application. We measured the time during which the concentration was above a level of 100 μg/L (Figure 6.5.7) and the maximal amplitude of the drug (Figure 6.5.8), and found that both depend on the size of the treated area. This information can help us to estimate the ideal treatment size for clinical use. The maximum concentration in the case of adults can be determined by equation (24)

$$C_{b\_\max}\left[\mu g / L\right] = \frac{82.95}{m[kg]} \times area\left[cm^2\right] \qquad (24)$$

in the range of 55 – 85 kg.

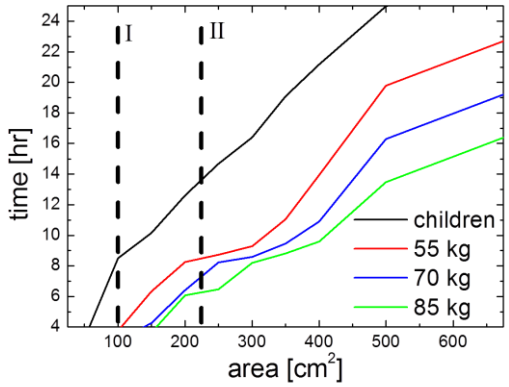

Figure 6.5.7: Time required for the concentration of the drug in blood to decrease to less than 100 μg/L. Time is measured from beginning of application. I – represents 100 cm^2 (10×10 cm), II – represents 225 cm^2 (15×15 cm).

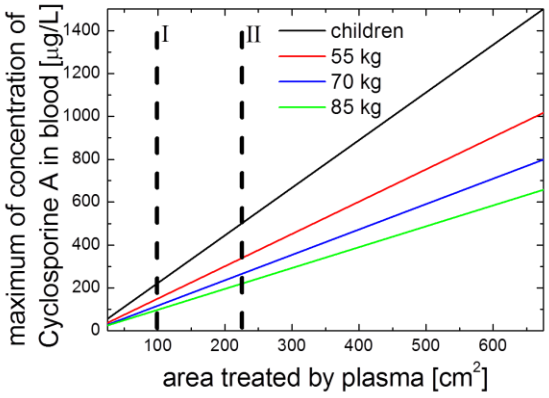

Figure 6.5.8: Amplitude of concentration of drug in blood. I – represents 100 cm^2 (10×10 cm), II – represents 225 cm^2 (15×15 cm).

We chose two sizes of treated area for investigation of the amount of drug in blood, 100 cm^2 (I in Figure 6.5.7 and Figure 6.5.8) and 225 cm^2 (II in Figure 6.5.7 and Figure 6.5.8) which could be considered acceptable. However, 100 cm^2 is too small for adults because the concentration is above 100 μg/L for too short of a time (Figure 6.5.7).

When we compared the chosen sizes with patches on the market, most of them have a size less than 100 cm^2. They deliver drugs with molecular weight less than 500 Da, but it is possible to find some large sizes when Lidocain 140 cm^2, Diclofenac epolamine 140 cm^2, or Capsaicin 280 cm^2 is delivered for reducing pain [73]. It would be an ideal case if plasma treatment could be realized as rarely as possible or at least only one time during the day. On the other hand, the treated area should not be too large.

6.6.2.2 *One treatment of the skin and drug application*

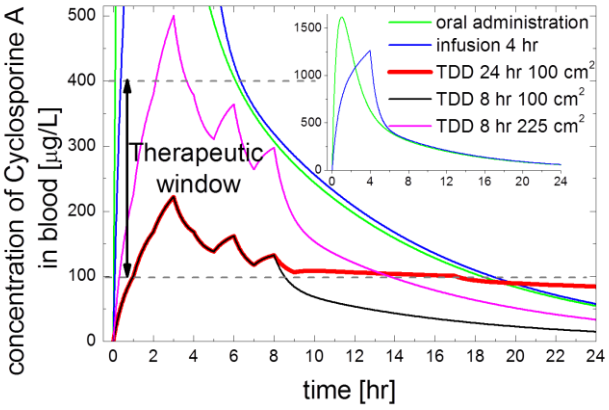

Figure 6.5.9: Oral administration of 8 mg/kg of Cyclosporine A (green) applied to a 30 kg child, infusion delivery of 3 mg/kg applied to a 30 kg child for 4 hours (blue), transdermal delivery of Cyclosporine A with a concentration of 400 mg/mL during 24 hours applied on a 100 cm^2 large area (red), transdermal delivery of Cyclosporine A with a concentration of 400 mg/mL during 8 hours applied on a 100 cm^2 large area (black), transdermal delivery of Cyclosporine A with a concentration of 400 mg/mL during 8 hours applied on a 225 cm^2 large area (pink). The two peaks at 6 and 8 hours come from experimental data of drug flux containing some errors.

We compared oral administration and infusion of the drug sufficient for one day with the drug delivery using the microplasma DBD with the treated area (100 cm^2 and 225 cm^2). We also determined the time which the concentration of the drug in blood was in the therapeutic range after plasma treatment.

Oral delivery of 8 mg/kg of Cyclosporine A given to a child weighing 30 kg will keep the concentration above 100 μg/L for almost 20 hours, but a high concentration of the drug in the blood will appear after delivery. Similar results will be achieved by infusion delivery of 3 mg/kg with a delivery rate of 0.75 mg/hr during four hours (Figure 6.5.9). The advantage of transdermal delivery is a lower peak value of concentration in the blood. During application over 24 hours we can observe an almost constant concentration because of the constant drug flow through the skin (red line in Figure 6.5.9). However, this is an average flow and some samples showed flow close to 0 and we cannot expect that the drug will always be delivered after 8 hours. That is the reason why we studied only cases when the drug was applied 8 hours with a higher drug flux. In Figure 6.5.9 (pink line), 8 hours of application of Cyclosporine A is depicted, when the treated area was 225 cm^2, and it remained for 13 hours in the therapeutic range. The same result but with higher peak values would be achieved by 5 mg/kg of oral delivery or 1.8 mg/kg of 4 hour infusion. If the treated area were 100 cm^2, the concentration of the drug remaining in the therapeutic range would be almost 9 hours,

which would be equivalent to 2 – 3 mg/kg of oral delivery or 0.8 – 1 mg/kg of four-hour infusion.

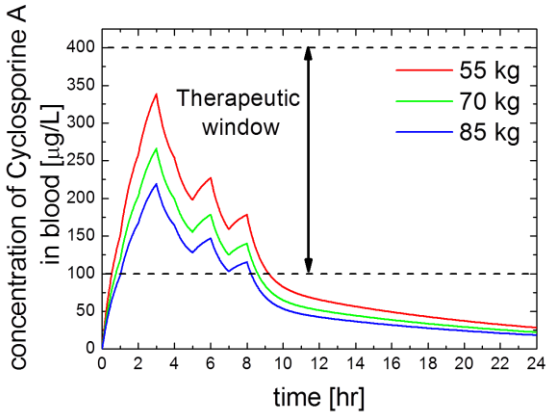

Figure 6.5.10: Concentration of Cyclosporine A in blood of adults 55 kg, 70 kg and 85 kg weigh. Two peaks at 6 and 8 hours come from experimental data of drug flux containing some errors.

In the case of adults, Figure 6.5.10 shows 8 hours of application of the drug on a treated area 225 cm^2 in size. A patient of 85 kg is equivalent to children when the drug is applied on a surface 100 cm^2 in size. These results are not sufficient for whole-day delivery, so using multiple applications of the drug during the day was also investigated.

6.6.2.3 Repeated treatment and drug application

Cyclosporine A needs to be delivered/taken over a long term of several months. The concentration of the drug in blood usually increases until equilibrium between the drug delivery and elimination is achieved. Next, we present required delivery interval for safe administration. As shown in Figure 6.5.11A, safe values represent application of drug and skin treatment every 8 – 10 hours for 55 kg adults, or every 6 – 8 hours for 56 – 85 kg adults on an area of 225 cm^2 (applied concentration 400 mg/mL of Cyclosporine A).

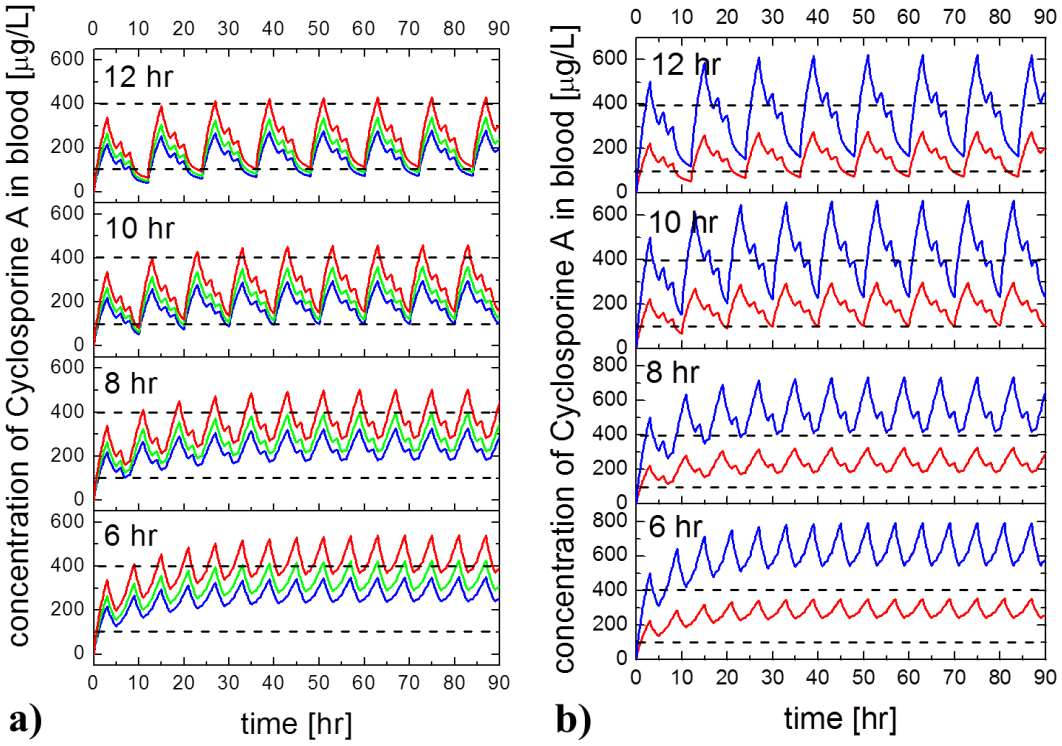

Figure 6.5.11: Evolution of Cyclosporine A in blood after repetitive treatment and application of drug
a) every 6 hours, 8 hours, 10 hour and 12 hours of adults weigh 55 kg (red), 70 kg (green), 85 kg (blue).
b) every 6 hours, 8 hours, 10 hour and 12 hours of children with treated surface 100 cm^2 (red) and 225 cm^2 (blue).

If a 100 cm^2 area is used for treatment of children, the treatment of skin and drug application has to be realized every 6 – 8 hours, and 6 – 12 hours when a 225 cm^2 area is used. But in the case of 6 and 8 hours, the concentration of the applied drug has to be decreased. However, whether the same place for repeated application can be used, and the effects of multiple treatments on the skin, have yet to be investigated.

6.6.2.4 Skin metabolism

In this section, we will discuss the estimation of the change of concentration of the drug in blood by skin metabolism. The presence of enzymes confirm the capability to metabolize a drug in the skin. It can have an influence on the amount of cutaneous delivered drugs and the toxicity. Unlike the first-pass metabolism in the liver, the drug is exposed to only a low fraction of metabolizing enzymes in a small region in the skin. This reduces the metabolizing effect in comparison with the liver [74] and cutaneous delivery can have higher bioavailability than oral delivery. Al-Qallaf *et al.* [75] introduced a transdermal delivery

model of the drug Verapamil with a correcting factor for skin metabolism. Their results showed a significant change in the amount of delivered drug after including this correction. Vickers *et al.* [76] showed that Cyclosporine A metabolizes in the dermal layer, but not in the epidermal layer. They observed a linear increase of metabolites during six days in an amount of 4 $pmol \cdot h^{-1}cm^{-2}$. If we suppose that increasing metabolites is equal to decreasing Cyclosporine A, the latter is decreased by 4.8×10^{-3} $\mu g \cdot h^{-1}cm^{-2}$. The drug will spend time in dermal layer according to

$$t_{lag} = \frac{h_{dermis}^2}{6D_{dermis}}, \tag{25}$$

where h_{dermis} is the thickness of the dermal layer, approximately 2 – 3 mm thick [46]. Diffusion in the dermal layer of Cyclosporine A is not known, but if we take Dextran with a molecular weight of 40 kDa with a diffusion coefficient in the dermal layer of 23 $\mu m^2/s$ as a reference molecule [77], Cyclosporine A would spend from 8 to 18 hours in the dermal layer. The drug flux will decrease about 0.09 – 0.04 $\mu g \cdot h^{-1}cm^{-2}$. As we suppose that diffusion coefficient for Cyclosporine A is higher, drug flux will decrease by a lower value. A comparison of the drug concentration in blood with and without metabolism is shown in Figure 6.5.12A where 55 kg and 85 kg adults were compared. As shown in the figure, the metabolism can decrease the time over which the concentration of the drug remains in the therapeutic range. The treatment and drug application have to be repeated every 8 hours for 85 kg adults and every 10 hours for 55 kg adults. The skin metabolism decreased the concentration in blood by a maximum value about 32.5 μg/L for the 85 kg adult and by about 50 μg/L for the 55 kg adult.

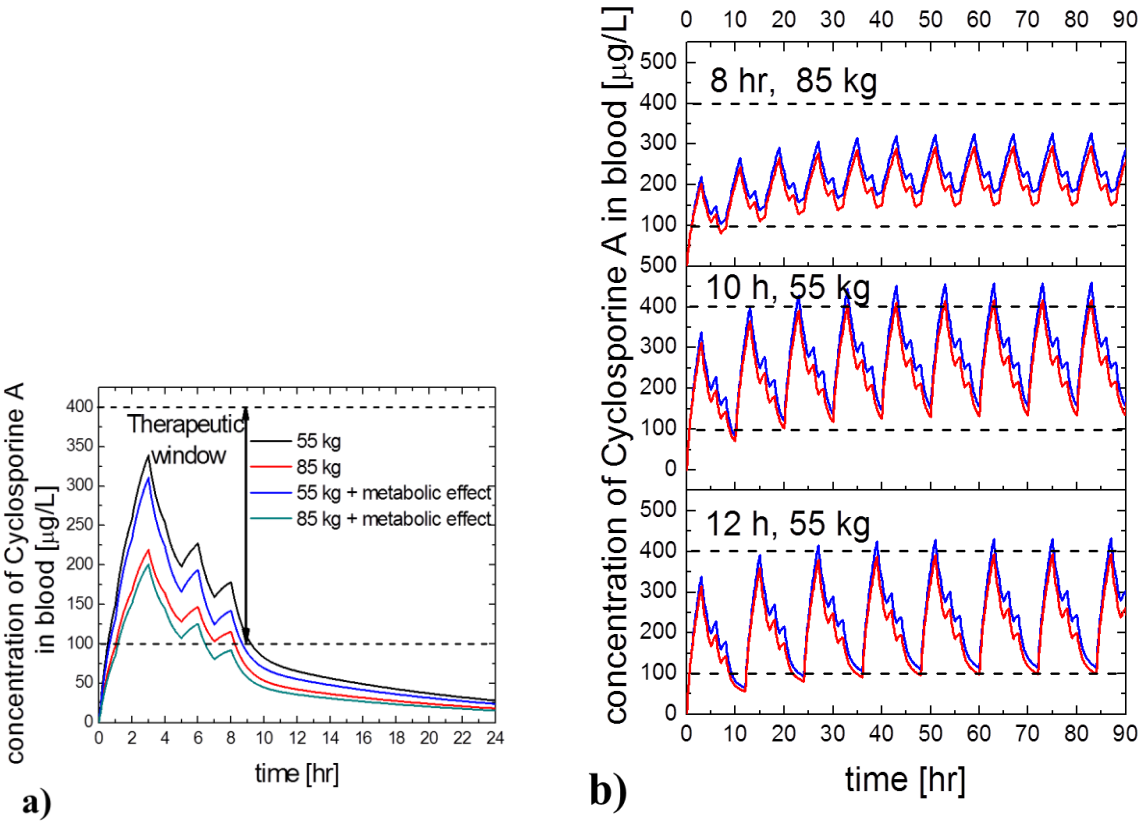

Figure 6.5.12: Evoulution of Cyclosporine A in blood

A) of 55 kg adult with skin metabolism (blue), without skin metabolism (black), and of 85 kg adult with skin metabolism (red), without skin metabolism (green). Two peaks at 6 and 8 hours come from experimental data of drug flux containing some errors.

B) after repetitive treatment and application of drug every 8 hours for an 85 kg adult, every 10 hours 55 kg adult, 12 hours 55 kg adult with skin metabolism (red), and without skin metabolism (blue) applied on a 225 cm^2 area.

6.6.2.5 Combination of oral drug delivery with transdermal drug delivery

Drug delivery can have an influence on the quality of life. When the drug has to be applied too often, there is a risk of failure of the patient. Also, application can be avoided because of the actual situation in the life. On the other hand, if administration method is too complicated, there is a risk of any mistake. This mistake can be fatal in the case of Cyclosporine A, if it is followed by the dramatic change of the concentration in the bloodstream. Our model in Figure 6.5.13A illustrates oral administration of 3.5 mg/kg every 24 hours. 10 hours after the drug application, the concentration in the bloodstream decreased below the therapeutic level of 100 μg/l. To achieve the level above therapeutic level, it is needed take 9 mg/kg of the drug every 24 hours (Figure 6.5.13C). This amount resulted in a

high peak of 1744 μg/l 1 hour after application, what is a toxic level according Ragab et al. [66]. Oral delivery of Cyclosporine A is usually administered 2 times a day every 12 hours. In our model, 3.5 mg/kg given every 12 hours could maintain a level of the drug above 100 μg/l (Figure 6.5.13B).

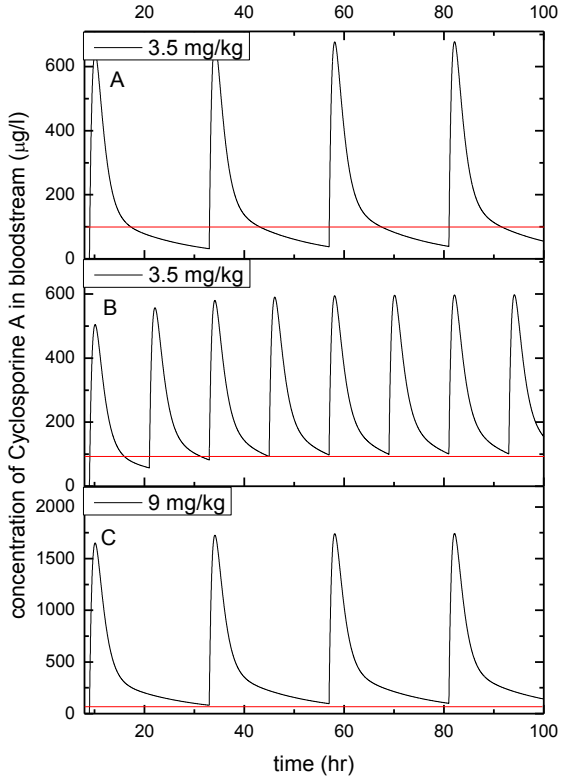

Figure 6.5.13.A. Oral delivery of 3.5 mg/kg of Cyclosporine A every 24 hours. B. Oral delivery of 3.5 mg/kg of Cyclosporine A every 12 hours C. Oral delivery of 9 mg/kg of Cyclosporine A every 24 hours. The weight of the patient was 55 kg in the model. The red line indicates the lowest therapeutic concentration.

The average weight of a Japanese man was less than 70 kg and the average weight of Japanese woman was less than 55 kg. In the calculations of our model, we used the weight of an average Japanese woman (55 kg). Results for men were very similar. The application of plasma drug delivery every 24 hours would not allow holding of Cyclosporine A concentration in the therapeutic range and the concentration would decreased below 100 μg/l 9.5 hours after the application. But the plasma drug delivery applied every 12 hours allowed maintaining of the therapeutic level (Figure 6.5.12B).

Oral drug delivery represents a simple method of the administration, but because of the influence of other drugs or even drinks on the metabolism of Cyclosporine A, it is needed

to be very careful. Investigation of the influence, for example, of grapefruit juice on Cyclosporine A metabolism was demonstrated in Murray *et al.* [78]. After oral administration of Cyclosporine A and drinking of 250 ml of grapefruit juice, the bioavailability of the drug increased about 62%. But they did not observe any influence of the grapefruit juice if the drug was administered intravenously. We also did not expect any influence of grapefruit juice on microplasma drug delivery and we can avoid the metabolic effect. Changes of the bioavailability following other drugs and substances can sometimes have fatal results [79].

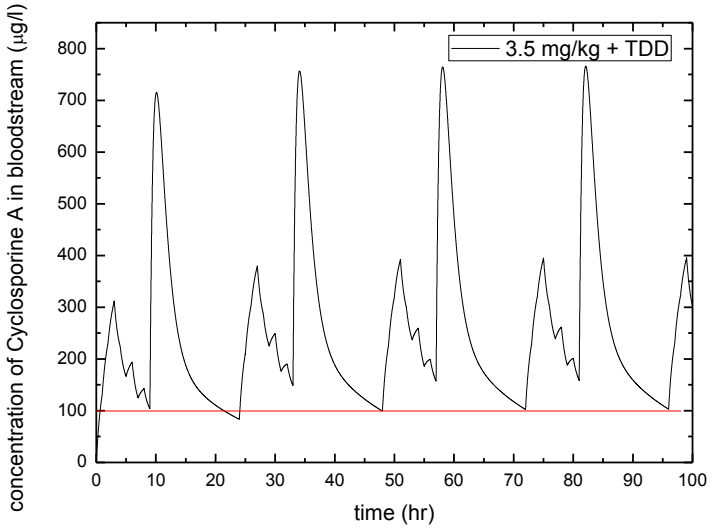

Figure 6.5.14.Oral delivery of 3.5 mg/kg of Cyclosporine A with combination of transdermal drug delivery (TDD) of Cyclosporine A every 24 hours. Delay between transdermal drug delivery and oral delivery is 9 hours and patient weight was 55 kg in the model. The red line indicates the lowest therapeutic concentration.

Combination of microplasma transdermal delivery and oral delivery is demonstrated in Figure 6.5.14. 3.5 mg/kg was administered every 24 hours, 9 hours after transdermal delivery. The peak values appeared every 24 hours for approximately 3 hours (value above 400 μg/l). Oral delivery was reduced to half and also the risk of side effects (caused by gastrointestinal tract) as Cyclosporine A was administered every 24 hours instead of every 12 hours. The time shift between the both administrations can be adjusted to microplasma transdermal delivery in the evening and to oral administration in the morning. This setting can improve the quality of life of the patient and partially decrease the effect of the interaction of Cyclosporine A with other substances because of oral administration.

References.

[1] J. Luque and D.R. Crosley. Lifbase: Database and spectral simulation program (version 2.1.1), http://www.sri.com/cem/lifbase. Technical report, SRI International, 1999.
[2] K. K. Petersen, M. L. Rousing, C. Jensen, L. Arendt-Nielsen, and P.
Gazerani, Int. J. Physiol. Pathophysiol. Pharmacol. 3, 236 (2011).
[3] D. G. Wood, M. B. Brown, S. A. Jones, European Journal of Pharmaceutics and Biopharmaceutics 81, 642 (2012).
[4] S. Venkatraman, R. Gale, Biomaterials 19, 1119 (1998).
[5] M. E. Ginn , C. M. Noyes , E. Jungmann, Journal of colloid and interface science 26, 146 (1968).
[6] A. Mavon, H. Zahouani, D. Redoules, P. Agache, Y. Gall, Ph. Humbert, Colloids Surfaces B: Biointerfaces 8, 147 (1997).
[7] S.O. Majekodunmi, O. A. Itiola, International Journal of Pharmacy and Pharmaceutical Science Research 4(4), 65 (2014).
[8] P. Capra, G. Musitelli and P. Perugini, International Journal of Cosmetic Science 39, 393 (2017).
[9] A. F. Azarbayjani, H. Lin, Ch. W. Yap, Y. W. Chan, S. Y. Chan, JPP 62, 770 (2010).
[10] A. E. Kovalev, K. Dening, B. N. J. Persson, S. N. Gorb, Beilstein J. Nanotechnol. 5, 1341 (2014).
[11] M. Wagner, A. Mavon, H. Haidara, M.-F. Vallat, H. Duplan, V. Roucoules,International Journal of Cosmetic Science 34, 55 (2012).
[12] H. Yasuda, A. K. Sharma, Journal of Polymer Science: Polymer Physics Edition 19,1285 (1981).
[13] S.A.W. Hollak, J.H. Bitter, J. van Haveren, K.P. de Jong, D. S. van Es, RSC Adv. 2, 9387 (2012).
[14] Stevens, Joana S., Schroeder, Sven L. M. (2017). X-ray photoelectron spectroscopy In Z. Wang (Ed.), Encyclopedia of Physical Organic Chemistry (pp. 3241). Hoboken, USA, New Jersey: Wiley.
[15] E. A. Bernardelli, M. Mafra, A. M. Maliska, T. Belmonte, A. N. Klein, Materials Research 16(2): 385-391 (2013) .
[16] E. A. Bernardelli, T Souza, M. Mafra, A. M. Maliska, T. Belmonte, A. N. Klein, Materials Research 14(4): 519-523 (2011)
[17] E. A. Bernardelli, T. Belmonte, D. Duday, G. Frache, F. Pncin-Epaillard, C. Noel, P. Choquet, H.-N. Migeon, A. M. Maliska, Plasma Chem Plasma Process 31:189–203 (2011).
[18] C. Noel, D. Duday, S. Verdier, P. Choquet, T. Belmonte, H.-N. Migeon, Plasma Process. Polym. 6, S187 (2009).
[19] X. Zhang, L. Santonja-Blasco, K. B. Wagener, E. Boz, M. Tasaki, K, Tashiro, R. G. Alamo, J. Phys. Chem. B 121 (43), 10166 (2017).
[20] B. Xie, G Liu, S. Jiang, Y. Zhao, D. Wang, J. Phys. Chem. B 112 (42), 13310 (2008).
[21] M. B. Sajwan, S. Aggarwal, R.B. Singh, THE INDIAN JOURNAL OF CRIMINOLOGY & CRIMINALISTICS VOLUME XXIX (1), 55 (2008).
[22] S. Zhu,M. Heppenstall-Butler, M. F. Butler, P. D. A. Pudney, D. Ferdinando, K. J. Mutch, J. Phys. Chem. B 109(23),11753 (2005).
[23] P. Garidel, A. Blume, W. Hubner, Biochimica et Biophysica Acta 1466, 245 (2000).
[24] D. J. Moore, M. E. Rerek, J. Phys. Chem. B 101, 8933 (1997).
[25] Kalghatgi S, Tsai C, Gray R, and Pappas D. Transdermal drug delivery using cold plasmas . In: 22nd Int'l Symposium on Plasma Chemistry; 5-10 July; Antwerp, Belgium. 2015. p. O-22-6.
[26] L. Brancaleon, M. P. Bamberg, T. Sakamaki, and N. Kollias, Journal of Investigative Dermatology 116(3), 380 (2001).
[27] M. Picardo, M. Ottaviani, E. Camera, and A. Mastrofrancesco, Dermatoendocrinol. 1(2), 67, 2009.
[28] G. Cakmak, I. Toqan, F. Severcan, Aquatic Toxicology 77, 53 (2006).
[29] A. Barth, "Infrared spectroscopy of proteins", Biochimica et Biophysica Acta 1767, 1073, 2007.
[30] Hill J. R., Wertz P.W., Biochimica et Biophysica Acta1616, 121 (2003).
[31] T.-K. Lin, D. Crumrine, B.S.1, L. D. Ackerman, B.A.1, J.-L. Santiago, T. Roelandt, Y. Uchida, M. Hupe, G. Fabriàs, J. L. Abad, R. H. Rice, P. M. Elias,J Invest Dermatol. 132(10), 2430 (2012).
[32] B. D. Kahan, The New England Journal of Medicine 321(25), 1725 (1989).
[33] J. D. Bos, M. M. Meinardi, Exp Dermatol. 9(3), 165 (2000).
[34] L. B. Lopes, M. V. L. B. Bentley, Brazilian Journal of Pharmaceutical Sciences 41(4), 477 (2005).
[35] J. Guo, Q. Ping, G. Sun, C. Jiao, C., A. Int.J.Pharm. 194, 201 (2000).
[36] H. K. Choi, G.L. Fflynn, G. L. Amidon, J.Pharm.Sci. 84(5), 581 (1995).
[37] D.-P. Wang, Ch.-Y. Lin, D.-L. Chu, L.-Ch. Chang, Drug Development and Industrial Pharmacy 23(1), 99 (1997).

[38] H. Pinkus, J. Invest. Dermatol. 16, 383 (1951).
[39] S. Wang, M. Kara, T.R. Krishnan, Journal of Controlled Release 50, 61 (1998).
[40] J. Guo, Q. Ping, G. Sun, Ch. Jiao, International Journal of Pharmaceutics 194, 201 (2000).
[41] H. Liu, S. Li, W. Pan, Y. Wang, F. Han, H. Yao H., International Journal of Pharmaceutics 326, 32 (2006).
[42] H. Liu, S. Li, Y. Wang, H. Yao, Y. Zhang. International Journal of Pharmaceutics 311, 182 (2006).
[43] H. Liu, Y. Wang, F. Han, H. Yao, S. Li, Journal of Pharmaceutical Sciences 96(11), 3000 (2007).
[44] B. Steffansen, B. Brodin, C. U. Nielsen, Molecular Biopharmaceutics: Passive diffusion of drug substances: the concepts of flux and permeability (Pharmaceutical Press, 2009).
[45] A.P. Raphael, S. C. Meliga, X. Chen, G. J.P. Fernando, Ch. Flaim, M. A.F. Kendallet, Journal of Controlled Release 166, 87 (2013).
[46] A. Z. Alkilani, M. T.C. McCrudden, R. F. Donnelly, Pharmaceutics 7, 438 (2015).
[47] H. Takruri, U.S. Patent No.20150352176 A1, (10 Dececember 2015).
[48] P. Augustijns, M. Brewster, Solvent Systems and Their Selection in Pharmaceutics and Biopharmaceutics, New York: Springer Science & Business Media (2007).
[49] Y. Ran, L. Zhao, Q. Xu, S. H. Yalkowsky, AAPS PharmSciTech. 2(1), 23 (2001).
[50] H. Tanojo, J. A. Bouwstra, H. E. Junginger, H. E. Bodde, Journal of Thermal Analysis and Calorimetry 57, 313 (1999).
[51] S. J. Jiang, Y. K. Kim and S. H. Lee, Ann Dermatol. 10(3), 153 (1998).
[52] J.-H. Choi, S.-H. Nam, Y.-S. Song, H.-W. Lee, H.-J. Lee, K. Song, J.-W. Hong, G.-Ch. Kim, Arch. Dermatol. Res. 306(7), 635 (2014).
[53] G.M. Gray, H.J. Yardley, J. Lipid Res. 16, 434 (1975).
[54] U. Jacobi, M. Kaiser, R. Toll, S. Mangelsdorf, H. Audring, M. Otberg, W. Sterry, Lademann, 131, 19 (2007).
[55] F. Muhammad, J.D. Brooks, J.E. Riviere, Toxicol. Lett. 150, 351 (2004).
[56] R.C.Wester, J. Melendres, L. Sedik, H. Mailbach, J.E. Riviere, Toxicol. Appl. Pharmacol. 151, 159 (1998).
[57] B. Godin, E. Touitou, Adv. Drug Deliv. Rev. 59(11), 1152 (2007).
[58] F.P. Schmook, J.G. Meingassner, A. Billich, Intl. J. Pharmaceutics 215, 51(2001).
[59] S. A. Ranamukhaarachchi, S. Lehnert, S. L. Ranamukhaarachchi, L. Sprenger, T. Schneider, I. Mansoor, K. Rai, U. O. Häfeli, B. Stoeber, Scientific Reports 6, 32074 (2016).
[60] A. Mehrabi, M. Wiesel, M. Zeier, A. Kashfi, P. Schemmer, T. Kraus, M. W. Buchler, J. Schmidt, Nephrol. Dial. Transplan.t 19 (Suppl 4), iv48–iv54 (2004).
[61] T. Yagisawa, M. Mieno, N. Yoshimura, K. Yuzawa, S. Takahara, Renal Replacement Therapy 2, 68 (2016).
[62] U. Christians and K.-F. Sewing, Clinical Biochemistry 28(6), 547 (1995).
[63] Y. N. Gavhane and A. V. Yadav, Saudi Pharm J. 20(4), 331 (2012).
[64] B. Koch, I. Rubino, F.-S. Quan, B. Yoo, and H.-J. Choi, Materials 9, 646 (2016).
[65] L. A. Bauer, Applied Clinical Pharmacokinetics, McGraw-Hill Professional Publishing, 2008.
[66] A. R. Ragab, M. K. Al-Mazroua, S. Abd-Elziz Al-Dakrory, J Clinic Toxicol 3, 154 (2013).
[67] N. P. Chau, Journal of Pharmacokinetics and Biopharmaceutics 5(4), 391 (1977).
[68] M. Gibaldi, Journal of Pharmaceutical Sciences 58(9), 1133 (1969).
[69] R. A. Ronfeld and L. Z. Benet, Journal of Pharmaceutical Sciences 66(2), 177 (1977).
[70] G. F. Cooney, K. Habucky, K. Hoppu, Clin, Pharmacokinet 32(6), 481 (1997).
[71] S. C. L. M. Cremers, E. M. Scholten, R. C. Schoemaker, E. G. W. M. Lentjes, P. Vermeij, L. C. Paul, J. den Hartigh, J. W. de Fijter, Nephrol Dial Transplant 18, 1201 (2003).
[72] A. J. Willemze, S. C. Cremers, R. C. Schoemaker, A. C. Lankester, J. Den Hartigh, J. Burggraaf, J. M. Vossen, British Journal of Clinical Pharmacology 66, 539 (2008).
[73] M. N Pastore, Y. N Kalia, M. Horstmann, M. S Roberts, British Journal of Pharmacology 172, 2179 (2015).
[74] C. K. Svensson, DMD 37, 247 (2009).
[75] B. Al-Qallaf, D. Mori, L. Olatunji, D. B. Das, Z. Cui International Journal of Chemical Reactor Engineering 7, A69 1 (2009).
[76] A. E. M. Vickers, W. A. Biggi, R. Dannecker, V. Fischer, Life Sciences 57(3), 215 (1995).
[77] A. M. Romgens, D. L. Bader, J. A. Bouwstra, F. P. T. Baaijens, C. W. J. Oomens, Biomedical Materials 50, 215 (2015).
[78] M. P. Ducharme, L. Warbasse, D. J. Edwards, Clinical Pharmacology and Therapeutics 57(5), 485 (1995).
[79] A. Tafazoli: Accidental Overdose of Oral Cyclosporine in Haematopoietic Stem Cell Transplantation: A Case Report and Literature Review. Drug Saf - Case Rep 2, 20 (2015).

7 Conclusion

Interaction of plasma and skin was investigated to enhance permeability. Our research is concluded in the six points. In the first point we conclude which plasma source is suitable for skin treatment. The second point indicates how the drug flow through the skin can be increased. The third point demonstrates interaction between the skin lipids and plasma showing possible ways of increasing permeability. The fourth point, based on FTIR observation of the stratum corneum explains the reason of the increased permeability. The fifth point demonstrates of permeability of Cyclosporine A and the sixth point applicability in medical praxis and risks of skin damage.

1. Two plasma sources were used – plasma jet and microplasma. Plasma jet is ignited by high voltage and because high temperature and possible skin damage, it is not suitable for skin treatment. Different design and construction of plasma jet must be done to be possible to apply on human skin. Microplasma requires low voltage in several hundred of volts and it can be used for skin treatment without any problem. Because of low distance between microplasma electrode and skin, very low amount of air is mixed with working gas – argon. This amount is lower than in the case of plasma jet. It was confirmed by FTIR and also by emission measurements.
2. Characterization of surface properties by measuring contact angle showed functionalization of the skin surface after plasma treatment. Treatment by Ar microplasma was the most effective in comparison with other gases. Ar microplasma treatment decrease contact angle from more than 80° to close to 35° when skin is in contact with electrode during treatment. Ageing of skin surface is relatively fast and it takes from several minutes up to 1.5 hours. This time is in inverse correlation with contact angle. Plasma treatment of the skin by any gas increased oxygen and nitrogen atoms on the surface. However, reorientation of molecules of the skin can be dominant effect. Skin roughness has minor effect on water contact angle because the skin is not flat surface. Etching skin by microplasma was saturated after 60 s of treatment. Thickness of stratum corneum decreased from 30 μm to 15 μm. Plasma jet decreased thickness of startum corneum to 10 μm. Plasma did not etch the strongest layer of the skin – last 10 μm. Functionalization and etching of the skin surface cannot increase permeability of the skin but it can increase of flow of the drug through the stratum corneum. In the case of etching, it is because stratum corneum thickness is thinner so less of the drug remains in the skin. Higher drug flow caused by functionalization of the skin surface (measured by

contact angle), it is because the drug solution will have better contact with stratum corneum layer and it will ensure increase of contact area which induces higher drug flow.

3. Observation of microplasma treatment of lipids such as stearic acid, erucic acid, cholesterol and ceramide C4 can demonstrate possible changes of these lipids inside of stratum corneum. Etching by Ar ions was effective in decreasing of C-C and C-H bonds in the case of erucic acid and also in the cholesterol. When C-C, C-H bonds decrease, the number of carbon bonded to oxygen by single bonds increase (number of oxygen double bonds decrease). On the other hand, C-C and C-H bonds of ceramide and stearic acid were very stable to etching by argon ions but number of carbons bonded to oxygen decreased. Plasma treatment of lipids decrease number of C-C and C-H bonds about 10 % in the case of stearic acid and erucic acid and 25% in the case of cholesterol. Number of oxygen and nitrogen bonds increased (erucic acid had no nitrogen bonds.). In the case of ceramide, number of C-C, C-H bonds was not changed but number of oxygen bonds was decreased. Structure of stearic acid and erucic acid was orthorhombic with increase of lattice after plasma treatment. Cholesterol and ceramide was structurally more seriously changed after plasma treatment but no increase of lattice as observed. These results demonstrate that fatty acids are oxidized. And presence of oxygen in molecule induces increase of the lattice. If this effect happens in lipid barrier, it means that density of lipids decrease and because of more empty space, permeability of the skin can increase. Plasma can also destroy molecule of cholesterol. Cholesterol has very important function in barrier function. If amount of cholesterol is reduced in lipid matrix, permeability of the skin will increase. Plasma can also induce structural changes to ceramides but their effect on skin permeability has to be investigated more to be clear.
4. Plasma jet treated skin showed that plasma increase space in lipid bilayer. This observation is in agreement with increasing of lattice in point 3. Increase of the space in lipid bilayer means increase of skin permeability. Extraction of lipids and breaking lipid chain was also observed. As it as mentioned in chapter 2, shorter lipid chains and extraction of lipids also increase the skin permeability. It was shown that these effects could not be due to UV irradiation or heating of the skin. Skin treatment at different distances from electrode showed that presence of air species is important for increasing of permeability but optimal concentration of air ha to be found. Observation of lipid lamellae of pig skin by plasma jet confirmed spots with increased lacular space (empty

space). In the case of microplasma treatment, we could observe areas with lipid extractions and altered lipid lamellae as proof of permeability increase.

5. Increase of the skin permeability was confirmed by increase water increased of evaporation after plasma treatment. This effect was possible to repeat with the same sample. Cyclosporine A with molecular weight 1203 Da could permeate after plasma treatment of skin in comparison with non-treated samples. Increased permeability was temporary and after approximately 3 h, it started to decrease. No significant difference between plasma jet treatment and microplasma dielectric barrier discharge treatment was observed.
6. After 24 h of application of the drug, 14 μg of Cyclosporine A penetrated through the epidermal layer of skin after 5 min of microplasma dielectric barrier discharge treatment and 12.5 μg after 1 min of plasma jet treatment. Our pharmacokinetics study showed that after plasma treatment of the skin, it is possible to deliver a therapeutic amount of Cyclosporine A to blood if a saturated concentration of drug of 400 mg/ml in propylene glycol is used. We found out that a 100 cm^2 area has to be treated for successful delivery in the therapeutic range in the case of children from 1.8 to 16 years. Treatment and application have to be repeated every 6–8 h. In the case of adults with weights in the range of 55–85 kg and a 225 cm^2 large area, a repeated treatment and application every 6–10 h are needed, depending on the weight of the patient. Skin metabolism can decrease the concentration in blood from 35.2–50 μg/l depending on the weight of the patient. The effect of skin metabolism was estimated, and other measurements are needed for more precise corrections of the amount of delivered drug. Plasma drug delivery represents a promising method of delivery of drugs, but additional research is needed to improve drug flux and the delay of enhanced permeability of skin. Combination of microplasma transdermal delivery and oral delivery is possible according pharmacokinetic study. Delivery of 3.5 mg/kg orally every 24 hours, 9 hours after transdermal delivery can reduce of side effects (caused by gastrointestinal tract) as Cyclosporine A was administered every 24 hours instead of every 12 hours. The time shift between the both administrations can be adjusted to microplasma transdermal delivery in the evening and to oral administration in the morning. This setting can improve the quality of life of the patient and partially decrease the effect of the interaction of Cyclosporine A with other substances because of oral administration.

Skin damage can be done mostly by surface etching. If conditions of treatment are set correctly, stratum corneum is not removed completely. Microplasma removed 15 μm of stratum corneum in our case. But upper part of stratum corneum is easy to penetrate and it is not serious barrier in reality. This part is approximately 12 μm in our case. It means that we did not remove the strongest barrier of the skin. So, in this case, it is not risk for any infection. However, we changed barrier properties of the skin. Barrier recovery start around 2-4 hours after disruption and it can take over 24 hours to complete recovery depending on disruption. Usually, the largest particle which was tested for penetration through the stratum corneum after plasma treatment has dimension in nanometers. This is very far from dimension of bacteria (1-10 μm) or fungi (3-200 μm), so there is no risk from them. However, the most of viruses are has diameter from 20 – 450 nm. In this case, it is possible that it can be some risk of infection. The most of drugs are smaller than 1 nm and plasma cause as a disinfection agent because of the sterilization effect and the treatment place is covered by the patch which can reduce risk of infection by virus. Ability of penetration of the skin decreases with size/weight of molecule. It means that larger molecules penetrate in a lower concentration. Large molecules can be interesting for cosmetic companies and they want to incorporate them to the skin, maybe in large areas. In such case, risk of infection has to be considered.

All these results show that plasma can enhance permeability of the skin and it gives hope for successful plasma drug delivery in medicine in future.

List of publications

Related to plasma-skin interaction:

2018:

K. Shimizu and ***J. Krištof*** (2018). **Microplasma Drug Delivery.** In Y. Tutar (Ed.), Plasma Medicine - Concepts and Clinical Applications (pp. 101-120). London, England: IntechOpen Limited.

Kristof J., Miyamoto H., Blajan M., Shimizu K., **XPS analysis of the skin treated by microplasma**, Advanced Material Letter 9:301 (2018).

2017:

J. Kristof, H. Miyamoto, A. N. Tran, M. Blajan, and K. Shimizu, **Feasibility of transdermal delivery of Cyclosporine A using plasma discharges**, Biointerphases 12(2):02B40, (2017).

K. Shimizu and ***J. Kristof*** (2017). **Enhancement of Percutaneous Absorption on Skin by Plasma Drug Delivery Method**. In S. Maiti (Ed.), Advanced Technology for Delivering Therapeutics (pp. 111-136). London, England: IntechOpen Limited

Kristof J., Tran A.N., Blajan M.G., Shimizu K., **Pharmacokinetics of Cyclosporine A of Transdermal Delivery Using Microplasma and Oral Administration**. Recent Advances in Technology Research and Education, vol. 660:161 (2017).

2016:

J. Kristof, A. N. Tran, M. Blajan, and K. Shimizu, **A Study of the Influence of Plasma Particles for Transdermal Drug Delivery**, Advances in Intelligent Systems and Computing, Vol. 519:167 (2016).

Shimizu K, Tran A N, ***Kristof J***, and Blajan M G. **Investigation of atmospheric micro-plasma for improving skin permeability**. In: Proceedings of the 2016 Electrostatics Joint Conference; 13-18 June; Lafayette, USA. 2016. p. I4

Other topics:

2018:

Veis P., Marin R. A., ***Kristof J.***, **Simultaneous vacuum UV and broadband UV-NIR plasma spectroscopy for LIBS improvement of light elements analysis**, 2018 submitted to Plasma Sources Science and Technology by Article reference: PSST-102384.R1

K. Shimizu, S. Muramatsu, ***J. Kristof***, M. Blajan, **Analysis of Hexadecane Decomposition by Atmospheric Microplasma**, IEEE Transactions on Industry Applications Vol. 54(1):605 (2018).

2017:

M. Suchonová, ***J. Krištof***, M. Pribula, M. Veis, F.L. Tabarés, P. Veis, **Analysis of LiSn alloy at several depths using LIBS**, Fusion Engineering and Design 117:175 (2017).

M. Blajan, A. Ito, ***J. Kristof***, K. Shimizu, **Flow Control by Dielectric Barrier Discharge Microplasma**, Recent Advances in Technology Research and Education, vol. 660:169 (2017).

K. Shimizu, A. Ito, M. Blajan, ***J. Kristof***, and H. Yoneda, **Basic Study of Fine Particle Transfer Using Electrostatic Force Generated by a Microplasma Actuator Type Electrode**, International Journal of Plasma Environmental Science & Technology Vol.11(1):87 (2017).

K. Shimizu, A. Ito, M. Blajan, ***J. Kristof*** and H. Yoneda, **Basic study of fine particle removal using microplasma and its electrostatic effect**, Jpn. J. Appl. Phys. 56:01AC03 (2017).

K. Shimizu, A. Ito, M. Blajan, ***J. Kristof,*** H. Yoneda, **Study of Fine Particle Removal from the Surface of a Microplasma Electrode Using the Electrostatic Force**, J. Inst. Electrostat. Jpn. vol. 41(1):26 (2017）.

2016:

Kristof J., Annušová A., Anguš M., Veis P., Yang X., Angot T., Roubin P., Cartry G., **Diagnostics of low-pressure hydrogen discharge created in a 13.56 MHz RF plasma reactor**, Physica Scripta Vol. 91(7):74009 (2016).

Pribula M., ***Kristof J.***, Suchoňová M., Horňáčková M., Plavčan J., Hakola A., Veis P., **Use of the near vacuum UV spectral range for the analysis of W-based materials for fusion applications using LIBS**, Physica Scripta No.T169:014045 (2016).

A. Annušová, ***J. Kristof***, C. Foissac, P. Supiot, P. Veis, **Experimental Study of a Water Vapour RF Discharge with/without Ar Admixture at Low and Moderate Pressure**, Acta Physica Universitatis Comenianae Vol. LIII:37 (2016).

M. Anguš, A. Annušová, ***J. Kristof***, P. Veis, **Molecular Hydrogen Lyman Band System in Vacuum UV Emissions of H_2-Ar Glow Discharge**, Acta Physica Universitatis Comenianae Vol. LIII:27 (2016).